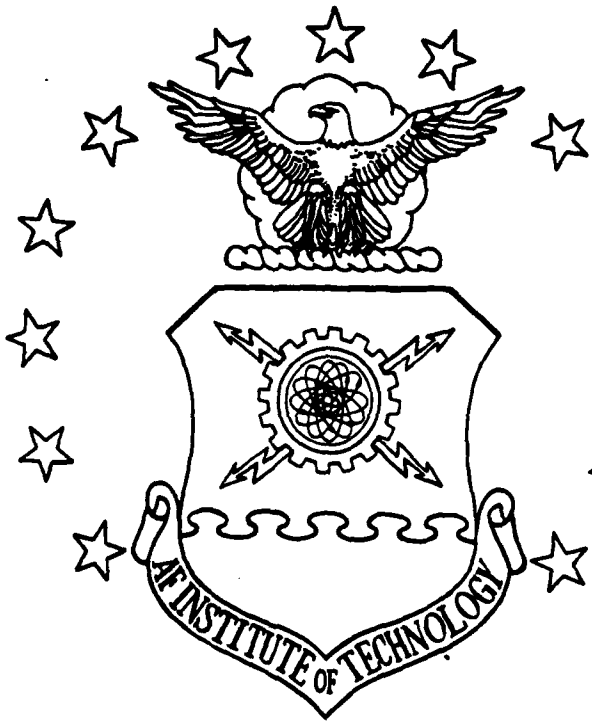

PREDICTION OF LONGITUDINAL PILOT INDUCED OSCILLATIONS USING THE OPTIMAL CONTROL MODEL

THESIS

Steven W. Lindsey
Captain, USAF

AFIT/GAE/ENY/90M-1

DEPARTMENT OF THE AIR FORCE
AIR UNIVERSITY
AIR FORCE INSTITUTE OF TECHNOLOGY
Wright-Patterson Air Force Base, Ohio

(1

PREDICTION OF LONGITUDINAL PILOT INDUCED OSCILLATIONS USING THE OPTIMAL CONTROL MODEL

THESIS

Steven W. Lindsey
Captain, USAF

AFIT/GAE/ENY/90M-1

AFIT/GAE/ENY/90M-1

PREDICTION OF LONGITUDINAL PILOT INDUCED OSCILLATIONS USING THE OPTIMAL CONTROL MODEL

THESIS

Presented to the Faculty of the School of Engineering

of the Air Force Institute of Technology

Air University

In Partial Fulfillment of the

Requirements for the Degree of

Master of Science in Aeronautical Engineering

Steven W. Lindsey, B.S.

Captain, USAF

December 1989

PREFACE

The purpose of this study was to determine if the Optimal Control Model (OCM) could be used to predict pilot induced oscillations (PIO) in a variety of aircraft configurations prior to flight test. The OCM was first applied to two existing data bases and correlations attempted with several OCM outputs. Based on analytical results, the two most promising prediction schemes were used to predict pilot handling qualities ratings (PHQR) and PIOs of 12 different flight test configurations. A flight test was performed in the approach and landing task for each of these configurations using the USAF/CALSPAN variable stability NT-33A.

The flight test results confirmed that the OCM was capable of predicting both PHQRs and PIOs prior to flight. 80 percent of the flight test PHQRs were within one pilot rating of the OCM predicted PHQRs. 96 percent of the flight test PIOs were within one PIO rating of the OCM predicted PIO ratings. The data base obtained during flight test was considered reliable and accurate and should be valuable data to use in future research.

The joint AFIT/USAFTPS program under which this research was conducted provided a unique opportunity to apply academic research to an actual flight test. It also provided the author new insight into handling qualities and

the ability to "bridge the gap" between the flight test and engineering communities. In accomplishing this research I was helped by several people. I would like to thank my thesis advisor, Dr. R. A. Calico, for providing me with the original idea. Additionally, I would like to thank my academic advisor and TPS advisor, Maj Dan Gleason, for providing assistance and motivation during this extended program.

I also wish to thank my test management project team, which included Capt Clarke Manning, Capt Rodney Liu, Capt Kurt Baum, and Capt Steve Thomas for their efforts in making our flight test go extremely smoothly. I would like to thank Russ Easter and John Ball of CALSPAN corporation for keeping us safe during those divergent PIOs 50 feet above the ground, as well as their insight and experience in handling qualities and the use of the handling qualities rating scale.

Table of Contents

	Page
Preface	ii
List of Figures	vi
List of Tables	ix
List of Symbols	xi
Abstract	xvi
I. Introduction	1
Background	1
Objectives	4
Method	5
Limitations	6
II. Equations of Motion and the Optimal Control Model	8
General Equations of Motion	8
The Optimal Control Model	12
Mathematical Development of the OCM	15
Computer Implementation	23
Choosing OCM Parameters	28
Modeling the Approach and Landing Task	31
OCM LAHOS Example	35
III. Analytical Results	42
Correlation Between Pilots	43
LAHOS Analysis	46
Flight Path Error Versus Control Rate	48
Flight Path Error	50
Crossover Frequency	53
Frequency at 180 Degrees of Phase	55
HAVE PIO Analysis	57
Correlation of LAHOS and HAVE PIO Results	63
Prediction Schemes	64

		Page
IV.	Flight Test Method	69
	Test Item Description	69
	Instrumentation and Data Reduction	70
	Test Methods and Conditions	72
V.	Flight Test Results and Analysis	78
	Flight Path Error	78
	Crossover Frequency	82
	Comparison Between Pilots	88
VI.	Conclusions and Recommendations	92
Appendix A:	NT-33A Stability Derivatives and Flight Control Configurations	94
Appendix B:	LAHOS 1-C Sample Input and Output Files	105
Appendix C:	Inflight Pilot Rating Scales	115
Appendix D:	Aircraft Description and Test Instrumentation	120
Appendix E:	Inflight Pilot Comment Cards	127
Appendix F:	NT-33A Configuration Identifications	155
Bibliography		171
Vita		173

List of Figures

Figure		Page
1.	Kleinman et. al. Linear Model	13
2.	The Optimal Control Model	21
3.	Flight Path Tracking Task	33
4.	LAHOS Pilot Rating Comparisons	43
5.	HAVE PIO Pilot Rating Comparisons	44
6.	LAHOS Flt Path Error vs Control Rate (PHQRs)	48
7.	LAHOS Flt Path Error vs Control Rate (PIO Ratings)	50
8.	Pilot Ratings vs Flt Path Error (LAHOS)	52
9.	PIO Ratings vs Flt Path Error (LAHOS)	52
10.	Pilot Ratings vs Crossover Frequency (LAHOS)	54
11.	PIO Ratings vs Crossover Frequency (LAHOS)	54
12.	Pilot Ratings vs Frequency at 180 Degrees (LAHOS)	56
13.	PIO Ratings vs Frequency at 180 Degrees (LAHOS)	57
14.	HAVE PIO Flt Path Error versus Control Rate (PHQRs)	59
15.	HAVE PIO Flt Path Error vs Control Rate (PIO Ratings)	59
16.	Pilot Ratings vs Flt Path Error (HAVE PIO)	60
17.	PIO Ratings vs Flt Path Error (HAVE PIO)	60
18.	Pilot Ratings vs Crossover Frequency (HAVE PIO)	61
19.	PIO Ratings vs Crossover Frequency (HAVE PIO)	61

Figure		Page
20.	Pilot Ratings vs Frequency at 180 Degrees (HAVE PIO)	62
21.	PIO Ratings vs Frequency at 180 Degrees (HAVE PIO)	62
22.	PHQRs vs Flight Path Error	67
23.	PIO Ratings vs Flight Path Error	67
24.	PHQRs vs Crossover Frequency	68
25.	PIO Ratings vs Crossover Frequency	68
26.	HAVE CONTROL Baseline Dynamics	73
27.	HAVE CONTROL PHQRs vs Flight Path Error	80
28.	HAVE CONTROL PIO Ratings vs Flight Path Error	81
29.	HAVE CONTROL PHQRs vs Crossover Frequency	82
30.	HAVE CONTROL PIO Ratings vs Crossover Frequency	85
31.	Revised PIO Ratings vs Flight Path Error	87
32.	Revised PIO Ratings vs Crossover Frequency	87
33.	Pilot A and B PHQR Comparison	89
34.	Pilot B and C PHQR Comparison	89
35.	Pilot A and C PHQR Comparison	90
36.	Pilot Handling Qualities Rating Scale	117
37.	PIO Rating Scale	119
38.	NT-33A Variable Stability Aircraft	121
39.	Variable Stability NT-33A Block Diagram	122
40.	Control System Layout	123
41.	System Verification by Calspan - Configuration 1-1	156

Figure		Page
42.	System Verification by Calspan - Configuration 2-1	157
43.	System Verification by Calspan - Configuration 3-1	158
44.	System Verification - Configuration 1-1	159
45.	System Verification - Configuration 1-3	160
46.	System Verification - Configuration 2-1	161
47.	System Verification - Configuration 2-D	162
48.	System Verification - Configuration 2-2	163
49.	System Verification - Configuration 2-5	164
50.	System Verification - Configuration 2-7	165
51.	System Verification - Configuration 3-1	166
52.	System Verification - Configuration 3-3	167
53.	System Verification - Configuration 3-5	168
54.	System Verification - Configuration 3-6	169
55.	System Verification - Configuration 3-8	170

List of Tables

Table		Page
1.	OCM Parameters	34
2.	LAHOS 1-C OCM Outputs	41
3.	Average Pilot and PIO Ratings, LAHOS Data	47
4.	Flight Path Error Trends, LAHOS Data	51
5.	Average Pilot and PIO Ratings, HAVE PIO Data	58
6.	Pilot Rating Correlations, LAHOS and HAVE PIO Data	63
7.	PIO Rating Correlations, LAHOS and HAVE PIO Data	63
8.	Pilot Rating Correlations, Combined Database	65
9.	PIO Rating Correlations, Combined Database	65
10.	Flight Test Prediction Equations	66
11.	HAVE CONTROL Flight Test Configurations	74
12.	Task Performance Standards	77
13.	Flight Path Error Pilot Rating Results	79
14.	Flight Path Error PIO Rating Results	80
15.	Crossover Frequency Pilot Rating Results	83
16.	Crossover Frequency PIO Rating Results	84
17.	Project Pilot Experience	88
18.	NT-33A Parameters	96
19.	LAHOS Baseline Configurations	97
20.	HAVE PIO Baseline Configurations	98
21.	NT-33A Flight Control Prefilters	99

Table | Page

22. LAHOS Flight Control System and Aircraft Dynamics Combinations 100

23. HAVE PIO Flight Control System and Aircraft Dynamics Combinations 101

24. HAVE CONTROL Baseline Configurations 103

25. HAVE CONTROL Flight Control System and Aircraft Dynamics Combinations 104

26. Test Instrumentation 126

List of Symbols

A	Controlled system state matrix
A_a	Airframe state matrix
A_b	Additional control system dynamics state matrix
A_c	Shaping filter state matrix
B	Controlled system control matrix
B_a	Airframe control matrix
C	Controlled system observation state matrix
C_a	Airframe observation state matrix
C_b	Additional control system dynamics observation state matrix
D	Controlled system observation control matrix
D_a	Airframe observation control matrix
D_b	Additional control system dynamics observation control matrix
E	Controlled system driving noise matrix
E_c	Shaping filter driving noise matrix
f_c	Fraction of attention allocated to the primary control task
f_{other}	Fraction of attention designated to side tasks
f_{tot}	Fraction of attention lost when switching from one displayed variable to another
F_{e_s}	Pilot's stick deflection including additional control system dynamics, inches
g	Acceleration of gravity, ft/sec^2
$H_n(s)$	Transfer function for pilot's neuromuscular lag

J	Value of the cost function
K_q	NT-33A pitch rate loop feedback gain
K_α	NT-33A angle of attack loop feedback gain
l_i	Intermediate variable for determining the optimal feedback gains
l_x	Pilot's location forward of the aircraft center of gravity, feet
L^*	Optimal state feedback gains
L_m^*	Optimal control feedback gains
$M_{[]}$	$=(1/I_y)(\partial M/\partial[])$, dimensional moment stability derivative in the body axis, rad/sec^2 per []
N	Describing function for nonlinear dead zone element
q	Perturbed pitch rate in the body axis, rad/sec
Q_r	Diagonal weighting matrix, control rate
Q_u	Diagonal weighting matrix, control
Q_x	Diagonal weighting matrix, state
Q_y	Diagonal weighting matrix, observations
RMS	Root mean squared
s	Laplace transform variable
TH	Visual indifference threshold
u	Perturbed forward speed in the body axis, ft/sec
U_0	Equilibrium forward speed, ft/sec
$\bar{u}$	System control inputs
u_m	Motor noise control input

$\hat{u}_m$	Best estimate of the motor noise control input
$\bar{u}_p$	Pilot stick deflection, inches
$v_m(t)$	Gaussian white motor noise
$v_{y_i}(t)$	Gaussian white observation noise of the i^{th} displayed variable
V_m	Power spectral density of the motor noise
V_{y_i}	Power spectral density of the observation noises
$V_{y_i}^0$	Power spectral density of the observation noise when the pilot's attention is limited to the i^{th} displayed variable
w	Perturbed downward speed in the body axis, ft/sec
$w(t)$	Random external disturbances
W_0	Equilibrium downward speed, ft/sec
W	Power spectral density of the disturbance or shaping filter
x_a	Airframe state vector
x_b	Additional control system dynamics state vector
x_c	Shaping filter state vector
$\hat{x}(t)$	Best estimate of the system state
$\hat{x}(t-\tau)$	Best estimate of the delayed system state
$X_{[]}$	$=(1/m)(\partial X/\partial[])$, dimensional x-force stability derivative in the body axis, ft/sec^2 per []
$\bar{y}$	Observation vector
$Z_{[]}$	$=(1/m)(\partial Z/\partial[])$, dimensional z-force stability derivative in the body axis, ft/sec^2 per []
α	Perturbed angle of attack in the body axis, rad

α_i	Half width of nonlinear deadzone element
β	Perturbed sideslip angle in the body axis, rad
γ	Flight path angle, rad
γ_c	Flight path driving signal, rad
γ_e	Flight path error, rad
δ_e	Elevator deflection input, deg
δ_{e_s}	Pitch stick deflection, inches
$\delta(t-\tau)$	Delta dirac function
$\xi(t)$	Intermediate variable for determining $\hat{x}(t)$
ρ_i	Noise to signal ratio, i^{th} displayed variable, db
$\sigma_{F_{es}}$	RMS control input, inches
σ_i	Standard deviation of the i^{th} displayed variable
σ_γ	RMS flight path, rad
σ_{γ_e}	RMS flight path error, rad
σ_θ	RMS pitch angle, rad
σ_{θ_c}	RMS attitude driving signal, rad
Σ	Error covariance matrix
ω_c	Open loop crossover frequency, rad/sec
ω_d	Dutch roll natural frequency, rad/sec
ω_{n_1}	Second order flight control system natural frequency, rad/sec
ω_{n_2}	Fourth order additional control system dynamics natural frequency, rad/sec

ω_p	Phugoid mode natural frequency, rad/sec
ω_{sp}	Short Period mode natural frequency, rad/sec
ω_{180}	Open loop frequency at 180^0 of phase, rad/sec
ϕ_c	Open loop phase at crossover frequency, deg
τ	Pilot's observation delay, sec
τ_n	Pilot's neuromuscular lag, sec
τ_R	Roll mode time constant, sec
τ_s	Spiral mode time constant, sec
τ_{θ_1}	Phugoid mode numerator time constant, sec
τ_{θ_2}	Short period mode numerator time constant, sec
τ_1	Additional control system dynamics first order numerator time constant, sec
τ_2	Additional control system dynamics first order denominator time constant, sec
θ	Perturbed pitch angle in the body axis, rad
θ_0	Equilibrium pitch angle, rad
θ_c	OCM attitude driving signal, rad
$\|\|_{180}$	Open loop gain at 180^0 of phase, db

Abstract

The purpose of this study was to evaluate the Optimal Control Model (OCM) in predicting handling qualities and PIO pilot ratings during the approach and landing task. Using two existing PIO databases, analytical prediction schemes were developed using the OCM. The two prediction schemes used were flight path error and crossover frequency. The prediction schemes were then applied to twelve different aircraft/flight control system landing configurations. The twelve configurations were flight tested using a USAF/Calspan variable stability NT-33A.

The OCM was able to predict pilot handling qualities ratings (PHQR) accurately (within one pilot rating) 80 percent of the time. PIO ratings were predicted accurately 96 percent of the time. Due to a PIO rating problem in the original databases, the PIO prediction schemes were modified using flight test data. Additional flight test configurations should be flown to verify the revised flight path error and crossover frequency PIO prediction schemes.

Because of the subjective nature of PHQRs and PIO ratings, the flight test results varied between pilots. Flight test results showed that the fighter pilot gave configurations poorer PHQRs and PIO ratings than the multiengine pilots. Additionally, the correlation between multiengine pilots was better than with the fighter pilot.

The crossover frequency prediction scheme was the most accurate predictor of pilot ratings, while the flight path error prediction scheme was slightly more accurate for PIO ratings. Both predictors agreed with classical control theory, showing correlation between flight path error, crossover frequency, and pilot/PIO ratings. The flight path error and crossover frequency rating prediction methods should be used as a tool in flight control system design.

PREDICTION OF LONGITUDINAL PILOT INDUCED OSCILLATIONS USING THE OPTIMAL CONTROL MODEL

I. INTRODUCTION

Background

According to Ralph H. Smith(1:6), a pilot induced oscillation (PIO) is "an unwanted, inadvertent and atypical closed loop coupling between a pilot and two or more independent response variables of an aircraft". Smith posed this definition to eliminate certain categories of aircraft that merely exhibit deficient handling qualities and not a true tendency to PIO.

PIOs have been encountered since the beginning of manned flight. Two examples of PIOs that nearly resulted in the loss of an aircraft was the inadvertent first flight of the YF-16 as well as a divergent PIO in the YF-17 (as simulated in the USAF/CALSPAN NT-33). A longitudinal PIO was also encountered during space shuttle testing when the pilot was tasked to land on a concrete runway. Before this test, the shuttle had shown no PIO tendencies and only by increasing the pilot's gain (by landing on the concrete runway instead of the large dry lakebed) was this PIO exposed. PIOs have traditionally been difficult to duplicate in fixed-base simulation, and as a result are

often not detected until the latter stages of flight test.

Since a PIO is difficult and sometimes impossible to stop, it can and has had in the past catastrophic consequences. An example of a catastrophic PIO was one in which an F-4 was destroyed at high speed and low altitude when the pitch augmentation failed.

PIOs have been defined previously as only occurring in a multi-task situation. Typical situations where PIOs have been encountered are in takeoff and landing, formation/air refueling, and air-air tracking. From this definition it appears that PIOs occur in demanding, high pilot "gain" tasks and do not otherwise show up. The most common cause of PIOs are excessive demands on the pilot (2:17). Assuming that the pilot is motivated and well trained, the amount of gain, lead and lag a pilot can provide in a given task is limited. When this limitation has been exceeded, a PIO will probably occur. It has been shown (1:4) that pilot handling qualities ratings (PHQR) do not necessarily correlate with PIO ratings; that is, an aircraft with good handling qualities may have strong PIO tendencies, while an aircraft with poor handling qualities may not PIO at all.

In MIL-STD-1797, the requirement states that "There shall be no tendency for pilot induced oscillations, that is, sustained or uncontrollable oscillations resulting from efforts of the pilot to control the aircraft." (3:22). The Mil-STD also references the research done by Smith when

applying this qualitative requirement. Smith's research was done using frequency domain techniques with a particular pilot model assumed in each case. Frequency domain techniques have been quite successful in the past, but they do not account for nonlinearities such as pilot remnant. Since a pilot in the loop is a requirement for a PIO to occur, it seems logical that the most important element to model in any analytical PIO study would be the pilot.

The Optimal Control Model (OCM) was developed in 1970 by Kleinman, Baron, and Levison (4). This was one of the first attempts to model the human pilot using state space techniques. State space models have become more popular in recent years because of advances in digital computers. According to Curry, Hoffman, and Young (5:19-20), there are several advantages to the OCM over describing function pilot models. First, the OCM more easily handles multiple input, multiple output control tasks. This is due to the state space nature of the model. Secondly, the model appears to provide an empirically verified measure of workload related to attention. Therefore, it will work for several different levels of displayed information, accounting for the increased or decreased attention required. It will also account for the source of the observation, i.e. whether the variable is observed under IMC (Instrument Meteorological Conditions), implying that the cockpit displays are being used, or VMC (Visual Meteorological Conditions), implying

that the pilot is looking outside the cockpit. Finally, the OCM is more adaptable to calculating time-varying statistical behavior over the ensemble of possible trajectories. It takes into account random system 'noises' as well as pilot 'noises'.

Objectives

The overall objective of this project was to evaluate the Optimal Control Model in predicting PHQRs and PIO pilot ratings during the approach and landing task. The advantage of using the approach and landing task is that it forces the pilot into a high gain situation, thereby exposing PIOs if they exist. The aircraft/flight control configurations modeled using the OCM came from two studies done with the USAF/Calspan variable stability NT-33.

The LAHOS (Landing Approach Higher Order System) study was completed in 1978 and evaluated several different aircraft configurations (6). This longitudinal study encompassed the entire spectrum of handling qualities and along the way encountered several longitudinal PIO's. The second study used was the HAVE PIO test project (7). In this study several different aircraft/control system configurations were evaluated, in which more longitudinal PIOs were encountered. The theory used was an application of the Optimal Control Model (OCM). The OCM has been applied primarily to handling qualities predictions in the

past, although some PIO work has been done by Hess (8). The ultimate goal of this effort was to predict beforehand whether or not a particular aircraft configuration will encounter PIO. The specific objectives of this project were:

1. Determine what parameters obtained from the OCM correlate with pilot handling qualities and PIO ratings.

2. Use OCM correlations to predict PHQRs and PIO tendencies for several aircraft/flight control system configurations.

3. Conduct a flight test of the aircraft/flight control system configurations chosen above and obtain actual PHQR and PIO data.

4. Determine if there is a correlation between the Optimal Control Model predictions and the actual flight test results in the approach and landing task.

5. Determine the percentage of correct pilot and PIO ratings predictions made by the OCM.

Method

The procedure used to accomplish the objectives presented above was the following:

1. The OCM was applied to the 1978 Calspan Landing Approach Higher Order System (LAHOS) data. The results were recorded for each aircraft/control system configuration.

2. The OCM was applied to the HAVE PIO data and the results recorded for each aircraft/control system configuration.

3. The results from both the HAVE PIO data and the LAHOS data were correlated versus pilot rating (to verify the OCM) and PIO rating/tendency. Prediction schemes based on these results were developed.

4. A set of aircraft/flight control system configurations were developed to implement and flight test on the Calspan NT-33 aircraft. These configurations had varying lead, lag, and corresponding time delay designed to cover the spectrum of pilot handling qualities and PIO ratings.

5. Using the prediction schemes developed from the OCM, the PHQR and PIO ratings of the newly developed configurations were predicted.

6. The configurations were flight tested on the NT-33 in the approach and landing task and the predicted ratings were compared to the actual ratings.

Limitations

This study applied the OCM in a slightly different way than it had been applied in the past. The intent of this application was to come up with a straightforward way to predict PIO tendency over a wide variety of aircraft configurations. The OCM was chosen to accomplish this

primarily because it is relatively simple to implement. Because of the inherent difficulty of modeling the human pilot, this study did not attempt to put any specific meaning on the absolute values of the various output parameters from the OCM. The goal was to keep the input model parameters constant throughout all of the aircraft/control system configurations and look for trends in the OCM outputs versus pilot handling qualities and PIO ratings.

II. EQUATIONS OF MOTION AND THE OPTIMAL CONTROL MODEL

In this section the equations of motion for longitudinal PIO analysis are developed in state space form from the Laplace transformed equations found in McRuer (8). These equations are further simplified using "lumped" stability derivatives in accordance with the LAHOS and HAVE PIO study. The additional control system dynamics for the NT-33 are then added to the state space formulation of the aircraft dynamics. The theory and mathematical development of the Optimal Control Model (OCM) is next presented. The computer implementation of the OCM is briefly discussed and a description of how the OCM parameters were chosen for this application is presented. Then the modeling of the approach and landing task is developed. Finally, the OCM is applied to a specific example from the LAHOS NT-33 study to include additional control system dynamics.

General Equations of Motion

The longitudinal equations of motion are found in McRuer (8:256). These linearized perturbation equations are based on steady state flight and are presented in the body axis. In this application, the equations were presented using "lumped" stability derivatives as described in the LAHOS study (6:211). Since the parameter identification technique used in the LAHOS study identified the transfer function directly, some stability derivatives were lumped together.

The equations relating the identified derivatives to actual derivatives were

$$M_q = M_q + U_0 M_w \qquad M_w = M_w + M_{\dot{w}} Z_w$$

The estimated stability derivatives and dynamic characteristics for the LAHOS, HAVE PIO, and HAVE CONTROL (flight test) configurations are in Appendix A. The equations presented below assumed negligible gust inputs:

$$\begin{aligned} du/dt + W_0 d\theta/dt + g\cos\theta_0\theta &= X_u u + X_w w + X_q q + X_{\delta_e}\delta_e \\ dw/dt - U_0 d\theta/dt + g\sin\theta_0\theta &= Z_u u + Z_w w + Z_q q + Z_{\delta_e}\delta_e \\ dq/dt &= M_u u + M_w w + M_q q + M_{\delta_e}\delta_e \\ d\theta/dt &= q \end{aligned} \qquad [1]$$

In the LAHOS longitudinal study, the only control input used during the landing phase was the elevator input. Since the thrust input during the landing phase was small, it was assumed negligible. X_q and Z_q were also considered negligible. Writing the equations in state space form yielded the following:

$$\begin{bmatrix} \dot{u} \\ \dot{w} \\ \dot{q} \\ \dot{\theta} \end{bmatrix} = \begin{bmatrix} X_u & X_w & -W_0 & -g\cos\theta_0 \\ Z_u & Z_w & U_0 & -g\sin\theta_0 \\ M_u & M_w & M_q & 0 \\ 0 & 0 & 1 & 0 \end{bmatrix} \begin{bmatrix} u \\ w \\ q \\ \theta \end{bmatrix} + \begin{bmatrix} X_{\delta_e} \\ Z_{\delta_e} \\ M_{\delta_e} \\ 0 \end{bmatrix} \begin{bmatrix} \delta_e \end{bmatrix} \qquad [2]$$

The definitions for the terms in equation [2] are as follows:

u = perturbed forward velocity

w = perturbed downward velocity

θ = perturbed pitch angle

q = perturbed pitch rate

δ_e = elevator control input

U_0 = equilibrium forward velocity

W_0 = equilibrium downward velocity

θ_0 = equilibrium pitch angle

$X_{[]}$ = x body axis stability derivatives

$Z_{[]}$ = z body axis stability derivatives

$M_{[]}$ = y body axis stability derivatives

The system output to the pilot $\bar{y}(t)$ can be modeled as a linear combination of the states $\bar{x}(t)$ and controls $\bar{u}(t)$. Therefore the set of equations representing the NT-33 aircraft in matrix form is

$$\dot{\bar{x}}_a(t) = A_a\bar{x}_a(t) + B_a\bar{u}(t) \qquad [3]$$

$$\bar{y}(t) = C_a\bar{x}_a(t) + D_a\bar{u}(t) \qquad [4]$$

where $[]_a$ is that quantity as related to the NT-33 airframe.

The equations of motion presented above do not include the additional control system dynamics found in most of the LAHOS and HAVE PIO configurations. The control system dynamics are given in transformed form as shown in Appendix A and can be easily converted to state space as required by the OCM. The NT-33 simulation also included a second order feel system and a second order elevator actuator. These two systems were not modeled in the analysis because their frequencies were well above the frequency band of interest. The set of additional control system dynamics can be represented by the following formulation:

$$\dot{\bar{x}}_b(t) = A_b\bar{x}_b(t) + B_b\bar{u}_p(t) \qquad [5]$$

$$\bar{u}(t) = C_b\bar{x}_b(t) + D_b\bar{u}_p(t) \qquad [6]$$

where $[]_b$ is that quantity as related to the additional

control system dynamics and $\bar{u}_p(t)$ is the stick deflection applied by the pilot. In addition a shaping prefilter (to be discussed later) is added in state space form

$$\dot{\bar{x}}_c(t) = A_c\bar{x}_c(t) + E_c\bar{w}(t) \qquad [7]$$

Equations [3], [4], [5], and [7] are combined to express the entire system of equations as

$$\dot{\bar{x}}(t) = A\bar{x}(t) + B\bar{u}_p(t) + E\bar{w}(t) \qquad [8]$$

$$\bar{y}(t) = C\bar{x}(t) + D\bar{u}_p(t) \qquad [9]$$

with $\bar{x}^T(t) = \left[\bar{x}_c^T(t),\ \bar{x}_a^T(t),\ \bar{x}_b^T(t)\right]^T$, $A = \left[A_c,\ A_a,\ A_b\right]^T$, etc.

The Optimal Control Model

This application of the Optimal Control Model (OCM) is based on the theory put forth by Kleinman, Baron, and Levison (4). The discussion and mathematical development that follows is based on that theory. After the OCM theory is developed completely, the computer application of the model is briefly discussed. Finally, an example of one LAHOS configuration is presented using OCM theory.

The basic assumption underlying the OCM approach is that the human is "optimal" in some sense; that is, the well trained, motivated pilot attempts to control the system the best that he or she can while at the same time minimizing the

amount of workload or amount of effort required (4:358). Obviously, as the difficulty of the task increases, the workload and effort required also increases. A simplified model of the OCM as first proposed by Kleinman et. al. (4:359) is shown in Figure 1:

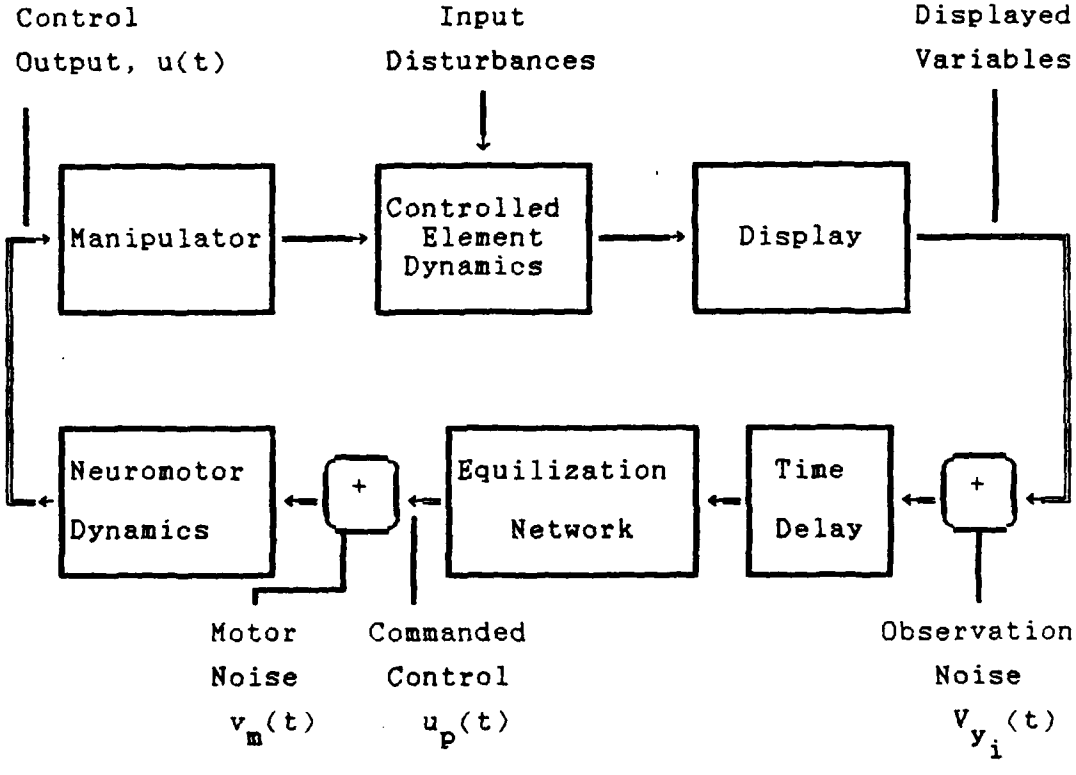

Figure 1. Kleinman et. al. linear model

In Figure 1 the controlled element dynamics are the mathematical model of the aircraft. The input disturbances are random variables representing all unmodelled inputs such as wind, weather, etc. The aircraft generates a display both

inside and outside the cockpit to the pilot. The output from the display is the information the pilot processes to close the feedback loop. However, what the pilot perceives is not necessarily what is actually being displayed.

To account for random "noises", such as instrument panel vibration, a dirty canopy, whether the pilot is viewing the instrument directly or peripherally, etc., an observation noise is added to the displayed variables. After passing through the observation noise, the displayed variables go through the pilot's perceptual time delay. This time delay accounts for visual and brain processing delays. After passing through this delay, the displayed variables finally enter the pilot's equalization network.

The equalization network is what the pilot uses to optimize his/her control strategy, depending on the situation and task at hand. The equalization network therefore depends on the situation and the controlled element. The pilot then provides a commanded control to the system. The double lines shown in Figure 1 represents situations where more than one control is used and one or more variables are observed. Added to this commanded control is a motor noise. This motor noise represents any random errors the pilot makes in applying the controls. It also accounts for the pilot's imperfect knowlege of the commanded control input. After passing through the input summing junction, the signal passes through the pilot's neuromuscular lag, which accounts for

neuromotor delays in the pilot. Finally, the input passes through the manipulator which represents the control system dynamics. These dynamics include anything external to the actual aircraft dynamics such as servos, feel system, or stick filters.

Mathematical Development of the OCM

The complete set of vehicle dynamics are represented by the linear, time-invariant equations of motion:

$$\dot{x}(t) = Ax(t) + Bu(t) + Ew(t) \qquad [10]$$

The vector x(t) represents the vehicle states, u(t) is a vector representing the pilot's control input, and w(t) represents the random external disturbances discussed above. In the OCM development, w(t) is a zero-mean, gaussian white noise with autocovariance:

$$E\{ w(t)w^{T}(\sigma) \} = W\delta(t-\sigma) \qquad [11]$$

The pilot observations y(t) are represented by a linear combination of the states and controls:

$$y(t) = Cx(t) + Du(t) \qquad [12]$$

These observations are presented to the pilot

continuously through the instrument panel or some outside reference. The OCM assumes that if the pilot explicitly observes a displayed output, he can extract the rate of change of that output. Recall that an observation noise $v_{y_i}(t)$ is added to the observed variables. In addition, recall that a motor noise $v_m(t)$ is also added to the pilot's control input. Based on a study of controller remnant (9), the noises $v_{y_i}(t)$ and $v_m(t)$ are assumed to be sufficiently wideband so as to be considered white noise processes with autocovariance:

$$E\left\{ v_{y_i}(t)v_{y_i}(\sigma) \right\} = V_{y_i}\delta(t-\sigma) \qquad [13]$$

$$E\left\{ v_m(t)v_m(\sigma) \right\} = V_m\delta(t-\sigma) \qquad [14]$$

A single noise v_{y_i} is associated with each displayed output $y_i(t)$. After passing through the time delay, τ, the human pilot ends up perceiving the following:

$$y_{p_i}(t) = y_i(t-\tau) + v_{y_i}(t-\tau) \qquad [15]$$

or

$$y_p(t) = Cx(t-\tau) + Du(t-\tau) + v_y(t-\tau) \qquad [16]$$

This is a delayed, noisy replica of the system output, which is ready to be processed by the pilot's equilization network.

The pilot's equilization network processes the delayed, noisy observed data to produce the pilot's control input, $u_p(t)$. Added to the pilot's control input is a motor input $u_m(t)$, which accounts for random errors in executing the control input. $u_m(t)$ is generated by the first order noise process

$$u(t) = u_p(t) + u_m(t) \qquad [17]$$

$$\dot{u}_m(t) + l u_m(t) = v_m(t) \qquad [18]$$

where l is the feedback gain and $v_m(t)$ is defined in equation [14].

The optimal control gains, L^*, are chosen by the pilot to minimize a quadratic cost function which in its most general form is given by

$$J = E\left\{ \lim_{T\to\infty} \frac{1}{T} \int_0^T \left[y^T Q_y y + x^T Q_x x + \dot{u}^T Q_r \dot{u} + u^T Q_u u \right] dt \right\} \qquad [19]$$

subject to

$$Q_y \geq 0 \qquad Q_x \geq 0 \qquad Q_u \geq 0 \qquad Q_r > 0$$

where $Q_{()_{ij}} = q_{()_i}$, $i = j$ and $Q_{()_{ij}} = 0$, $i \neq j$. The Q's in equation [19] are diagonal weighting matrices for the display variables, state variables, control rate, and control displacement, respectively. The selection of the cost weightings is not an easy task, although they can be selected

either objectively (by the designer) or subjectively (by the pilot in performing the task). The solution of this problem is simply a well-defined linear regulator problem with time delay and observation noise. The usual assumptions of controllability and observability are required to solve this problem.

The pilot's neuromuscular lag has been modeled in the past by a first order lag:

$$H_n(s) = \frac{1}{\tau_n s + 1} \qquad [20]$$

The neuromuscular dynamics have not been represented in the cost function. However, included in the cost function is a weighting on the control rate, $\dot{u}(t)$. This control rate weighting has little physical meaning since a trained pilot rarely makes rapid control movements. Also, it can be shown (10) that including a control rate term in the cost function results in a first order lag being introduced into the optimal controller. Therefore, the control rate weightings, q_{r_i}'s, are chosen to yield the appropriate neuromuscular time constant, τ_n.

It can also be shown (11) that the single control input $u_p(t)$ that minimizes the cost function is the solution of the following linear feedback law:

$$\tau_n \dot{u}_p(t) + u_p(t) = -L^* \hat{x}(t) - L_m^* \hat{u}_m(t) \qquad [21]$$

In the above equation, $\hat{x}(t)$ is the best estimate of the system state $x(t)$ based on the observed variables $y_p(t)$, and $\hat{u}_m(t)$ is the best estimate of $u_m(t)$. The rest of the mathematical development in this section is based on the presentation in Curry et. al. (5:152-155) and assumes cost function weightings on observed variables and control rates only. The time constant τ_n and gains L^* are found from the following two equations:

$$\tau_n = l_{n+1}^{-1} \qquad [22]$$

$$L_i^* = \tau_n l_i \ , \ i=1, \ \ldots, \ n \qquad [23]$$

The l_i's (i=1, ..., n+1) are obtained from the equation

$$l = b_0^T K_0 / q_r \qquad [24]$$

where K_0 is the unique positive definite solution of the n+1 dimensional algebraic matrix Ricatti equation:

$$A_0 K_0 + K_0 A_0 + C_0^T Q C_0 - K_0 b_0 b_0^T K_0 / q_r = 0 \qquad [25]$$

$$Q = \text{diag}[q_{y_1}, \ q_{y_2}, \ \ldots, \ q_{y_n}]$$

$$b_0 = \text{col}\ [0,0, \ \ldots, \ 0,1]$$

$$A_0 = \left[\begin{array}{c|c} A & B \\ \hline 0 & 0 \end{array}\right] \qquad C_0 = \left[C \mid D\right]$$

The gain L_m^* due to the control $\hat{u}_m$ in equation [21] is determined from the following equation:

$$L_m^* = \tau_n[(\tau_{n-1} - A_0 + b_0 l)^{-1} b_0]^T (C_0^T Q_0 + K_0 \bar{b})/q_r \qquad [26]$$

$$\bar{b} = \text{col}[b_0, 0]$$

This equation assumes that the bandwidths of $u_p(t)$ and $u_m(t)$ are approximately equal. It is also assumed that

$$L_m^* u_m(t) << L^* x(t) \text{ or } u_m(t) \cong 0$$

With this assumption and the bandwidth assumption, equations [18] and [21] can be added to produce the following equation:

$$\tau_n \dot{u}(t) + u(t) = m(t) + v_m(t) \qquad [27]$$

$$m(t) = -L^* \hat{x}(t)$$

The state estimate with time delay $\hat{x}(t-\tau)$ is produced by a Kalman filter. To account for the observation time delay τ, the Kalman filter is cascaded with a least-mean-squared predictor as shown in Figure 2 (5:21). The Kalman filter least-mean-squared estimate of the delayed state is generated by

$$\dot{\hat{x}}(t-\tau) = A_1 \hat{x}(t-\tau) + \Sigma C_0^T V_y^{-1} [y_p(t) - C_0 \hat{x}(t-\tau)] \qquad [28]$$

$$+ b_0 \tau_n^{-1} m(t-\tau)$$

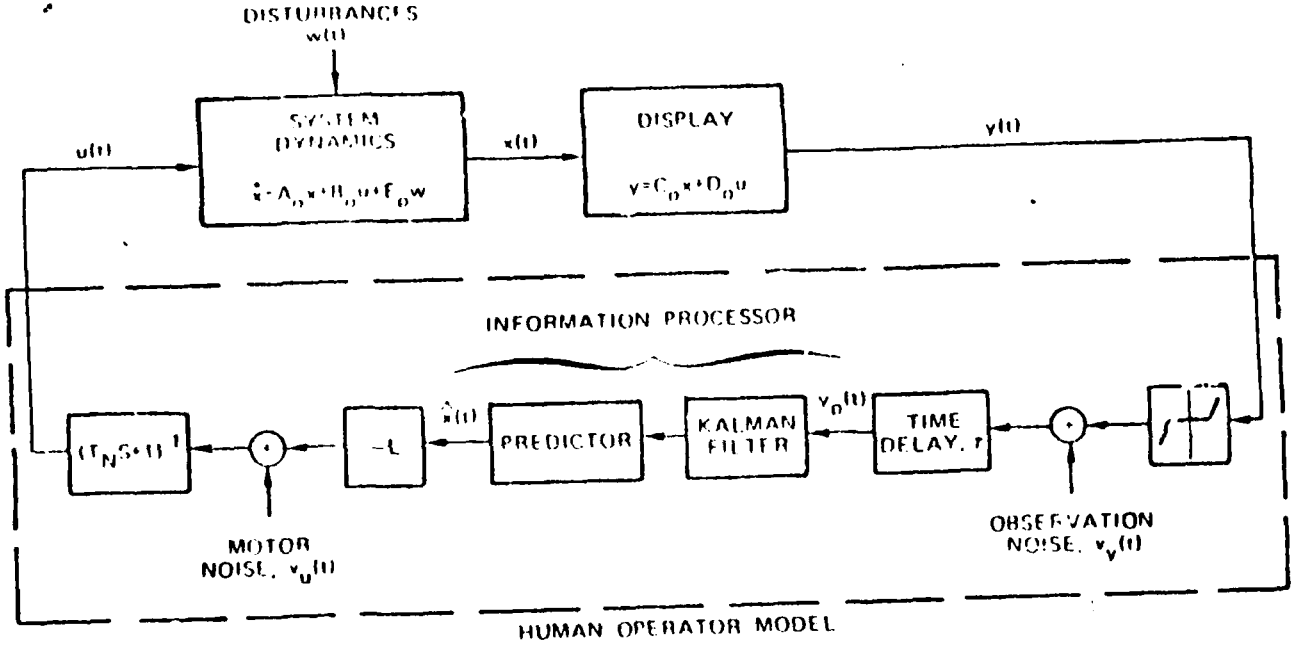

Figure 2. The Optimal Control Model

In this equation $x(t) = col[x(t),u(t)]$. The term Σ is the error covariance matrix. Σ is the unique positive definite solution to the steady state variance matrix equation

$$0 = A_1\Sigma + \Sigma A_1^T + W - \Sigma C_0^T V_y^{-1} C_0 \Sigma \qquad [29]$$

with the following definitions for A_1 and W:

$$A_1 = \left[\begin{array}{c|c} A & B \\ \hline 0 & -\tau_n^{-1} \end{array}\right] \qquad W = \left[\begin{array}{c|c} EE^T & 0 \\ \hline 0 & V_m \tau_n^{-2} \end{array}\right]$$

The predictor adjusts the delayed state estimate given by the Kalman filter output $p(t) = \hat{x}(t-\tau)$:

$$\hat{x}(t) = \xi(t) + e^{A_1\tau}[p(t) - \xi(t-\tau)] \qquad [30]$$

$$\dot{\xi}(t) = A_1\xi(t) + b_0\tau_n^{-1}m(t) \qquad [31]$$

Kleinman (12) was able to obtain a closed form expression for the covariance of $\hat{x}(t)$, thus explicitly relating the time delay and observation noise to system performance. By solving for the expected values of states, observed variables and controls, a quantitative least-mean-squared output of the OCM can be used to compare with experimental results. The closed form expressions from (12) are as follows:

$$E\left\{\hat{x}(t)\hat{x}^T(t)\right\} = e^{A_1\tau}\Sigma e^{A_1\tau} + \int_0^{\tau} e^{A_1\sigma} W e^{A_1{}^T\sigma} d\sigma \qquad [32]$$

$$+ \int_0^{\infty} e^{\bar{A}\sigma} e^{A_1\Sigma C_0{}^T V_y{}^{-1} C_0 \Sigma e^{A_1{}^T\tau} e^{\bar{A}^T\sigma}} d\sigma$$

where $\bar{A} = A_0 - b_0\tau$. The expected values of the OCM outputs are as follows:

$$E\left\{x_i{}^2(t)\right\} = X_i, \quad i = 1, 2, \ldots, n$$

$$E\left\{y_i{}^2(t)\right\} = \left[C_0 X C_0{}^T\right]_i, \quad i = 1, 2, \ldots, r \qquad [33]$$

$$E\left\{u^2(t)\right\} = X_{n+1,n+1} \qquad [34]$$

This completes the mathematical development of the OCM as originally developed by Kleinman, Baron, and Levison. This mathematical model of the pilot has been applied successfully many times and compared against experimental results.

Computer Implementation

The Optimal Control Model was implemented using a Fortran computer program called PIREP (5). PIREP is a powerful program that allows for some extra terms in the OCM. First of all, PIREP allows the user to input an observation threshold. This threshold sets the minimum value of a

variable that a pilot can observe. Any value below this, and the pilot will not notice the change in that variable. This threshold is put into the model as a dead zone element.(see Figure 2). Therefore, the observation noise is modified as follows:

$$V_{y_i} = \rho_i \left[\frac{\sigma_i}{N(\sigma_i, \alpha_i)} \right]^2 \qquad [35]$$

In this equation V_{y_i} is the covariance of the white observation noise, σ_i is the standard deviation of y_i, N is the describing function for the nonlinear dead zone element with half width α_i, and ρ_i is the noise to signal ratio. In PIREP, the covariance V_{y_i} is solved for iteratively; the user merely has to provide the noise to signal ratio ρ_i and the threshold value.

An estimate of pilot workload is also included in PIREP's implementation of the OCM. The type of pilot workload used by PIREP is known as task interference workload (13). The basic theory behind task interference workload is that the pilot is trying to accomplish some primary task and most of his attention is focused on that. However, other side tasks come up that interfere with the primary task. Since these side tasks must be accomplished, they take away some of the pilot's attention that would otherwise be spent on the primary task. Examples of side tasks include changing

radio frequencies, updating the inertial navigation system, clearing for other aircraft, and talking on/listening to the radio. Task interference workload is consistent with the OCM formulation. In the task interference workload model, the total fraction of attention by the pilot is composed of the following terms:

$$f_{tot} = f_c + f_o + f_{other} \qquad [36]$$

$$f_c = \sum_i f_{c_i}$$

In equation [36], f_c is the portion of attention allocated to the primary control task and f_{c_i} is that fraction of f_c allocated to each displayed variable. The term f_o is the fraction of attention lost by the pilot when switching from one displayed variable to another, or from the control task to the side task. Finally, f_{other} is the fraction of attention designated to the other side tasks (switching radios, talking to ground control, etc) that the pilot must perform.

To implement this model for task interference, the fractions of attention are accounted for by modifying equation [35]:

$$V_{y_i} = \frac{V_{y_i}^0}{f_{c_i}} = \frac{\rho_i}{f_{c_i}} \left[\frac{\sigma_i}{N(\sigma_i, \alpha_i)} \right]^2 \qquad [37]$$

In this equation, $V_{y_i}^{0}$ is the power spectral density of the observation noise of y_i when the pilot's attention is limited to that display variable alone, and f_{c_i} is the fraction of attention allocated to the i^{th} displayed variable. Note that to be consistent with the assumptions of the OCM, f_{c_i}'s have to be chosen for not only the displayed y_i's, but also chosen for the rates of change of the y_i's. If f_{c_i} is chosen to be 1.0, equation [37] reduces to equation [35]. In the PIREP implementation, only the f_{c_i}'s have to be chosen, it automatically accounts for f_o and f_{other}. Note that the maximum value of f_{total} is 2.0, not 1.0. This is because the observation rate fractions of attention are normally chosen to be the same as the observed y_i's, therefore the total attention allocation always adds up to 2.0.

Finally, a random noise w(t) needs to be added into the state equation to account for disturbances. What the noise w(t) actually does is provide a signal for the OCM to follow. The OCM attempts to minimize the mean squared error while following w(t). Typically w(t) is implemented as a linear system driven by white noise to generate a signal that approximates a specific task, such as air-air tracking or approach and landing. w(t) is placed in the A matrix as a shaping filter, as shown in equation [8]. After these modifications are chosen for the OCM, it can be implemented in PIREP. The parameters and variables that need to be

chosen by the user are as follows:

1. System matrices A, B, C, D, E
2. Cost functional weightings Q_x, Q_y, Q_u, Q_r
3. Controller time delay, τ
4. Variance of process or driving noise, W
5. Motor noise to signal ratio, V_m
6. Indifference thresholds for the observations, TH
7. Observation noise to signal ratio, V_{y_i}
8. Fractional attention allocations, f_{c_i}'s
9. Neuromuscular time constant, τ_n

In addition, PIREP will calculate frequency domain representations of the OCM. The most commonly used frequency domain output is a composite describing function of the system. The single axis Y_pY_c function is an "outer loop" representation of the OCM and is typically used to determine the gain and phase margin of the entire system. According to Kleinman et. al. (4:364), the OCM structure can be represented in the frequency domain as

$$y(s) = H(s)u(s) \qquad [38]$$

H(s) can be solved for directly from the OCM as follows:

$$H(s) = - \frac{l_e}{\tau_n s + 1} \left[(sI - \hat{A}) \int_0^{\tau} e^{(sI-A_1)\sigma} d\sigma (sI-\bar{A}) \right. \qquad [39]$$

$$\left. + sI-\hat{A} + b_1 l_e \right]^{-1} \Sigma C_0^T V_y^{-1}$$

In this equation, $l_e = [1^*,0]$, $\hat{A} = A_1 - \Sigma C_0^T V_y^{-1} C_0$, and $\bar{A}$ is defined in equation [32]. The next subject to be addressed is how to choose the particular parameters of the OCM.

Choosing OCM Parameters

Several methods have been recommended for choosing the cost functional weightings Q_x, Q_y, Q_u, and Q_r. The weighting Q_r is chosen consistent with the theory to yield the appropriate value of the neuromuscular time constant, τ_n. One method recommended by Bryson and Ho (14:149) is to weight each variable by the inverse of the maximum allowable deviation squared. For example, if the maximum flight path angle deviation allowed was five degrees, then the weighting on the flight path angle would be $(1/5)^2$. Another method is to vary the weightings to match the OCM output with the experimentally obtained output. Since we want to use to OCM to predict PIO's beforehand, it is not practical to vary the weightings to match experimental results. The method recommended by Bryson and Ho was attempted on a LAHOS

configuration, and the results were compared with just using a weighting of 1.0. The RMS error output of the OCM was exactly the same for both cases. The only noticeable difference in the two cases is the absolute value of the cost function. To keep the analysis as simple as possible, cost weightings of 1.0 are used in the OCM.

The controller time delay, which accounts for visual and brain processing delay has typical values of 0.1 to 0.3. For this study the controller time delay was chosen to be 0.2. The neuromuscular time constant, τ_n, for the fastest reaction time with a force-type manipulator has been experimentally determined to be about 0.1.

The observation thresholds depend upon the format of the display. A typical value for these thresholds would be ten percent of full scale deflection on the particular display. No assumptions made about the display format in this analysis, but thresholds have to be provided for the rate terms of the displayed variables. The thresholds were chosen to be .05 deg for the explicitly displayed variables and .18 deg/sec for their rates, which is consistent with the work done by Anderson and Schmidt (15).

The motor and observation noise to signal ratios have both been experimentally determined through man-machine human factors studies. Typically, the motor noise is chosen to be -25 db and the observation noise is set at -20 db. These values will be used for this application of the OCM.

Attention allocation is highly dependent upon the task, the display, and the training of the pilot. For example, in a VMC (visual meteorological conditions) situation, the pilot will probably spend most of his time on outside references, while in an IMC (instrument meteorological conditions) situation, the pilot is more likely to concentrate on his instruments. The cross check each pilot uses will be somewhat different, so it is difficult to specify attention allocations that will work for everyone. To keep the analysis simple, the fractional attention allocations were chosen to be the same and to add up to 1.0 across all observed variables and their rates.

As stated before, a driving noise, w(t) needs to be added to the system state equations to give the OCM a signal to track. The shaping filter to be used in this analysis is a second order filter taken from Anderson's work (15:189). This filter is a commanded aircraft attitude signal, generated by

$$\ddot{\theta}_c + 0.5\dot{\theta}_c + 0.25\theta_c = 0.25w(t) \qquad [38]$$

The statistics on this filter, using $\sigma^2_w = 64\delta(t)$ are

$$\sigma_{\theta_c} = 4 \text{ deg} \qquad \sigma_{\dot{\theta}_c} = 2 \text{ deg/sec}$$

This tracking task approximates the actual instrument tracking task performed in the Neal-Smith report (16).

Modeling the Approach and Landing Task

As stated previously, a PIO occurrence requires closed loop coupling between the pilot and two or more response variables. To simulate this situation in the OCM, the approach and landing task used was originally developed in the report by Anderson and Schmidt (15). In the approach and landing task, the aircraft's altitude and vertical velocity are important to the pilot. These two parameters can be related to the aircraft's flight path angle, γ. Therefore, Anderson and Schmidt reasoned that controlling the flight path angle is necessary if the pilot is to achieve good closed loop performance. Controlling the flight path angle is equivalent to minimizing the flight path error deviation around a desired flight path. This can be reflected in the cost functional as follows:

$$J(u_p) = E\left\{ \lim_{T\to\infty} \frac{1}{T} \int_0^T \left[q_y \gamma_e^2 + q_u u_p^2 + q_{\dot{r}} \dot{u}_p^2 \right] dt \right\} \qquad [39]$$

where γ_e is the flight path error and u_p is the pilot's control input. Flight path error is not displayed directly to the pilot, rather it is a linear combination of states. Other observations assumed available to the pilot in a VMC task are pitch attitude, pitch rate, vertical velocity (or sink rate), and vertical acceleration. This formulation assumes that due to the kinematic relationships between these

parameters, the pilot can close loops based on pitch attitude, pitch rate, flight path, and flight path rate as well as flight path error and flight path error rate. Therefore, the pilot observation vector chosen by Anderson and Schmidt was

$$y_p(t) = [\gamma_e,\ \dot{\gamma}_e,\ \gamma,\ \dot{\gamma},\ \theta,\ \dot{\theta}]^T \qquad [40]$$

The filter described by equation [38] is modified to generate a command flight path signal using the γ/θ relationship

$$\frac{\gamma_c(s)}{\theta_c(s)} = \frac{1}{\tau_{\theta_2} s + 1} \qquad [41]$$

In this equation, $1/\tau_{\theta_2} = 0.5s^{-1}$. Combining equation [41] with equation [38] and changing the command dynamics to state space form yields

$$\begin{bmatrix} \dot{\theta}_c \\ \ddot{\theta}_c \\ \dot{\gamma}_c \end{bmatrix} = \begin{bmatrix} 0 & 1 & 0 \\ -0.25 & -0.5 & 0 \\ 0.5 & 0 & -0.5 \end{bmatrix} \begin{bmatrix} \theta_c \\ \dot{\theta}_c \\ \gamma_c \end{bmatrix} + \begin{bmatrix} 0 \\ 0.25 \\ 0 \end{bmatrix} w \qquad [42]$$

This formulation can then be put into the system matrices as equation [8].

Using the observation vector shown in equation [40], Anderson and Schmidt showed that the solution of the OCM yields the following block diagram description of the pilot's control strategy:

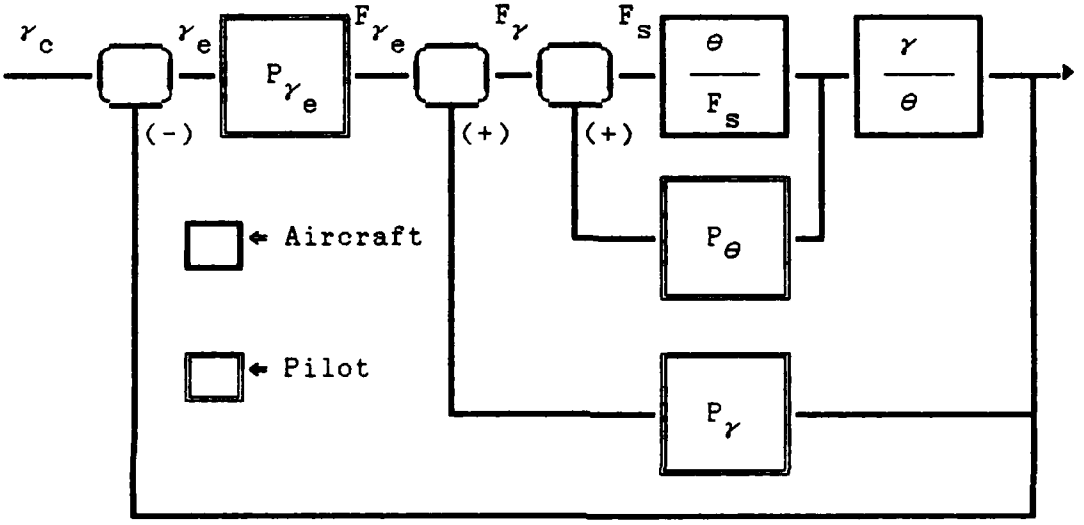

Figure 3. Flight path tracking task

From Figure 3 it can easily be seen that the pilot is closing loops on several observations, and therefore the task as modeled is realistic and meets the requirements for a PIO to take place. Since the term γ_e implicitly includes all of the pilot observations in equation [40], Anderson and Schmidt chose to weight only the observed variable γ_e. This method will be followed in this implementation. In summary, the OCM parameters chosen for this project are found in Table 1.

Table 1: OCM Parameters

Parameter	Chosen Value
Observation Vector	$y_p^T = \left[\gamma_e, \dot{\gamma}_e, \gamma, \dot{\gamma}, \theta, \dot{\theta}\right]$
Cost Function Weightings	Q_y = diag[1,0,0,0,0,0]
Observation Thresholds	$TH_{\gamma_e,\gamma,\theta}$ = 0.05 deg $TH_{\dot{\gamma}_e,\dot{\gamma},\dot{\theta}}$ = 0.18 deg/sec
Observation Noise/Signal Ratio	-20 db all observed variables
Motor Noise/Signal Ratio	-25 db all observed variables
Fractional Attention Allocations	f_{c_i} = .3333 all observed variables
Observation Delay	τ = 0.2 sec
Neuromuscular lag	τ_n = 0.1 sec

OCM LAHOS Example

The OCM theory and computer program PIREP will now be applied to LAHOS configuration 1-C. The equations of motion for the baseline configuration 1-1 (see appendix A for specific details), using equation [2] are as follows:

$$\begin{bmatrix} \dot{u} \\ \dot{w} \\ \dot{q} \\ \dot{\theta} \end{bmatrix} = \begin{bmatrix} -.041 & .11 & -25 & -32.08 \\ -.25 & -.75 & 205 & -2.52 \\ 0 & -.00232 & -.76 & 0 \\ 0 & 0 & 1 & 0 \end{bmatrix} \begin{bmatrix} u \\ w \\ q \\ \theta \end{bmatrix} \qquad [43]$$

$$+ \begin{bmatrix} .0032 \\ 1.1 \\ .33685 \\ 0 \end{bmatrix} \delta_{e_s}$$

Note that the term δ_{e_s} is the pilot's stick input in inches, which is in accordance with the parameter identification technique used in (6) The observation vector, $y = Cx + Du$, needs to be developed in the form specified in Table 1. Since γ is not explicitly shown in equation [43], γ can be

solved for using the following relationships:

$$\gamma = \theta - w/U_0 \qquad \gamma_e = \gamma_c - \gamma \qquad [44]$$

Using the relationships in [44], and the equations of motion, and shaping filter shown in equation [42], the observed variables γ_e, $\dot{\gamma}_e$, and $\dot{\gamma}$ can be expressed explicitly as

$$\gamma_e = \gamma_c + w/U_0 - \theta \qquad [45]$$

$$\dot{\gamma}_e = 0.5\theta_c - 0.5\gamma_c + (Z_u/U_0)u + (Z_w/U_0)w \qquad [46]$$

$$-(g\sin\theta_0/U_0)\theta + (Z_{\delta_e}/U_0)\delta_{e_s}$$

$$\dot{\gamma} = -(Z_u/U_0)u - (Z_w/U_0)w + (g\sin\theta_0/U_0)\theta - (Z_{\delta_e}/U_0)\delta_{e_s} \qquad [47]$$

With these relationships the observation vector can then be expressed in the proper form. For the LAHOS 1-1 baseline configuration, the observation vector is expressed below as

$$\begin{bmatrix} \gamma_e \\ \dot{\gamma}_e \\ \gamma \\ \dot{\gamma} \\ \theta \\ \dot{\theta} \end{bmatrix} = \begin{bmatrix} 0 & 0 & 1 & 0 & .0049 & -1 & 0 \\ 0.5 & 0 & -0.5 & -.0012 & -.0037 & -.0123 & 0 \\ 0 & 0 & 0 & 0 & -.0049 & 1 & 0 \\ 0 & 0 & 0 & .0012 & .0037 & .0123 & 0 \\ 0 & 0 & 0 & 0 & 0 & 1 & 0 \\ 0 & 0 & 0 & 0 & 0 & 0 & 1 \end{bmatrix} \begin{bmatrix} \theta_c \\ \dot{\theta}_c \\ \gamma_c \\ u \\ w \\ \theta \\ q \end{bmatrix}$$

$$+ \begin{bmatrix} 0 \\ .0054 \\ 0 \\ -.0054 \\ 0 \\ 0 \end{bmatrix} \delta_{e_s} \qquad [48]$$

In LAHOS configuration 1-C, there are additional control system dynamics that need to be included in the state equation. Filter C is a first order stick prefilter expressed in transfer function form as (6:8)

$$\frac{\delta_{e_s}}{F_{e_s}} = \frac{2(s + 5)}{s + 10} \qquad [49]$$

In this equation, F_{e_s} is the redefined pilot's input when the additional control system dynamics are included. Changing equation [49] to the time domain yields

$$\dot{\delta}_{e_s} = -10\,\delta_{e_s} + 2\dot{F}_{e_s} + 10\,F_{e_s} \qquad [50]$$

This equation in its current form cannot be used in the aircraft equations of motion. To include this term a new state needs to be defined. Integrating equation [50] yields

$$\delta_{e_s} = 2F_{e_s} + 10\int (F_{e_s} - \delta_{e_s})dt \qquad [51]$$

Defining $\dot{x} = 10(F_{e_s} - \delta_{e_s})$ yields the following equations:

$$\delta_{e_s} = 2F_{e_s} + x \qquad [52]$$

$$\dot{x} = -10x - 10F_{e_s} \qquad [53]$$

The additional control system dynamics added by the filter C can now be included in the state equation [48] by adding an additional state, x. Finally, the state equation to be implemented in PIREP for LAHOS configuration 1-C including additional control system dynamics and the shaping filter is

$$\begin{bmatrix} \dot{\theta}_c \\ \ddot{\theta}_c \\ \dot{\gamma}_c \\ \dot{u} \\ \dot{w} \\ \dot{q} \\ \dot{\theta} \\ \dot{x} \end{bmatrix} = \begin{bmatrix} 0 & 1 & 0 & 0 & 0 & 0 & 0 & 0 \\ -0.25 & -0.5 & 0 & 0 & 0 & 0 & 0 & 0 \\ 0.5 & 0 & -0.5 & 0 & 0 & 0 & 0 & 0 \\ 0 & 0 & 0 & -0.041 & .11 & -25 & -32.08 & .003 \\ 0 & 0 & 0 & -0.25 & -.75 & 205 & -2.52 & 1.1 \\ 0 & 0 & 0 & 0 & -.00232 & -.76 & 0 & .337 \\ 0 & 0 & 0 & 0 & 0 & 1 & 0 & 0 \\ 0 & 0 & 0 & 0 & 0 & 0 & 0 & -10 \end{bmatrix}$$

$$\begin{bmatrix} \theta_c \\ \dot{\theta}_c \\ \gamma_c \\ u \\ w \\ q \\ \theta \\ x \end{bmatrix} + \begin{bmatrix} 0 \\ 0 \\ 0 \\ .0064 \\ 2.2 \\ .6737 \\ 0 \\ -20 \end{bmatrix} F_{e_s} + \begin{bmatrix} 0 \\ 0.25 \\ 0 \\ 0 \\ 0 \\ 0 \\ 0 \\ 0 \end{bmatrix} w(t) \qquad [54]$$

The observation vector to be implemented with equation [54] is

$$\begin{bmatrix} \gamma_e \\ \dot{\gamma}_e \\ \gamma \\ \dot{\gamma} \\ \theta \\ \dot{\theta} \end{bmatrix} = \begin{bmatrix} 0 & 0 & 1 & 0 & .0049 & -1 & 0 & 0 \\ .5 & 0 & -.5 & -.0012 & -.0037 & -.0123 & 0 & .0054 \\ 0 & 0 & 0 & 0 & -.0049 & 1 & 0 & 0 \\ 0 & 0 & 0 & .0012 & .0037 & .0123 & 0 & -.0054 \\ 0 & 0 & 0 & 0 & 0 & 1 & 0 & 0 \\ 0 & 0 & 0 & 0 & 0 & 0 & 1 & 0 \end{bmatrix} \begin{bmatrix} \theta_c \\ \dot{\theta}_c \\ \gamma_c \\ u \\ w \\ \theta \\ q \\ x \end{bmatrix}$$

$$+ \begin{bmatrix} 0 \\ .0108 \\ 0 \\ -.0108 \\ 0 \\ 0 \\ 0 \end{bmatrix} F_{e_s} \qquad [55]$$

Equations [54], [55], and the OCM parameters as defined in Table 1 are input into PIREP. Sample input and output files for LAHOS configuration 1-C are shown in Appendix B. The pertinent OCM outputs are listed in Table 2.

Table 2: LAHOS 1-C OCM Outputs

OCM Output Description		Value
RMS Flight Path Error	σ_{γ_e} =	.6698 deg
RMS Flight Path Error Rate	$\sigma_{\dot{\gamma}_e}$ =	1.2542 deg/sec
RMS Flight Path	σ_{γ} =	3.2091 deg
RMS Flight Path Rate	$\sigma_{\dot{\gamma}}$ =	1.7189 deg/sec
RMS Pitch Angle	σ_{θ} =	4.4656 deg
RMS Pitch Angle Rate	$\sigma_{\dot{\theta}}$ =	4.6564 deg/sec
RMS Control	$\sigma_{F_{e_s}}$ =	.8063 inches
RMS Control Rate	$\sigma_{\dot{F}_{e_s}}$ =	5.687 inch/sec
Open Loop Crossover Frequency	ω_c =	1.91 rad/sec
Open Loop Crossover Phase	ϕ_c =	-151.3 deg
Frequency at 180^0 Phase	ω_{180} =	3.60 rad/sec
Gain at 180^0 Phase	$\lvert\rvert_{180}$ =	-3.773 db
Performance Cost	J =	.0001366

The information shown in Table 2 can be obtained for all of the LAHOS and HAVE PIO configurations. This data can be used to find correlations with pilot and PIO ratings.

III. ANALYTICAL RESULTS

To begin the analysis, 39 LAHOS configurations were put through the OCM as implemented by PIREP. It should be noted here that a few LAHOS configurations diverged when implemented by PIREP. The configurations that wouldn't run included fourth order lag prefilters. The HAVE PIO fourth order lag systems also did not converge. However, the vast majority of the LAHOS and HAVE PIO configurations did converge successfully.

The OCM parameters used are those found in Table 2. As stated previously, the OCM has in the past primarily been applied to determining pilot ratings, and not PIO ratings. Therefore, to verify that the model was consistent, the results from the LAHOS simulations were first compared to pilot handling qualities ratings (PHQR) and then to PIO ratings. After correlations were obtained with the LAHOS data, the same analysis was applied to the HAVE PIO data. The correlations found in the two databases were then compared and PHQR and PIO prediction schemes developed from the results.

The pilot ratings used in the 1978 Calspan study (6) and the HAVE PIO experiment (7) were based on the Cooper-Harper handling qualities rating scale shown in Figure 36 (Appendix C). The PIO flowchart and rating scale is in Figure 37. As can be seen from the scales, the pilot and

PIO ratings are highly subjective and may vary from pilot to pilot. The variability of pilot ratings make them difficult to quantify and develop a prediction scheme from. Typically, the best correlation achieved is usually 70-80 percent. To find out the variability between pilots in the LAHOS and HAVE PIO studies, some least squares regression analyses were performed on pilot and PIO ratings.

Correlation Between Pilots

To determine the typical correlations between pilots, two sample cases were analyzed. The first case was the correlation between two pilots in the LAHOS study. The correlation is shown in Figure 4 below:

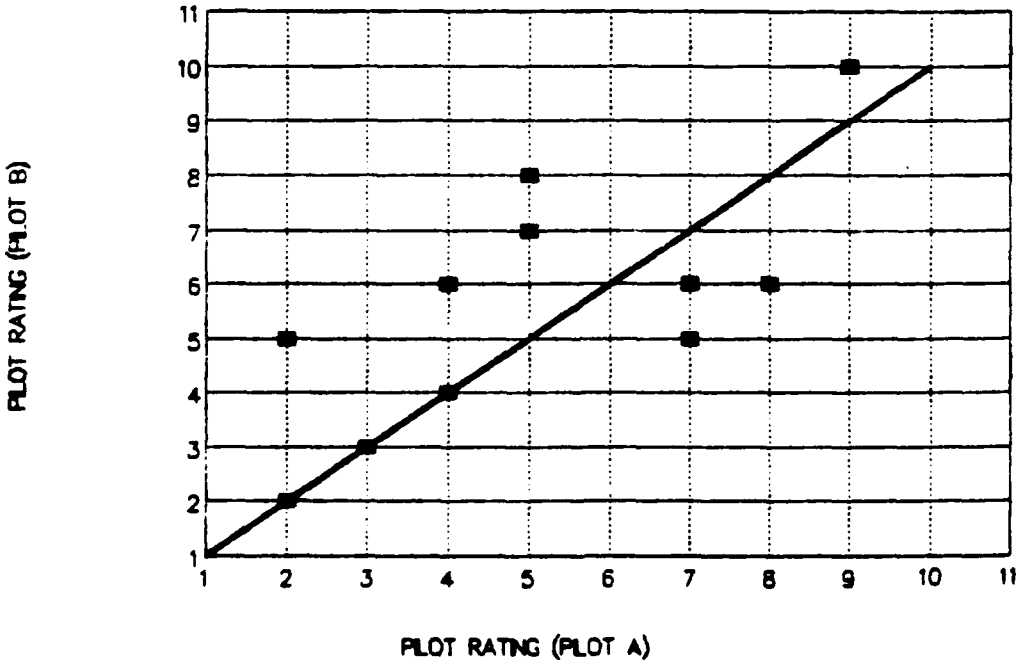

Figure 4. LAHOS Pilot Rating Comparisons

In Figure 4, the coefficient of correlation (R) between LAHOS pilot A and pilot B was 0.70. Figure 5 is a sample correlation between pilots in the HAVE PIO study:

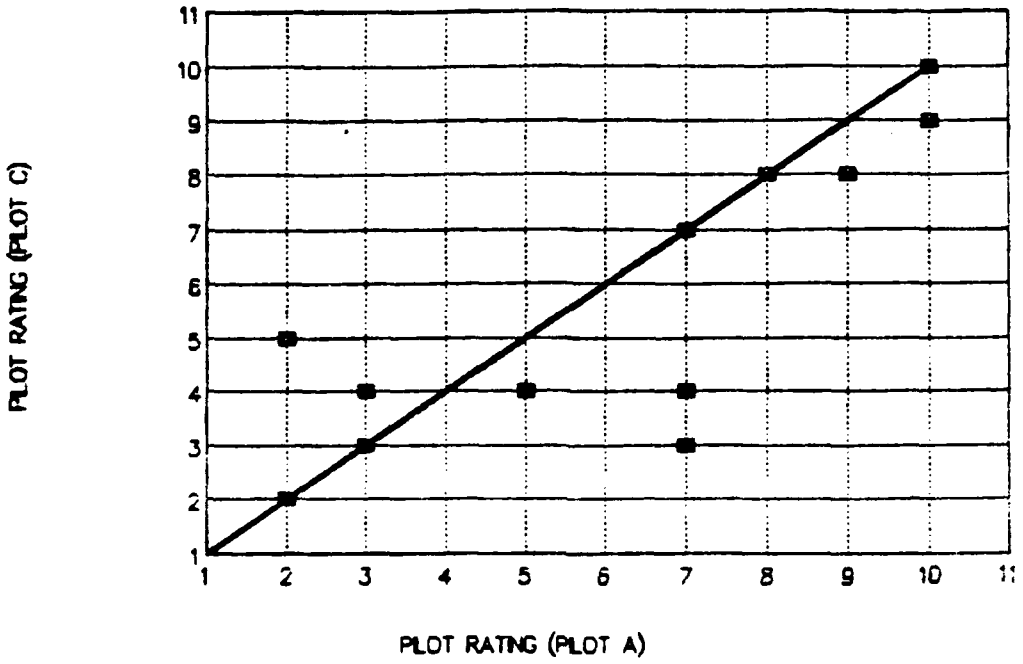

Figure 5. HAVE PIO Pilot Rating Comparisons

In Figure 5 the coefficient of correlation is 0.79, which is higher than that obtained in Figure 4. In the LAHOS study, correlations between pilots varied from 0.70 to 0.75, and in the HAVE PIO study, they varied from about 0.68 to 0.79. Similar correlations were found when comparing PIO ratings between pilots.

These results call into question whether or not PIO and pilot ratings should be averaged. There are arguments for and against this. One argument against is that the pilot

rating and PIO rating scales may not be linear, however, there is no way to prove or disprove this. Another argument against averaging is that not all configurations were flown more than once. In the LAHOS study, 22 of the 39 configurations analyzed were flown only once, while in the HAVE PIO study, every configuration was flown at least twice.

In this analysis both the pilot ratings and the PIO ratings were averaged for all of the configurations. The advantage in doing this was that none of the data points were lost; every rating was included in the analysis. Also, by averaging ratings, a particular handling qualities deficiency observed by one pilot but not observed by another pilot could be accounted for.

There are a few things to note before beginning the analysis. First of all, as stated before there were several LAHOS configurations that were flown only once. These configurations obviously could not be averaged. At the extremes of the rating scales, this is not a problem because a very poor aircraft will be consistently recognized as such by all pilots, and a very good aircraft will also be recognized as such. In the center of the scale, however, one pilot might rate a configuration as a 3 and another as a 5. If the configuration is flown only once, then the rating tends to be less objective. Secondly, the highest PIO rating given in the LAHOS study was a 4, while the highest

PIO rating given in the HAVE PIO study was a 5. During LAHOS pilot interviews conducted in (7:101), it was concluded that several LAHOS configurations had divergent PIO's and should have received 5's. The original LAHOS PIO ratings will be used but this inconsistency should also be taken into consideration.

LAHOS Analysis

A total of 40 LAHOS configurations were analyzed using PIREP. Configuration 1-A was thrown out because it was programmed incorrectly in the original LAHOS study. In addition, configurations 2-11, 4-11, and 5-11 would not converge and therefore were not included in this analysis A summary of the LAHOS configurations, pilot ratings, and PIO ratings are shown in Table 3:

Table 3: Average Pilot and PIO Ratings, LAHOS Data

Configu-ration	Number of Flights	Average Pilot Rating	Average PIO Rating
1-B	1	5	2
1-C	2	4	1
1-1	2	4	1.5
1-2	1	5	2
1-3	4	9.5	3.25
1-6	2	5	2
1-8	1	8	3
1-11	1	9	3.5
2-A	2	5	2.25
2-C	4	2.5	1.25
2-1	3	2	1
2-2	2	4	1.5
2-3	1	6	3
2-4	3	9	2
2-6	1	5	2.5
2-7	2	6.5	3
2-9	1	10	3
2-10	1	10	4
3-0	2	4	1.5
3-C	2	3.5	1.25
3-1	3	5.33	2.33
3-2	2	7	3
3-3	2	10	3.75
3-6	2	6.5	3
3-7	1	8	4
4-0	1	6	3
4-C	2	3	1.75
4-1	1	2	1
4-3	3	6.67	2.67
4-4	3	6.67	2.67
4-6	1	4	2
4-7	1	3	1
4-10	1	9	4
5-1	2	6	3
5-3	5	6.17	2.38
5-4	1	6	2.5
5-5	1	7	3
5-6	1	6	3
5-7	1	6	3

Flight Path Error Versus Control Rate

The first OCM outputs considered in this analysis were flight path error (performance) and control rate (workload). Schmidt (17:17) was able to show a link between pilot ratings and these two OCM based quantities. To verify this model, the same approach was used here. The plot of RMS flight path error versus RMS control rate is shown in Figure 6.

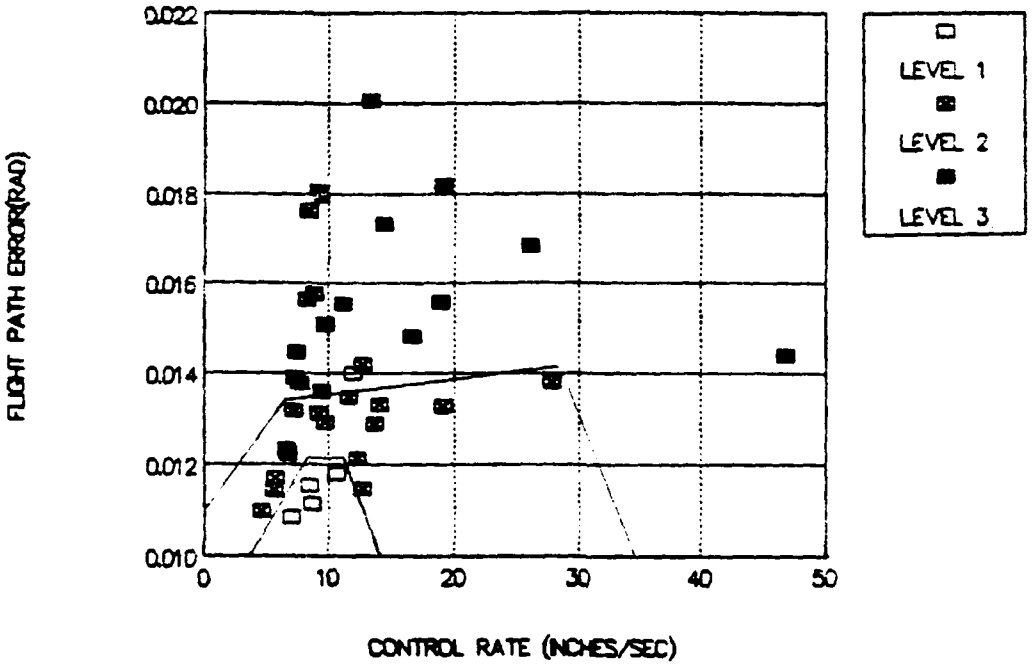

Figure 6. LAHOS Flight Path Error vs Control Rate (PHQRs)

The correlation obtained in Figure 6 is similar to that obtained by Schmidt. Level 1, 2, and 3 envelopes were subjectively drawn on the diagram. There does appear to be

a correlation. This graph will be compared to the HAVE PIO results later.

These same two OCM outputs were next applied to PIO ratings. In using this approach, a PIO tendency was defined as a PIO rating greater than 2, and a no PIO tendency was defined as less than or equal to 2. These were chosen because a PIO rating of 2 or less would probably not warrant a flight control design change. In the true definition of PIO, a 4 or greater would indicate an actual PIO. However, any undesirable motion (one requiring a flight control fix) will be detected using this prediction. It is not as important to predict actual PIO ratings as it is to predict whether or not a serious PIO exists. The correlation between flight path error, control rate, and PIO tendency is in Figure 7.

There seems to be a trend between flight path error, control rate, and PIO ratings similar to the trend noted with pilot ratings. It appears that as the control rate (pilot workload) and flight path error (pilot performance) increases, PIOs tend to occur. However, there is a lot of variability, and it would be difficult to predict PIO in borderline cases.

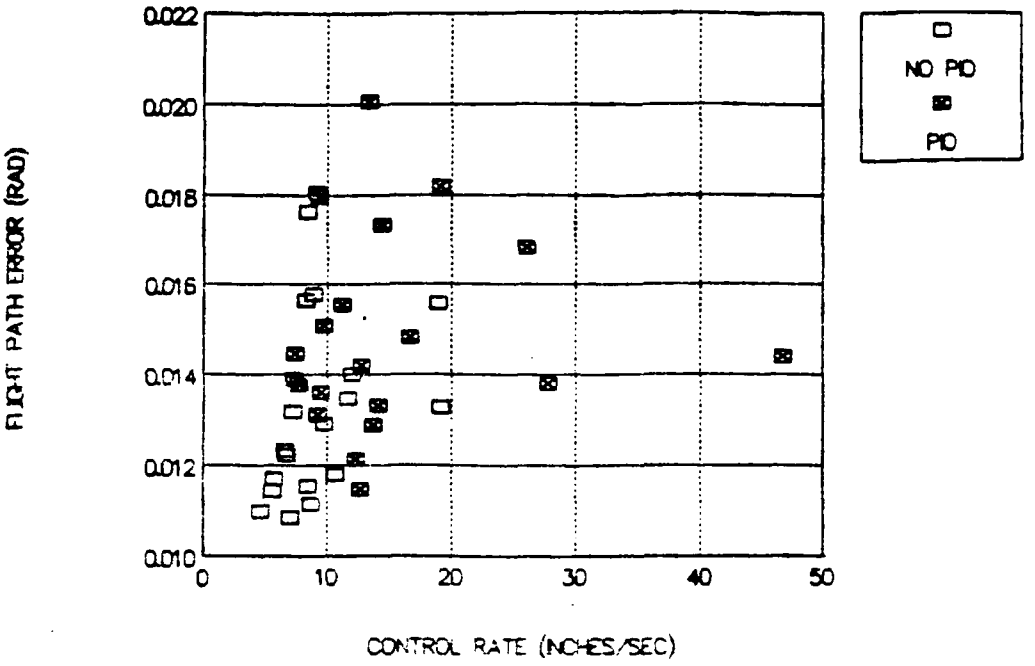

Figure 7. LAHOS Flight Path Error vs Control Rate (PIO Ratings)

Flight Path Error

The next OCM output evaluated was strictly a performance measure, flight path error. This parameter does not really reflect how hard the pilot is working; it merely shows the pilot's predicted performance in the tracking task. However, the size of the flight path error is directly related to the aircraft/control system dynamics. For example, LAHOS configurations 3-1, 3-2, and 3-3 represent the same basic airframe. LAHOS 3-1 had no additional control system dynamics, 3-2 had a first order pole at -10, and 3-3 had a first order pole at -4. Clearly,

the configurations degraded as the first order lag gets closer to the origin. The results obtained from the OCM for these three configurations were as follows:

Table 4: Flight Path Error Trends, LAHOS Data

Configu-ration	Flt Path Error (deg)	Pilot Rating	PIO Rating
3-1	.7007	4	2
3-2	.7884	7	3
3-3	.8646	10	4

Table 4 shows that larger OCM predicted flight path errors correlate with poorer pilot performance. The trend shown here was found consistently across all of the LAHOS and HAVE PIO data. To determine the relationship using pilot and PIO ratings, LAHOS pilot/PIO ratings and flight path error data is plotted in Figures 8 and 9.

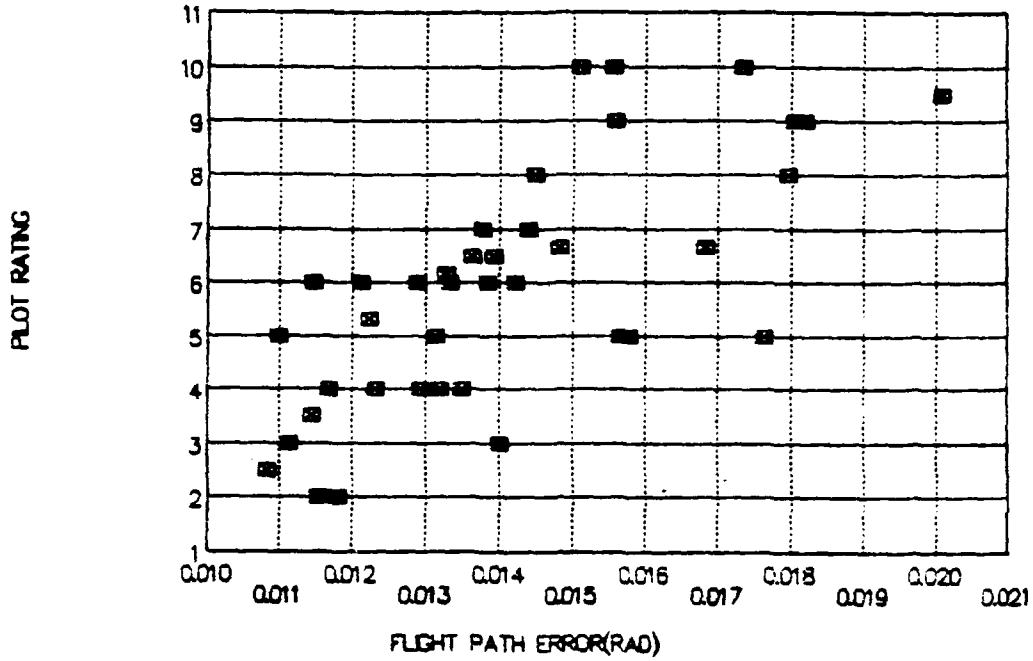

Figure 8. Pilot Ratings vs Flight Path Error (LAHOS)

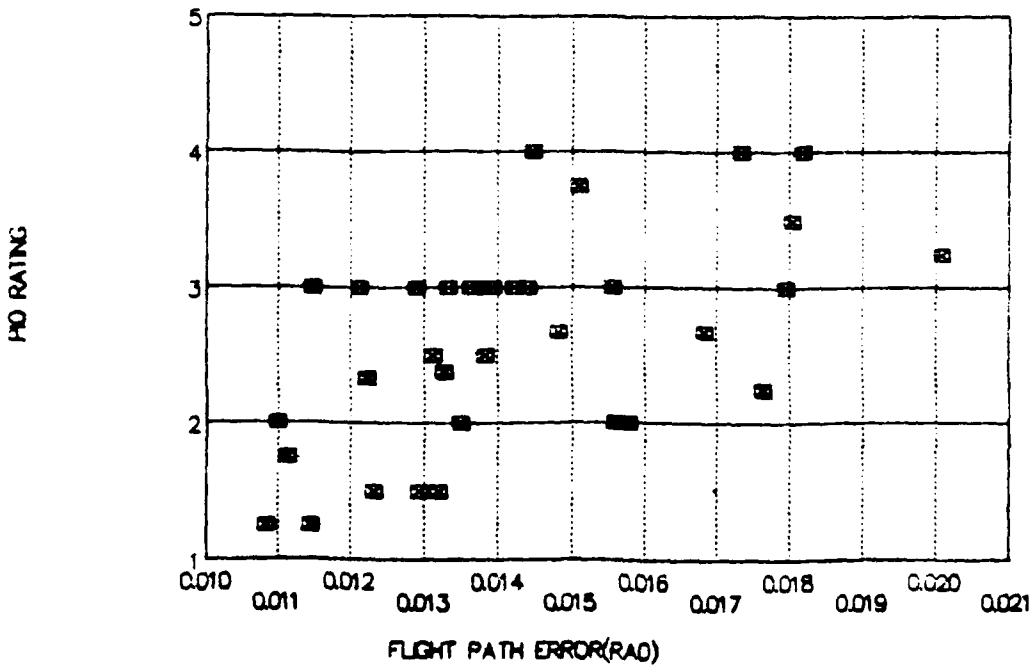

Figure 9. PIO Ratings vs Flight Path Error (LAHOS)

In Figures 8 and 9, there is a trend of increasing pilot/PIO rating with increasing flight path error. Note the conspicuous absence of any PIO ratings above 4 in Figure 9. This tends to skew any correlations found.

Several other OCM direct outputs were plotted in an attempt to identify correlations. These included pitch rate, stick displacement, flight path rate, and pitch angle. No significant correlation was found between pilot/PIO ratings and any of these parameters.

Crossover Frequency

As described in section II, the OCM as implemented by PIREP outputs a YpYc describing function of the entire man-machine system. This open loop describing function already includes the pilot's lead, lag, and gain compensation. PIREP's "optimal" describing function has the pilot-vehicle's crossover frequency occur such that there is a phase margin of 30-35 degrees. Plots of these crossover frequencies versus pilot and PIO ratings are shown in Figures 10 and 11.

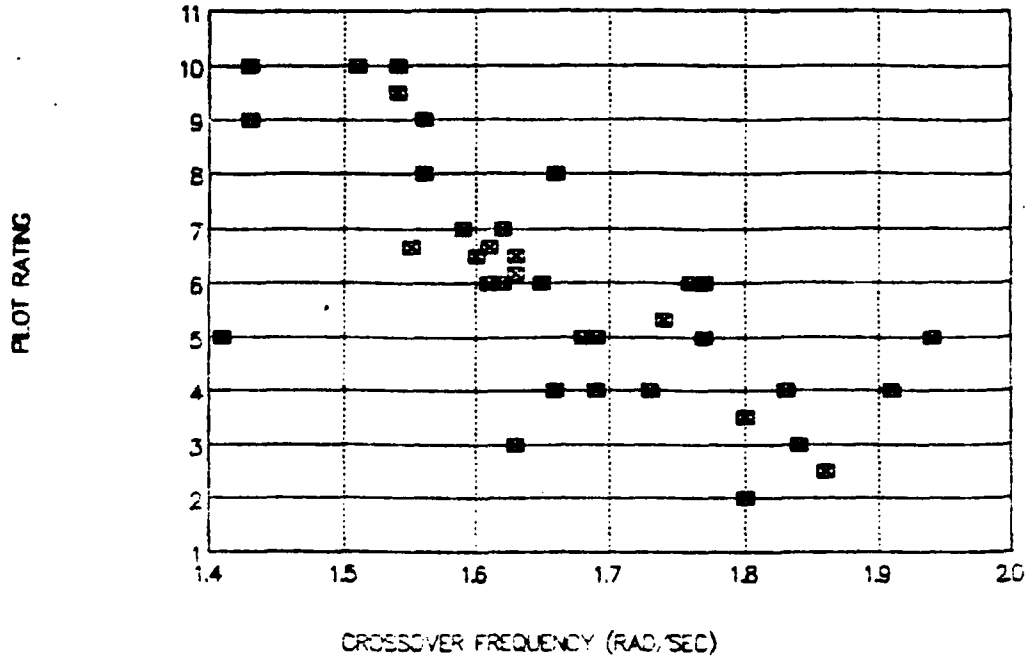

Figure 10. Pilot Ratings vs Crossover Frequency (LAHOS)

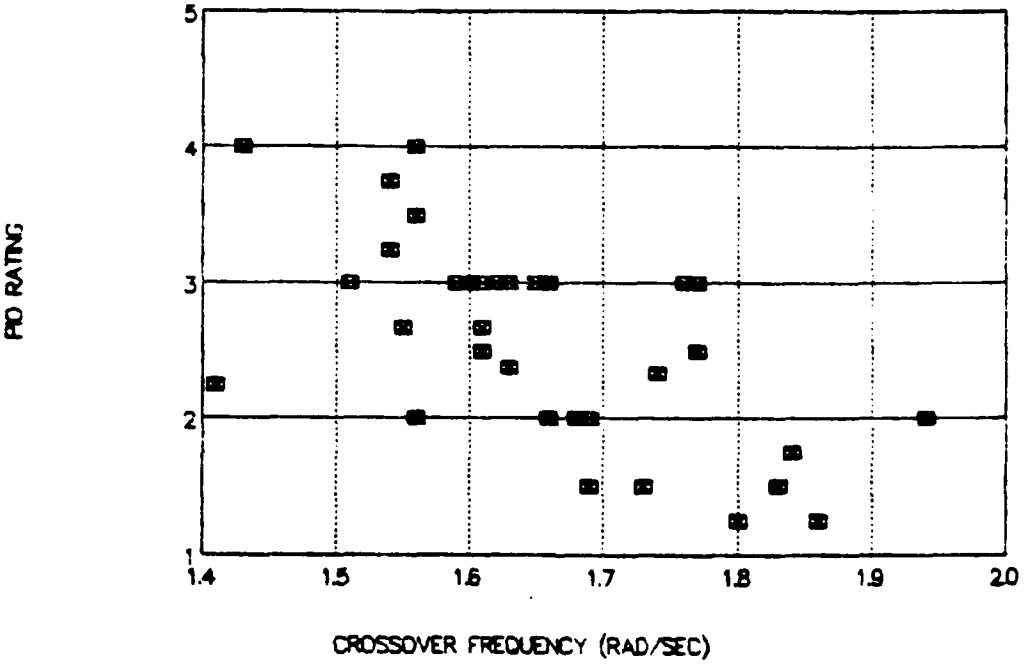

Figure 11. PIO Ratings vs Crossover Frequency (LAHOS)

Both Figures 10 and 11 show reasonable correlation between the predicted crossover frequency and pilot/PIO ratings. One observation from these figures is that the system's crossover frequencies are much lower than those predicted by frequency domain techniques. Typically, frequency domain techniques predict crossover frequencies of 2.5-3.5 rad/sec depending on the task. The trends shown in Figures 10 and 11 appear to be the best found so far. The pilot/PIO ratings improve as the bandwidth of the system increases, which agrees with classical control theory. Specifically, classical control theory implies that wider system bandwidths provide faster response of the closed loop system.

Frequency at 180 Degrees of Phase

An attempt was made to correlate OCM output with the frequency at which the PIO actually occurred. Assuming that the pilot's optimal gain is already in the describing function, an increase in gain will eventually drive the crossover frequency to where the phase margin goes to zero. At this frequency, the pilot-system should go unstable and a PIO is likely to occur. However, since the transfer function output by the OCM relates flight path error to control input rather than attitude to control input, the describing function and corresponding crossover frequencies will be different than typical analyses.

The frequencies obtained by increasing the gain to the zero phase margin point do not correlate with actual PIO frequencies. However, the pilot/PIO ratings do go up with decreasing frequencies, showing the same trend as the crossover frequencies do. Plots of the frequencies at 180 degrees of phase versus pilot/PIO ratings are shown in Figures 12 and 13.

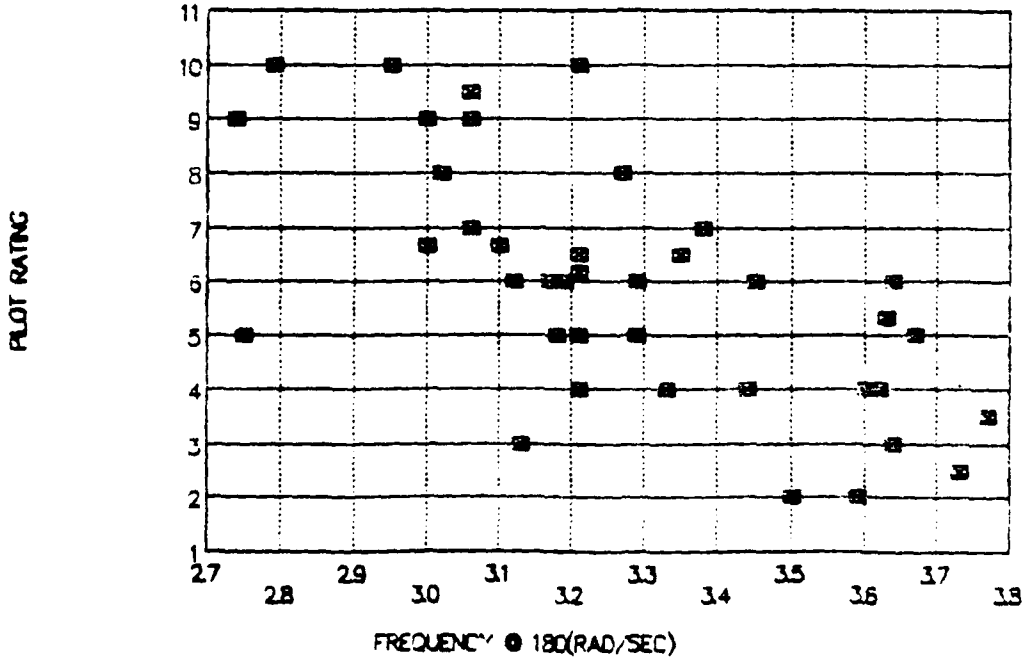

Figure 12. Pilot Ratings vs Frequency at 180°(LAHOS)

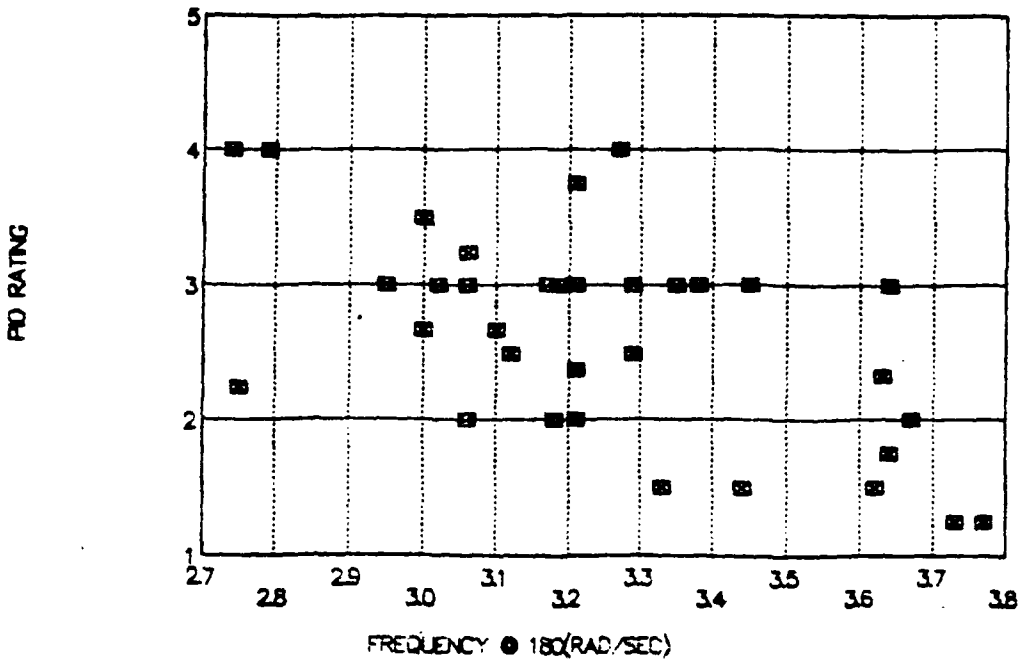

Figure 13. PIO Ratings vs Frequency at 180 °(LAHOS)

The correlations in Figures 12 and 13 are similar to that found for crossover frequencies; however, the correlations are not quite as good in these cases. It is interesting to note that the frequencies predicted by the OCM are closer to the typical aircraft/control system crossover frequencies.

HAVE PIO Analysis

The HAVE PIO OCM results were analyzed in the same way that the LAHOS data was. Seventeen of the eighteen HAVE PIO configurations were implemented in PIREP. HAVE PIO configuration 5-11 would not converge to a solution, so it was not included in the analysis. Table 5 contains a

summary of the HAVE PIO configurations, pilot ratings, and PIO ratings.

Table 5: Average Pilot and PIO Ratings, HAVE PIO Data

Configu-ration	Number of Flights	Average Pilot Rating	Average PIO Rating
2-1	3	2.3	1
2-5	3	9	4.3
2-7	3	5	3
2-8	3	8.7	4
2-B	4	4	2
3-1	3	4	2.3
3-3	3	4	1.7
3-6	2	4.5	2
3-8	3	7	3.7
3-12	2	8	4.5
3-13	2	10	4.5
3-D	2	2	1
4-1	3	2.7	1
4-2	3	4.3	1.3
5-1	2	3.5	1
5-9	2	7	4
5-10	2	10	5

Since each configuration in the HAVE PIO study was flown more than once, it was hoped that the correlations of the OCM outputs to pilot/PIO ratings obtained would be better than those obtained for the LAHOS data. The same plots were made for the HAVE PIO data. The plots for flight path error/control rate, flight path error, crossover frequency, and frequency at 180° of phase are shown in Figures 14-21.

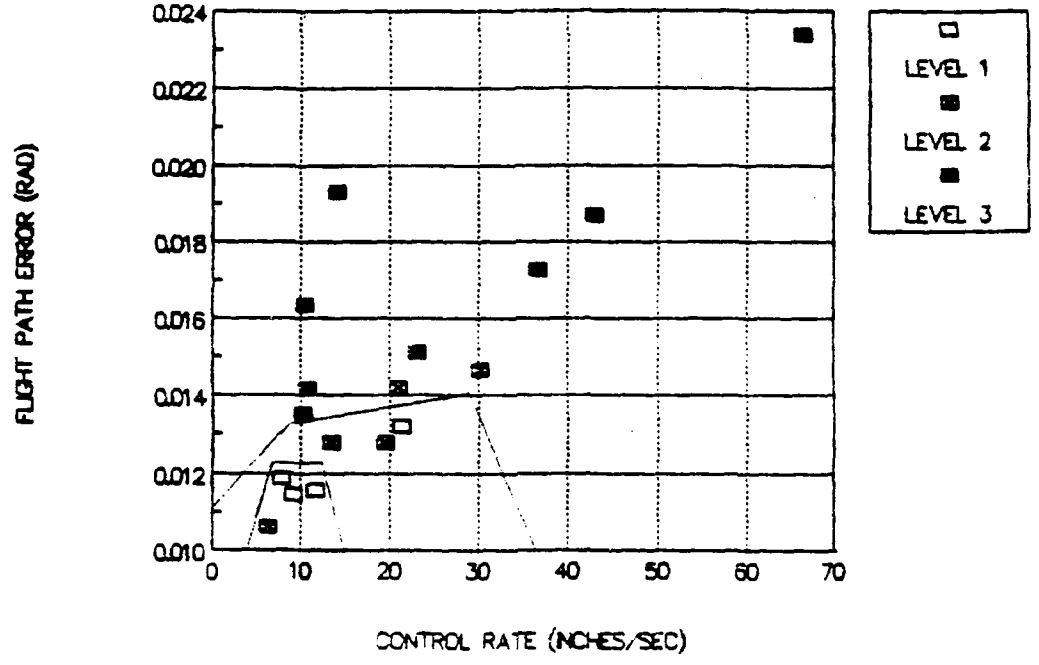

Figure 14. HAVE PIO Flight Path Error vs Control Rate (PHQRS)

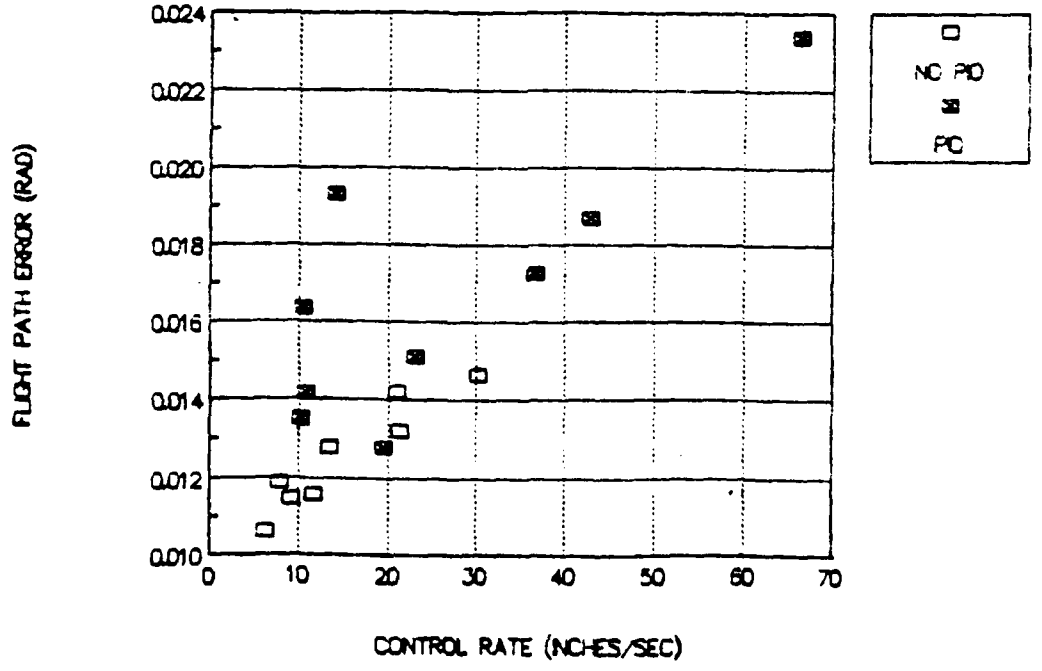

Figure 15. HAVE PIO Flt Path Error vs Control Rate (PIO Ratings)

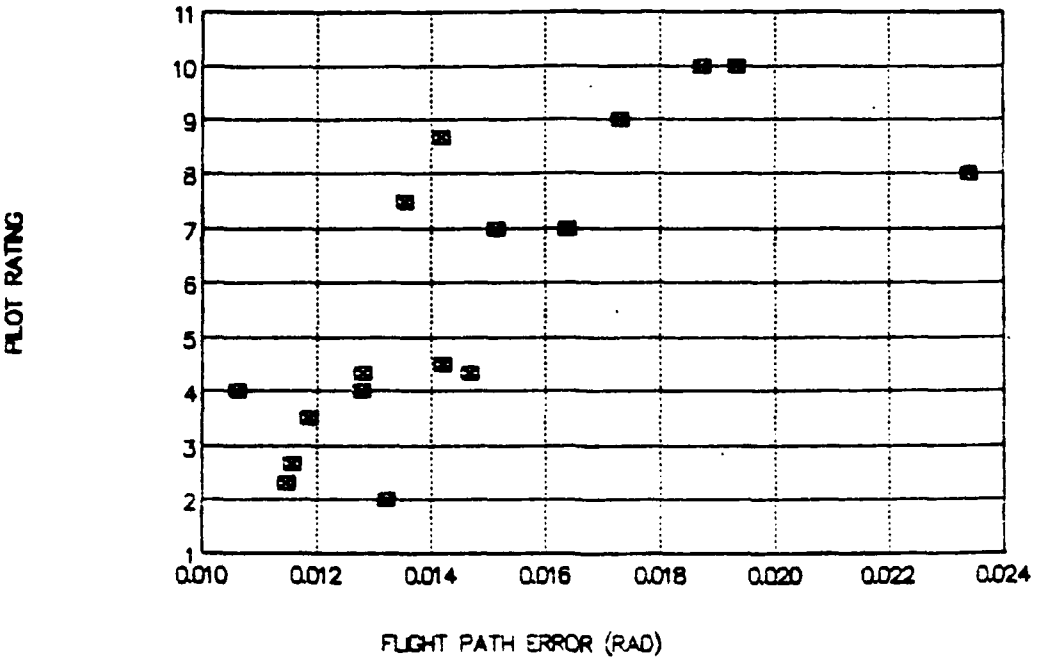

Figure 16. Pilot Ratings vs Flight Path Error (HAVE PIO)

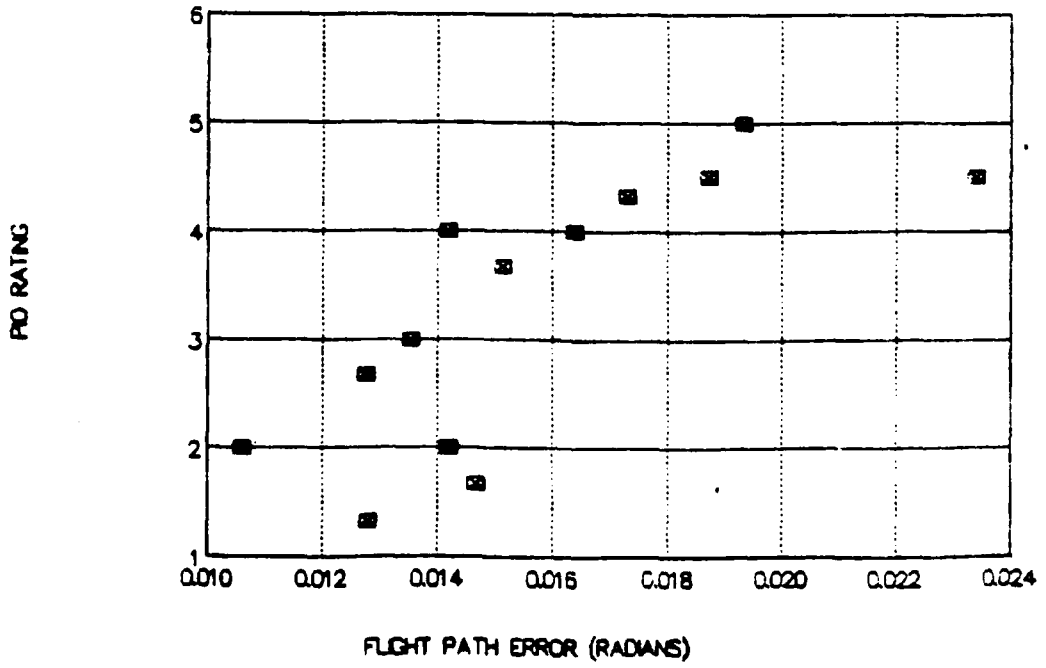

Figure 17. PIO Ratings vs Flight Path Error (HAVE PIO)

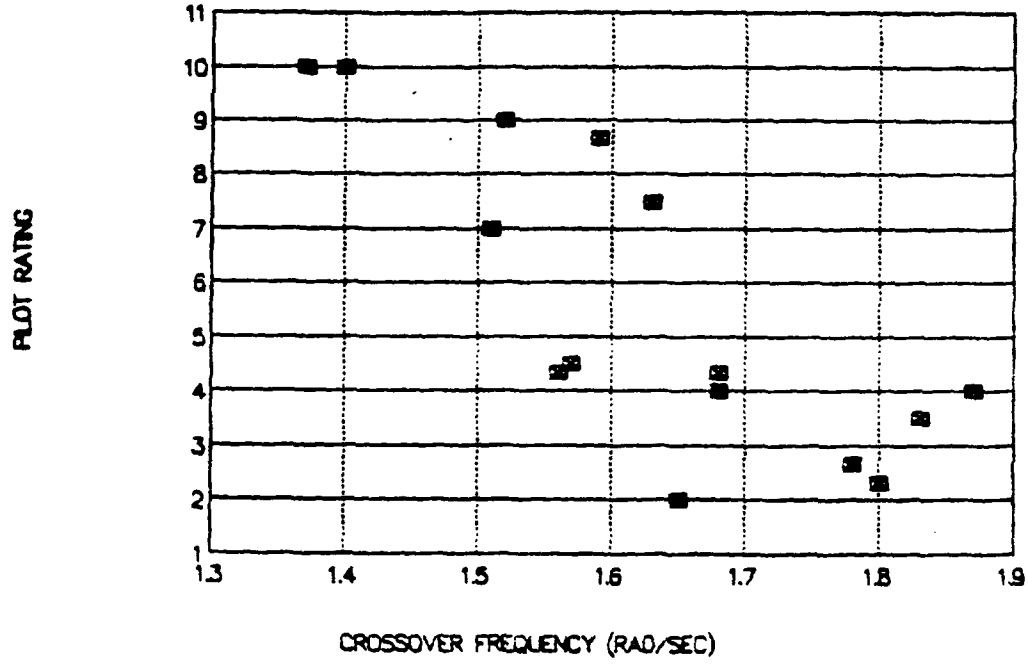

Figure 18. Pilot Ratings vs Crossover Frequency (HAVE PIO)

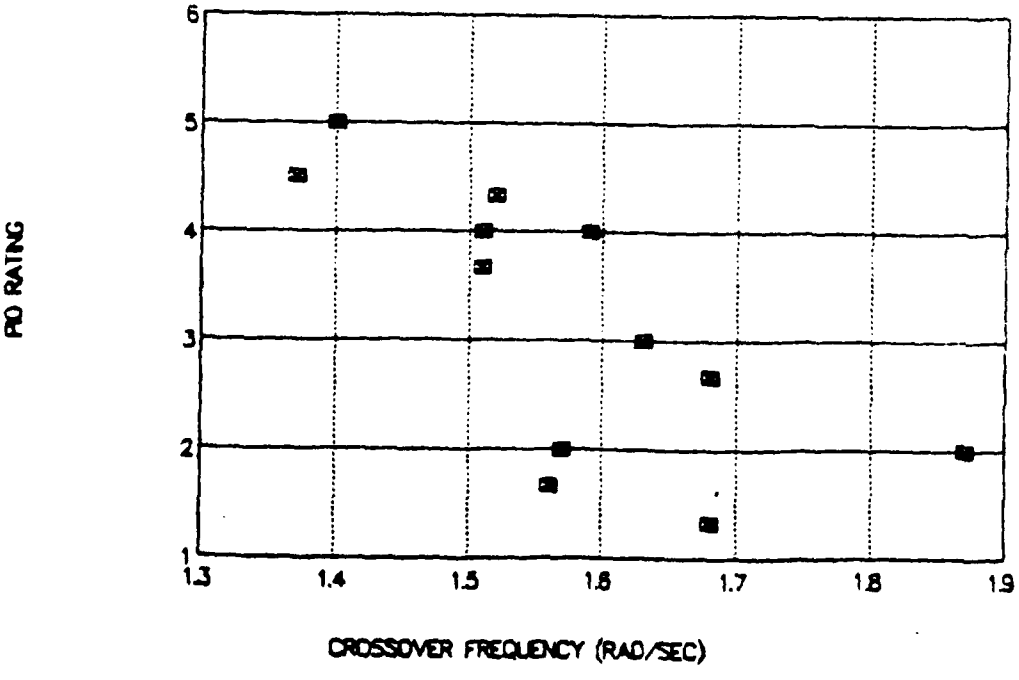

Figure 19. PIO Ratings vs Crossover Frequency (HAVE PIO)

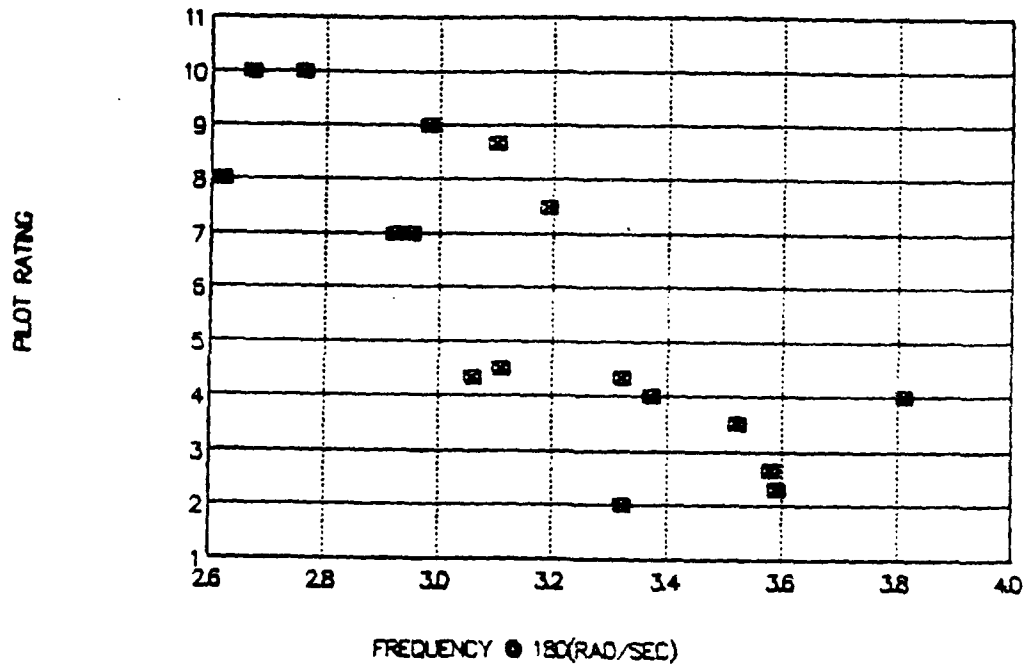

Figure 20. Pilot Ratings vs Frequency at 180° (HAVE PIO)

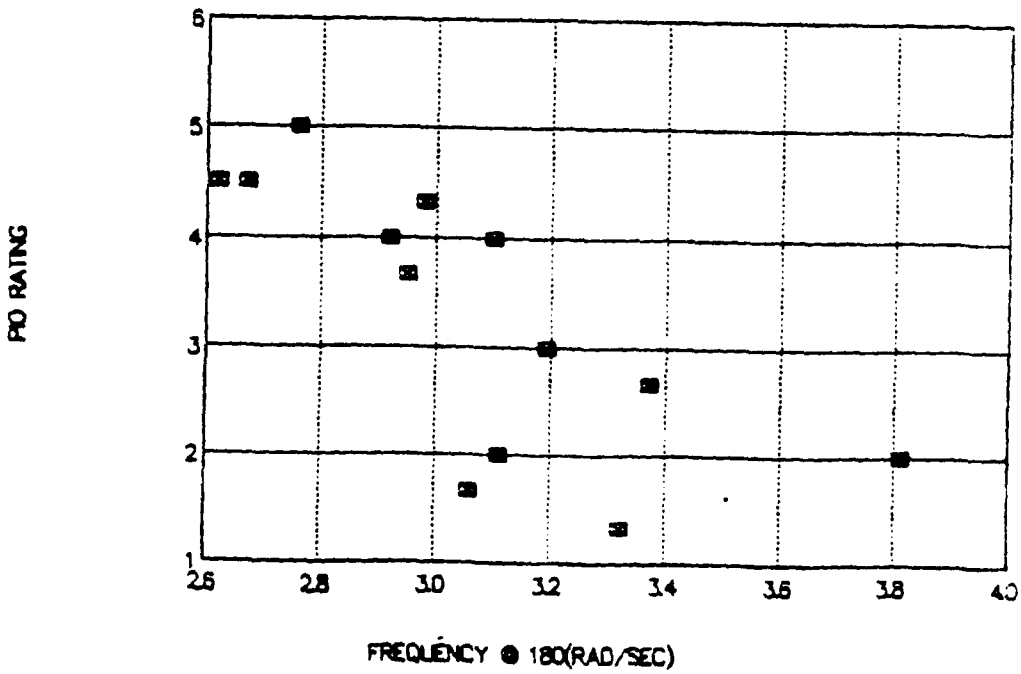

Figure 21. PIO Ratings vs Frequency at 180° (HAVE PIO)

Correlation of LAHOS and HAVE PIO Results

The trends found in Figures 14-21 are similar to the correlations shown in the LAHOS study. Visually, there appears to be a better correlation in the HAVE PIO data than there is in the LAHOS data. To determine the actual correlations a least squares regression analysis was performed on the LAHOS and HAVE PIO data. The results of a least squares fit between the pilot/PIO ratings and the OCM outputs for the LAHOS and HAVE PIO data are shown in Tables 6 and 7.

Table 6: Pilot Rating Correlations, LAHOS and HAVE PIO Data

OCM Outputs	Correlation Coefficient
Flight Path Error (LAHOS)	.72
Flight Path Error (HAVE PIO)	.76
Frequency at 180 (LAHOS)	.67
Frequency at 180 (HAVE PIO)	.81
Crossover Frequency (LAHOS)	.73
Crossover Frequency (HAVE PIO)	.78

Table 7: PIO Rating Correlations, LAHOS and HAVE PIO Data

OCM Outputs	Correlation Coefficient
Flight Path Error (LAHOS)	.57
Flight Path Error (HAVE PIO)	.81
Frequency at 180 (LAHOS)	.58
Frequency at 180 (HAVE PIO)	.82
Crossover Frequency (LAHOS)	.69
Crossover Frequency (HAVE PIO)	.82

As expected, the correlation in the LAHOS data was lower than that obtained in the HAVE PIO data. One possible explanation for this is that most of the LAHOS configurations were flown only once. Also the highest LAHOS PIO rating given was a 4, which tended to skew that regression.

The correlations obtained using the OCM show a definite relationship between the output variables and pilot and PIO ratings. Given the variability of the pilot ratings, the coefficients of correlations found here are probably about the best that can be obtained and are typical of results from other handling qualities research efforts. It appears that the best overall PIO correlation occurs when using the crossover frequency. One possible explanation for this is that the describing function is based on using all of the OCM output variables, whereas using a parameter such as flight path error looks at the RMS error of only one variable.

Prediction Schemes

To develop a method for predicting longitudinal PIO, the results from both the LAHOS and HAVE PIO analyses were first used. The LAHOS and HAVE PIO OCM outputs were both put into the same database and a least squares regression was done as before. The correlated results of the combined database are shown in Tables 8 and 9.

Table 8: Pilot Rating Correlations, Combined Database

OCM Output	Correlation Coefficient (R)
Flight Path Error	.73
Frequency at 180	.70
Crossover Frequency	.73

Table 9: PIO Rating Correlations, Combined Database

OCM Output	Correlation Coefficient (R)
Flight Path Error	.70
Frequency at 180	.70
Crossover Frequency	.75

The correlations obtained for the combined LAHOS and HAVE PIO results are about as good as those obtained during the LAHOS analysis, but poorer than those obtained using the HAVE PIO database. However these correlations show that both the LAHOS and the HAVE PIO OCM results agree. The correlations obtained here again are typical of those found in other handling qualities studies. It is interesting to note that there again appears to be a high correlation between crossover frequency and PIO ratings. It also appears that this OCM application predicts pilot ratings about as well as it predicts PIO ratings.

The best correlations obtained during this analytical study were using flight path error and crossover frequency.

Additionally, correlations with the HAVE PIO database were significantly higher than with the LAHOS data. One possible explanation was that most of the LAHOS configurations were flown only once. Also, the highest LAHOS PIO rating given was a 4, which is suspect and tended to skew that regression. Therefore, the prediction schemes chosen for flight test were based on flight path error and crossover frequency data from only the HAVE PIO database. Table 10 shows the flight test prediction equations.

Table 10: Flight Test Prediction Equations

	Flight Path Error	Crossover Frequency
Pilot Ratings	616.0 * (γ_e) - 3.3	-13.1 * (ω_c) + 26.9
PIO Ratings	353.4 * (γ_e) - 2.5	-7.4 * (ω_c) + 14.6

Linear regression flight test prediction lines and actual data for the HAVE PIO flight path error and crossover frequency predictions are in Figures 22 through 25.

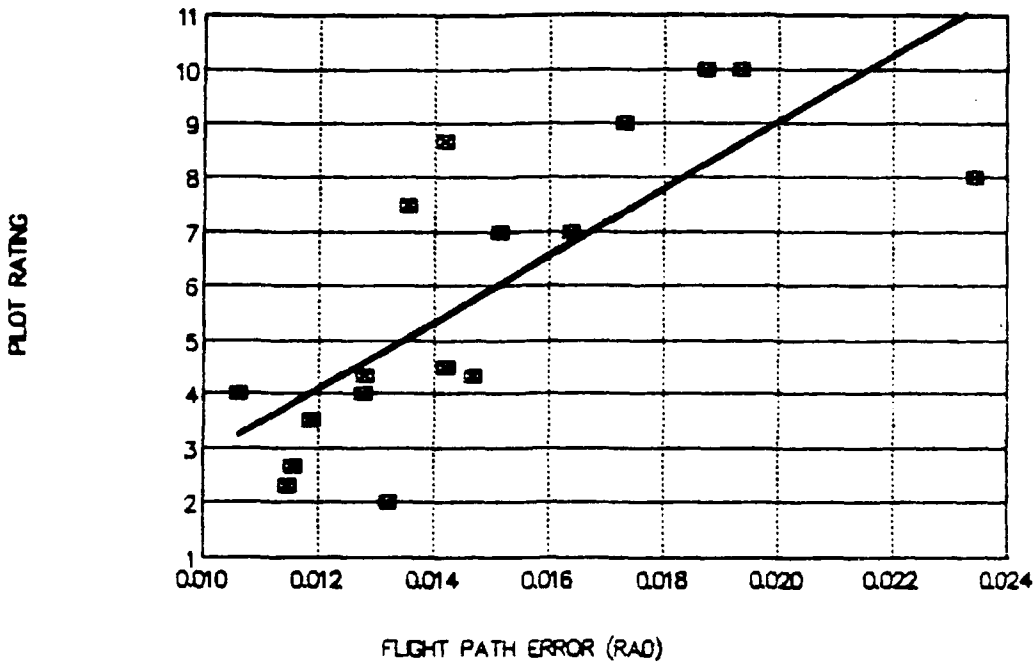

Figure 22. PHQR vs Flight Path Error

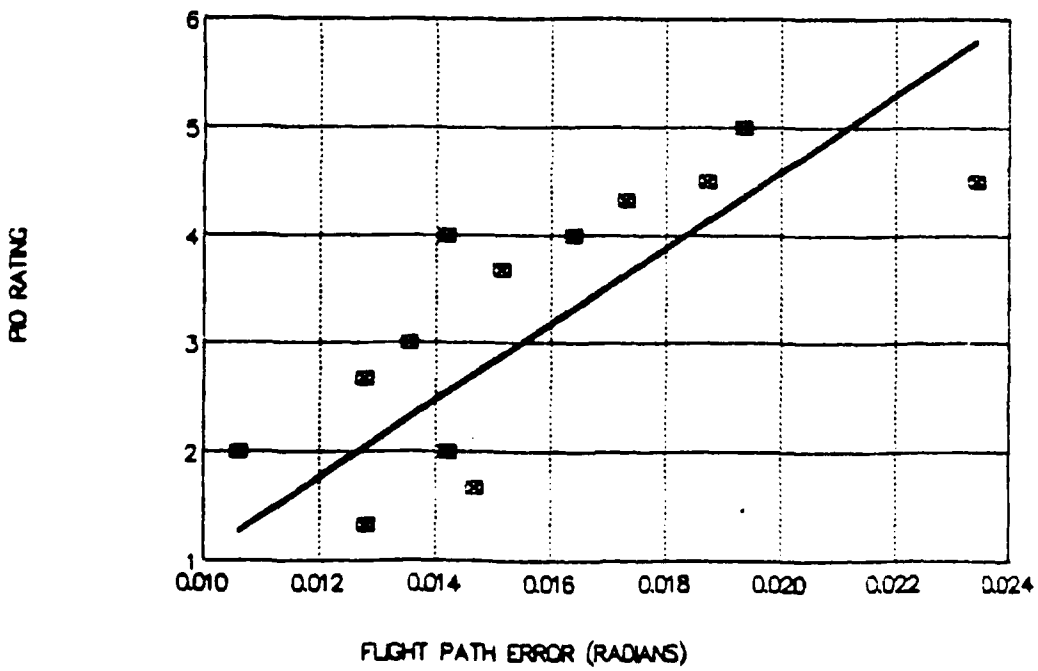

Figure 23. PIO Rating vs Flight Path Error

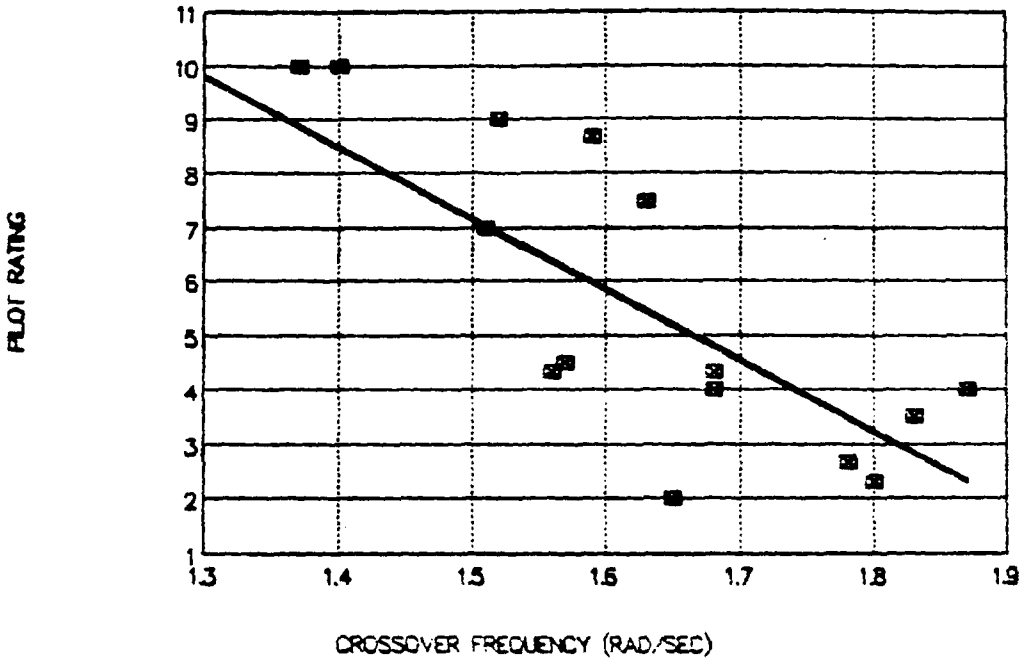

Figure 24. PHQR vs Crossover Frequency

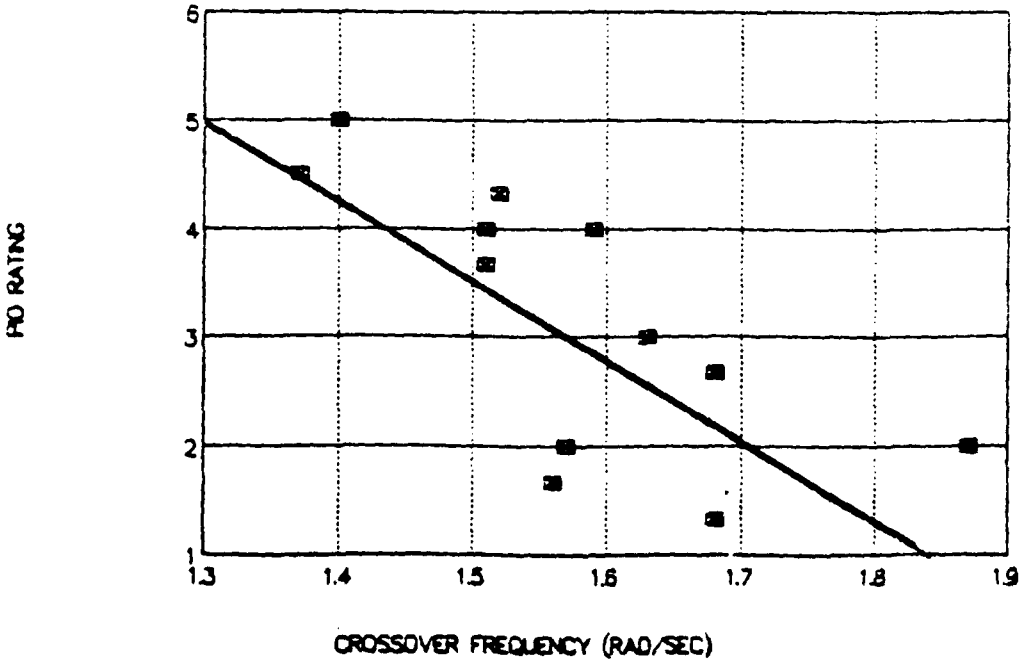

Figure 25. PIO Rating vs Crossover Frequency

IV. FLIGHT TEST METHOD

The flight test portion of this project was conducted as part of a USAF Test Pilot School systems project, called HAVE CONTROL. The test team consisted of three project pilots and two engineers, including the author. Additionally, two Calspan safety/instructor pilots acted as safety pilots during the flight test.

A total of twelve different aircraft/control system combinations were flown using the USAF/Calspan variable stability NT-33A. The test team flew twenty-five sorties totaling 27.8 flight hours between 12 September and 16 October 1989 at the Air Force Flight Test Center (AFFTC), Edwards Air Force Base, California. The flight test consisted of handling qualities evaluations of the twelve configurations in the approach and landing task.

Test Item Description

The NT-33A variable stability test aircraft, S/N 51-4120, was a modified, two seat jet trainer operated by the CALSPAN Corporation, Buffalo, New York and owned by the Flight Dynamics Laboratory, Wright Patterson AFB, Ohio. (18,19) The aircraft was capable of variable dynamic response and control system characteristics. (20) The Variable Stability System (VSS) modified the static and dynamic responses of the basic NT- 33A by commanding control

surface positions through full authority electro-hydraulic servos. A programmable analog computer, associated aircraft response sensors, control surface servos, and an electro-hydraulic force-feel system provided the total simulation capability. The instructor/safety pilot varied the computer gains through controls located in the rear cockpit, allowing changes in airplane dynamics and control system characteristics during the flight. Test aircraft center of gravity varied from 26.1 to 24.8 percent mean aerodynamic chord due to normal fuel consumption. Appendix D contains additional information concerning the aircraft systems, capabilities, and safety provisions.

The front cockpit AVQ-7 Heads Up Display (HUD) displayed several flight parameters, including airspeed, altitude, angle of attack, pitch attitude, heading, and the flight path marker (total velocity vector). The HUD was used during the test to closely simulate a representative fighter aircraft.

Instrumentation and Data Reduction

The NT-33 test instrumentation system contained the following items:

1. An on-board Ampex AR 700 magnetic tape recording system with 2.25 hours recording capability was used to record aircraft flight conditions, flight control positions, pilot voice, and aircraft states from the aircraft data

acquisition system (DAS).

2. An AN/ANH-2 voice recorder was used to record interphone and UHF radio communications.

3. A HUD video recorder was used to record all approaches and landings.

The NT-33A project pilot operated the HUD and an on-board voice recorder system. The NT-33A instructor/safety pilot operated the magnetic tape system and the HUD camera. A complete list of the instrumentation parameters are located in Appendix D. The AFFTC photographic branch provided ground videotape coverage of each landing task.

Following each NT-33 mission, the project pilots reviewed their HUD video and tape recorder audio and summarized their comments for each configuration flown on their inflight pilot comment card. Each comment card included the individual project pilot PHQR, PIO, and confidence rating factors for each configuration flown (Appendix C). Project pilot comments were used to qualitatively describe the aircraft PIO tendencies and handling qualities during the approach and landing task. In addition, pilot comments were used to ensure project pilots used similar criteria when assigning PHQRs. The PHQRs and PIO ratings for each NT-33A configuration were tabulated and included in chapter V.

Pilot comments, PHQRs, and PIO ratings were used to determine if the aircraft had a PIO tendency during the

approach and flare. The PIO was defined as an undesirable periodic motion which interferes with the accomplishment of the task and requires the pilot to reduce his gain or remove himself from the loop. The actual PIO tendencies were then compared to those predicted prior to flight.

Test Methods and Conditions

The landing longitudinal PIO tendencies and flying qualities were evaluated at three pairs of short period natural frequencies and damping ratios. All short period dynamics met MIL-STD-1797 Level 1 requirements for the landing approach (Category C). The configuration dynamics are depicted in Figure 26 and listed in Table 11, along with the flight control system filters, and predicted handling qualities levels. The phugoid and lateral-directional characteristics were held constant and are listed in Appendix A. The NT-33A instructor/safety pilot set the short period dynamics by adjusting the appropriate variable stability gain control in the rear cockpit. The rear seat pilot also selected the predetermined flight control system characteristics.

After takeoff, the project pilot took control of the aircraft, and climbed to approximately 5,000 feet pressure altitude. The instructor/safety pilot reconfigured the aircraft dynamics and established the landing configuration. The project pilot accomplished the auto-step and auto-ramp

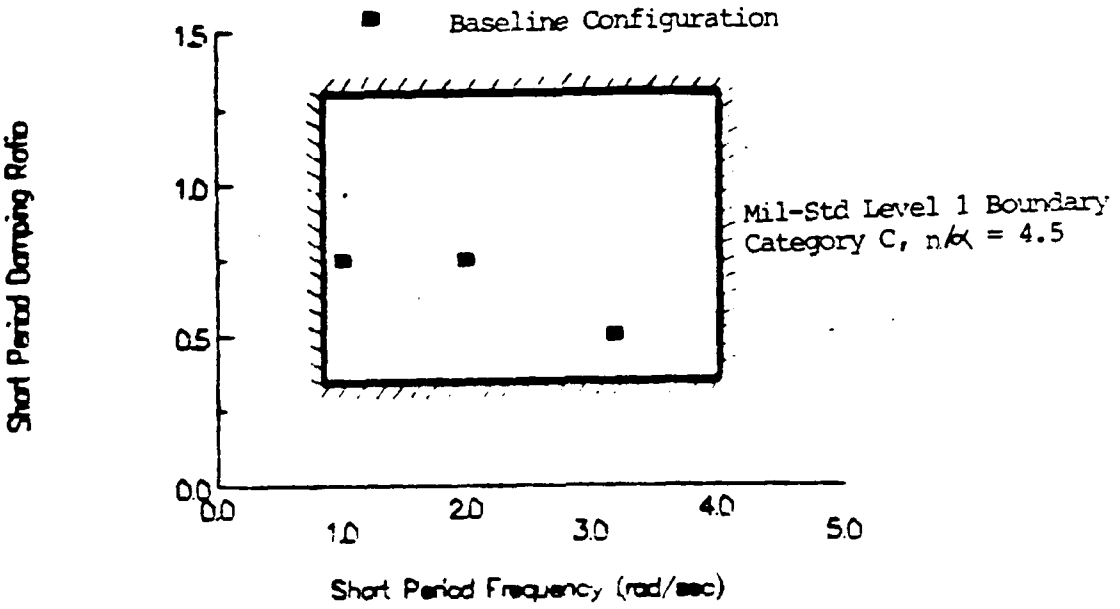

Figure 26. HAVE CONTROL Baseline Dynamics

inputs and then performed the hand-step and hand-ramp inputs used for system identification. The system identification tasks accomplished during the flight test were part of another research project and will not be discussed further.

After accomplishing the open loop tasks, the project pilot established a 1000 feet per minute descent in the landing configuration. Then at 50 feet above a 4000 feet mean sea level target altitude, the pilot simulated a landing task using an aggressive level off. As a safety precaution, if the configuration exhibited a divergent PIO

Table 11

HAVE CONTROL Flight Test Configurations

Primary Config	ζ_{sp}	$\omega_{n_{sp}}$	K	τ_1	τ_2	ζ_1	ω_{n_1}	Predicted HQ Level
1-1	0.75	1.0	1.0	--	--	--	--	1
1-3			4.0	--	4	--	--	2
1-10			16.0	--	--	0.7	4	3(8)*
2-1	0.75	2.0	1.0	--	--	--	--	1
2-D			0.5	20	10	--	--	2
2-2			10.0	--	10	--	--	2
2-5			1.0	--	1	--	--	3(8)
2-7			144.0	--	--	0.7	12	2
3-1	0.50	3.2	1.0	--	--	--	--	1
3-3			4.0	--	4	--	--	2
3-5			1.0	--	1	--	--	2
3-6			256.0	--	--	0.7	16	2
3-8			81.0	--	--	0.7	9	2

* Numbers in parentheses indicate the OCM predicted handling qualities rating.

First Order Filters: $\dfrac{K(s+\tau_1)}{(s+\tau_2)}$

Second Order Filters: $\dfrac{K}{s^2+2\zeta_1\omega_{n_1}s+\omega_{n_1}^2}$

or other Level 3 characteristics, that configuration was not tested any further. This never occurred during the flight test.

After the simulated landing was accomplished, the project pilot returned to the pattern and flew the approach and landing without an offset. After touching down, the instructor/safety pilot disengaged the VSS and performed the take off. The pilot then made preliminary comments on the configuration while the instructor/safety pilot flew the aircraft on an extended downwind. If, during the straight in approach, a divergent PIO occurred or adequate performance could not be achieved, then the offset landing task was not attempted. None of the flight test configurations were ever abandoned during straight in approaches. Two visual approaches with a lateral offset were then flown, with one offset to each side of the runway. After the first offset approach, the project pilot added to his preliminary comments. After the second offset approach, the project pilot summarized his overall comments and assigned a PIO rating and PHQR for that configuration. If the evaluation pilot felt confident enough to make an overall evaluation based on only two approaches he was allowed to eliminate the third approach. The evaluation pilot was allowed to assign separate ratings for the approach and flare if he deemed it necessary.

Two landing configurations were flown on each mission for a total of six approaches. During the last two sorties, which were slightly longer in duration, three configurations were evaluated.

The task for this project was a visual approach with a lateral offset and a correction to centerline prior to touchdown. The size of the lateral offset was approximately 150 feet. The 150 foot offset to the left was made by aligning with the left edge of the runway, and the 150 foot offset to the right was made by aligning with the right edge of the runway. The aircraft was flown on glidepath using the instrument landing system until the beginning of the overrun. The correction to centerline was initiated at 100 feet above ground level. The safety pilot assisted in maintaining a constant offset correction between the three project pilots.

The touchdown zone was 1000 feet long starting at 500 feet past the threshold. The touchdown aimpoint was 1000 feet from the threshold and within 5 feet of centerline. Each landing was treated as a "must land" situation, unless the instructor/safety pilot and/or project pilot determined that safety of flight would be compromised in an attempt to land. Table 12 summarizes the evaluation task performance criteria used to assign a PHQR to this visual landing task.

Table 12: Task Performance Standards

Desired	Adequate
No PIOs Touchdown within 5 feet of centerline (main wheels on centerline) Touchdown at aimpoint ±250 feet Approach airspeed ±5 kts	Touchdown within 25 feet centerline (tip tank on centerline) Touchdown at aimpoint ±500 feet Approach airspeed -5/+10 kts

The following test limitations were observed during the evaluation:

1. The NT-33A instructor/safety pilot assumed immediate and positive manual control of the aircraft at the first indication of any NT-33A system malfunction or if a dangerous situation developed.

2. Crosswind component was required to be less than 15 knots.

3. All testing was performed in accordance with the aircraft Flight Manuals (18,19) and AFFTCR 55-2 (21).

V. FLIGHT TEST RESULTS AND ANALYSIS

Twelve of the thirteen planned configurations were flown by at least two project pilots. Pilot comments are summarized in Appendix E. Time history plots showing Calspan baseline configuration identifications are shown in Appendix F. Plots of stick force and pitch rate for each HAVE CONTROL flight test configuration are also in Appendix F. Comparisons of the flight path error and crossover frequency prediction schemes with flight test results will be presented. Additionally, a comparison in PHQRs between project pilots will be analyzed.

Flight Path Error

Flight path error is an OCM output that reflects the pilot's predicted performance; that is, how close he is tracking a certain flight path angle. The OCM analysis showed that the size of the flight path error was directly related to the aircraft and control system dynamics. LAHOS and HAVE PIO data were correlated with flight path error and a prediction scheme was developed. As stated previously, the HAVE PIO correlations were much better than the LAHOS correlations. Therefore, the prediction scheme used for flight path error was based on the HAVE PIO database. Table 13 shows the actual and predicted handling qualities ratings using the flight path error prediction scheme.

Table 13: Flight Path Error Pilot Rating Results

Configuration	Predicted Pilot Ratings	Actual Pilot Ratings
1-1	5	2,4
1-3	9	7,7
2-1	4	3,2
2-D	4	4.5,3
2-2	5	4,2
2-5	9	8,10
2-7	5	4.5,5
3-1	4	2,3
3-3	5	3,3
3-5	6	6,5
3-6	5	5,6
3-8	5	3,7,4,4

From Table 13, 62 percent of the predictions were within one pilot rating of the actual flight test results. This predictor appears to only tell part of the story. The handling qualities rating scale is based on pilot workload and performance. However, this predictor doesn't take pilot workload into account, only performance. Figure 27 shows average flight test pilot rating versus flight path error and a comparison to the prediction line. In general, a smaller flight path error yielded a better pilot rating, which conforms to theory.

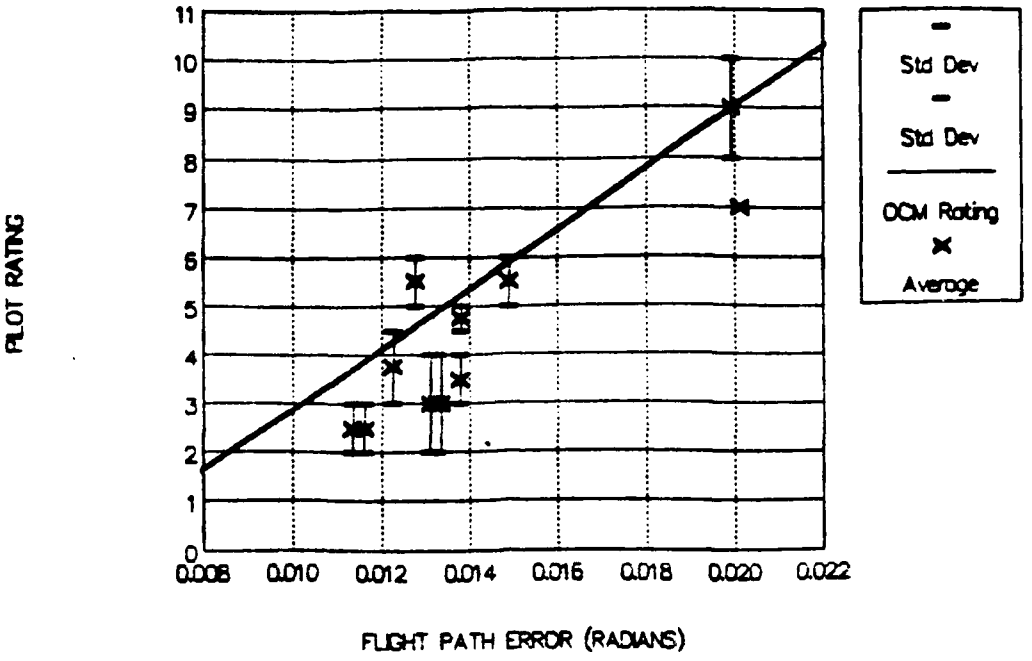

Figure 27. HAVE CONTROL PHQR vs Flight Path Error

Table 14 presents the actual and predicted PIO ratings using the flight path error prediction scheme.

Table 14: Flight Path Error PIO Rating Results

Configuration	Predicted PIO Ratings	Actual PIO Ratings
1-1	2	2,2
1-3	4	4,4
2-1	2	1,1
2-D	2	1,2
2-2	2	1,1
2-5	5	6,5
2-7	2	3,1
3-1	1	1,1
3-3	2	1,2
3-5	3	3,4
3-6	2	3,3
3-8	2	2,2,4,1

Table 14 shows that 96 percent of the predictions were within one PIO rating of flight test results. This prediction scheme was fairly accurate and reliable. Figure 28 plots the average PIO rating versus flight path error and the prediction line. A possible explanation for flight path error predicting PIO ratings more accurately than handling quality ratings is that in an actual PIO, deviation from normal flight path would be larger than flight path error in a stable approach. A linear correlation seems present in this plot.

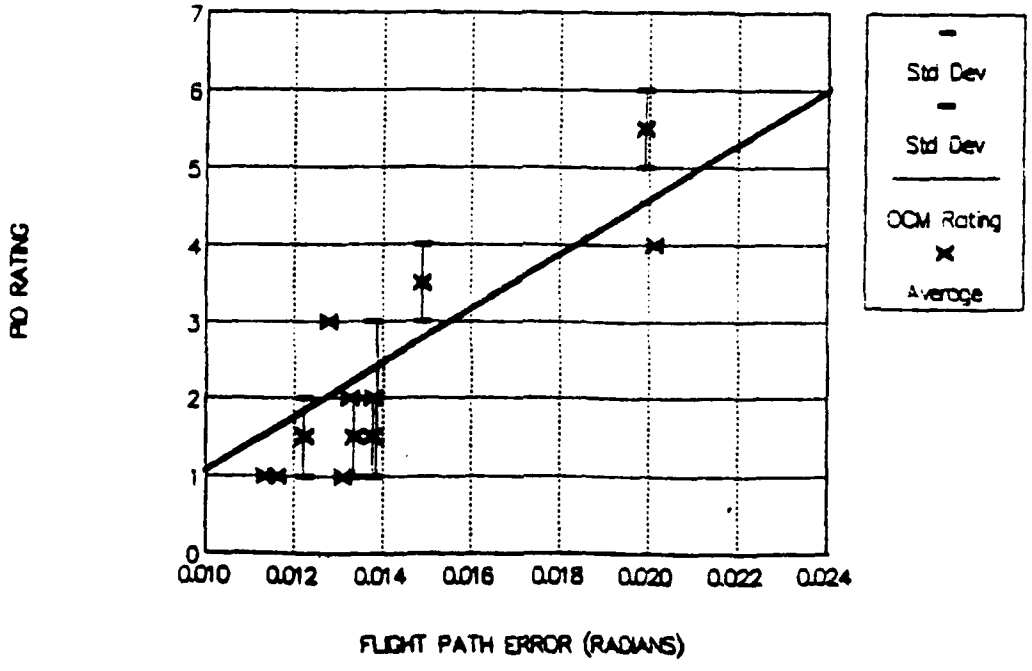

Figure 28. HAVE CONTROL PIO ratings vs Flight Path Error

Crossover Frequency.

As described previously, an OCM frequency domain output is a pilot in the loop transfer function, which includes the pilot's lead, lag and gain compensation. The transfer function's crossover frequency provides a phase margin of 30-35 degrees. This is in essence a measure of the pilot's workload. It defines the maximum amount the pilot can compensate before making the system unstable. The higher the crossover frequency, the better the pilot can control the system. Figure 29 shows the average flight test PHQRs plotted against the system's crossover frequency.

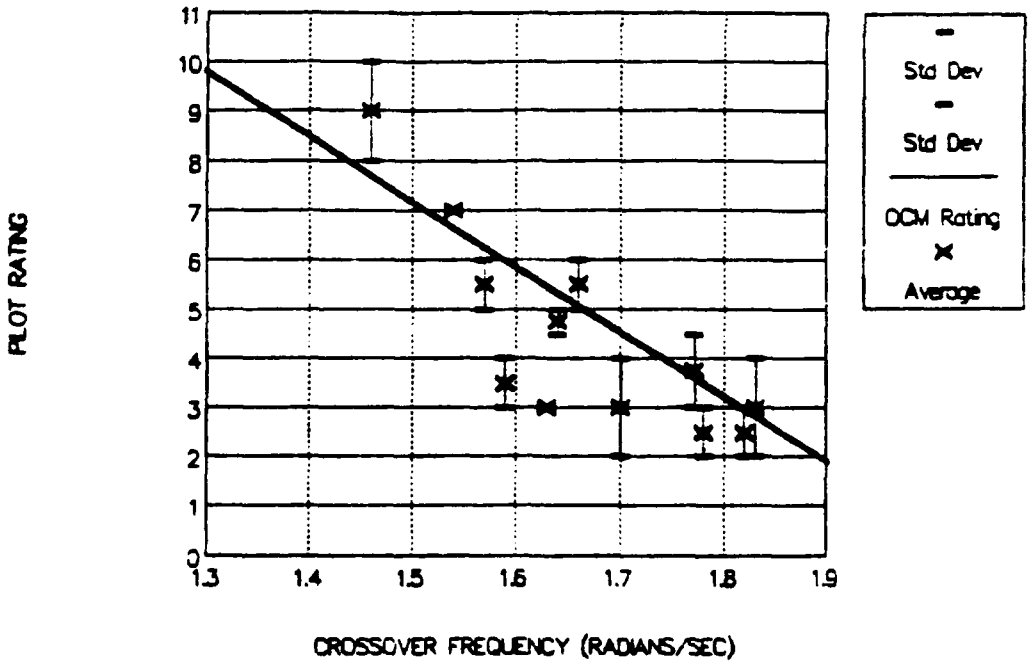

Figure 29. HAVE CONTROL PHQR vs Crossover Frequency

As expected, higher crossover frequencies yielded better pilot ratings, which conforms to theory. Table 15 presents the flight test and predicted pilot ratings using crossover frequency.

Table 15: Crossover Frequency Pilot Rating Results

Configuration	Predicted Pilot Rating	Actual Pilot Rating
1-1	3	2,4
1-3	7	7,7
2-1	3	3,2
2-D	4	4.5,3
2-2	4	4,2
2-5	8	8,10
2-7	5	4.5,5
3-1	3	2,3
3-3	5	3,3
3-5	6	6,5
3-6	5	5,6
3-8	6	3,7,4,4

Table 15 shows that 80 percent of the predictions were within 1 pilot rating of the flight test results. This predictor was much more accurate than flight path error. Results seem to conform to theory, in that pilot workload was a major factor in pilot ratings. For example, configuration 2-5 received a pilot rating of 8. However, task desired performance was achieved. The performance was only half of the story because the desired performance was achieved at the bottom of a PIO.

Table 16 presents the actual and predicted PIO ratings using the crossover frequency prediction scheme.

Table 16: Crossover Frequency PIO Rating Results

Configuration	Predicted PIO Ratings	Actual PIO Ratings
1-1	1	2,2
1-3	3	4,4
2-1	1	1,1
2-D	2	1,2
2-2	2	1,1
2-5	4	6,5
2-7	2	1,3
3-1	1	1,1
3-3	2	1,2
3-5	3	3,4
3-6	2	3,3
3-8	3	2,2,4,1

Table 16 shows that 92 percent of the predicted PIO ratings were within one PIO rating of the flight test results. Figure 30 plots average PIO ratings versus crossover frequency. Again, the higher crossover frequency yielded a better (lower) PIO rating, conforming to theory.

A trend developed in both the flight path error predictions and crossover frequency predictions. The PIO predictions were fairly accurate at the lower PIO ratings. However, neither scheme predicted a PIO rating higher than a four, yet configuration 2-5 consistently received test ratings higher than a four. To determine the cause of this, the original LAHOS and HAVE PIO data were reviewed. An

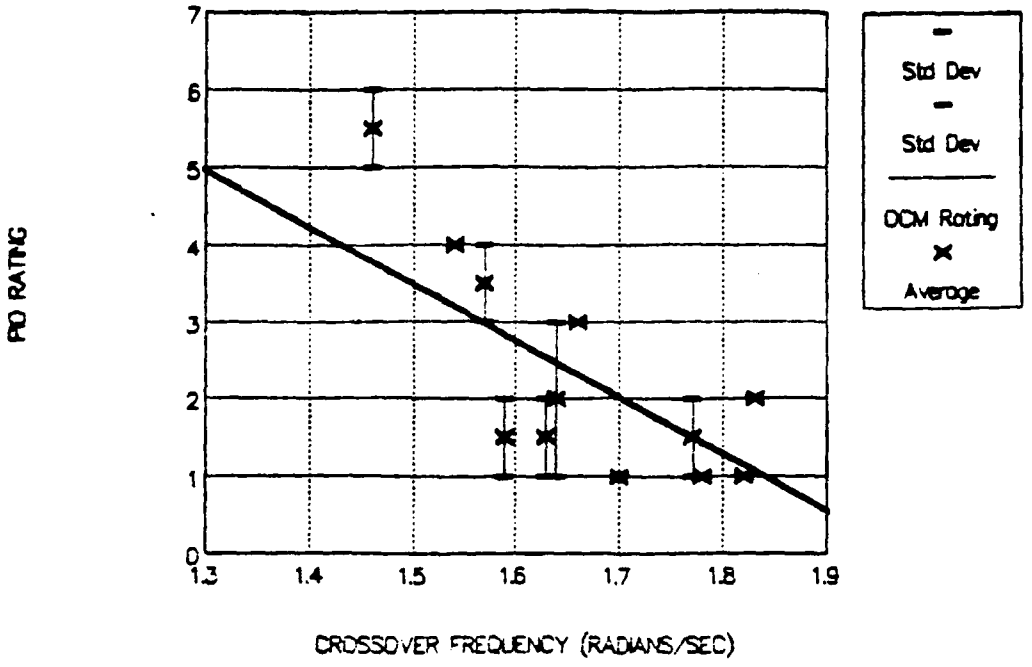

Figure 30. HAVE CONTROL PIO Ratings vs Crossover Frequency

inconsistency in using the PIO rating scale was uncovered. Specifically, a problem existed when interpreting the difference between an undesirable motion and a PIO. After consulting with Calspan, who originally wrote the PIO rating scale, the test team determined that an undesirable motion would be an uncommanded aperiodic aircraft response, and a PIO would be a periodic oscillation. By this definition, any periodic oscillation would fall into a PIO rating of four or higher. When reviewing the LAHOS and HAVE PIO data, it appeared that this same criteria had not been applied. For example, LAHOS configuration 2-9 received a pilot rating of 10 and a PIO rating of three. Pilot comments included

"Easy to over-rotate and get into damped PIO. Had to put in an input and wait. Got down to 20 feet, got into PIO due to delayed response." According to these comments the PIO rating should have been a 5 or 6. Inconsistencies such as this were found throughout both databases. The flight path error and crossover frequency prediction techniques skewed the predictions of the higher PIO ratings toward lower ones since they were based on these two databases. Therefore, the PIO prediction results could be improved at the higher end of the PIO scale. Based on this analysis, new PIO prediction schemes using flight path error and crossover frequency were developed using a least squares regression of the flight test data. The new PIO prediction equations developed were:

$$\text{Flight Path Error:} \quad 431.0 * (\gamma_e) - 3.8 \qquad [56]$$

$$\text{Crossover Frequency:} \quad -9.4 * (\omega_c) + 18.0 \qquad [57]$$

To determine the correlation between flight test data and the new prediction equations, a statistical analysis was performed on the regression. The coefficients of correlation for the flight path error and crossover frequency predictors were 0.88 and 0.78, respectively. The new prediction lines and flight test data are in Figures 31 and 32. These prediction schemes should be verified through additional flight test.

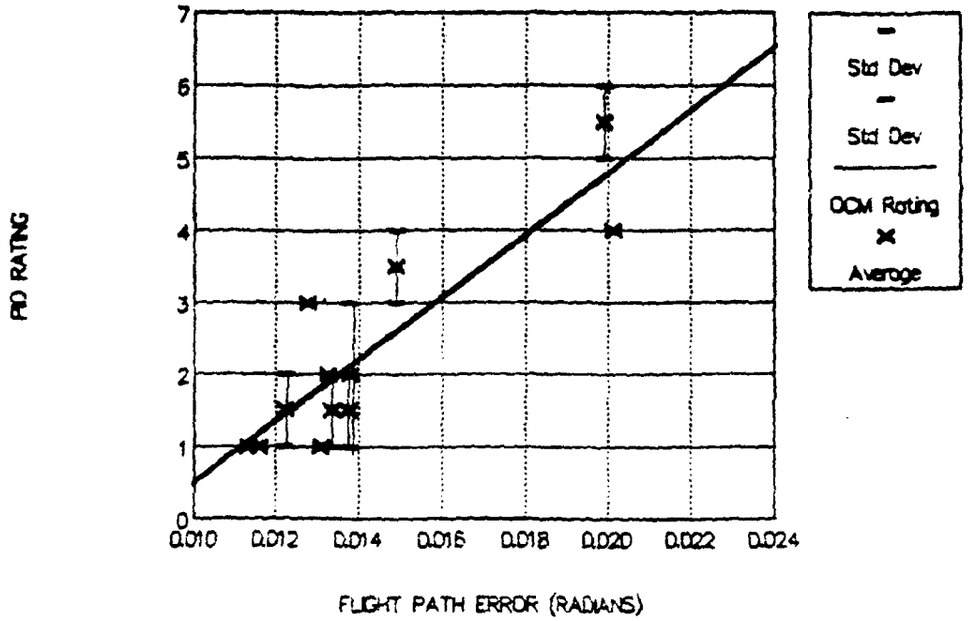

Figure 31. Revised PIO Rating vs Flight Path Error

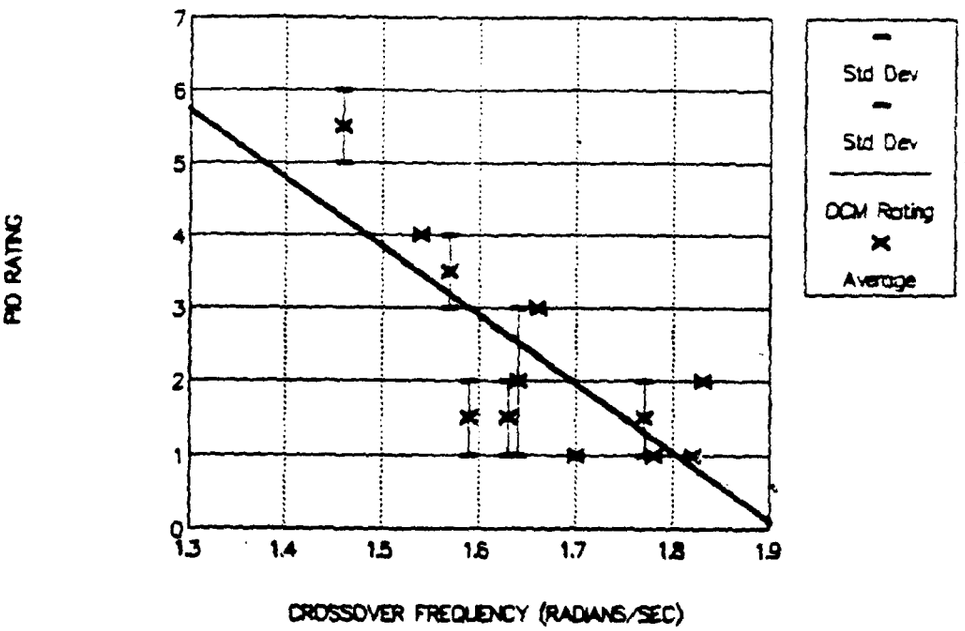

Figure 32. Revised PIO Rating vs Crossover Frequency

The crossover frequency prediction scheme was the most accurate predictor of pilot ratings, while the flight path error prediction scheme was more accurate for PIO ratings. Both predictors agreed with classical control theory, showing a definite correlation between flight path error, crossover frequency, and pilot/PIO ratings.

Comparison Between Pilots.

Three pilots flew and rated the flight test configurations. The pilots' operational experience and background are summarized in Table 17.

Table 17: Project Pilot Experience

Pilot	Aircraft	Hours
A	C-141	2500
B	F/RF-4	1000
	T-39	50
C	B-52	2200
	T-37	150

Because of the subjective nature of pilot and PIO ratings, the flight test ratings varied from pilot to pilot. To determine the variability and its influence on prediction scheme errors, correlations between pilots A, B, and C are presented in Figures 33 through 35. These figures show that the best correlations occurred between pilots A and C. A possible explanation for this is that pilots A and C had a

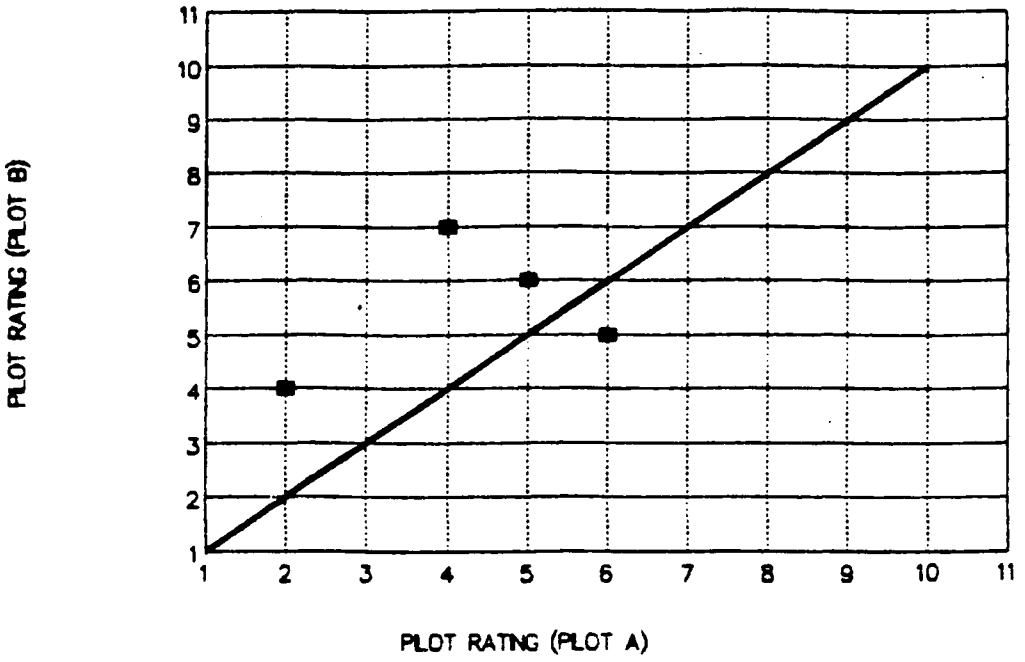

Figure 33. Pilot A and B PHQR Comparison

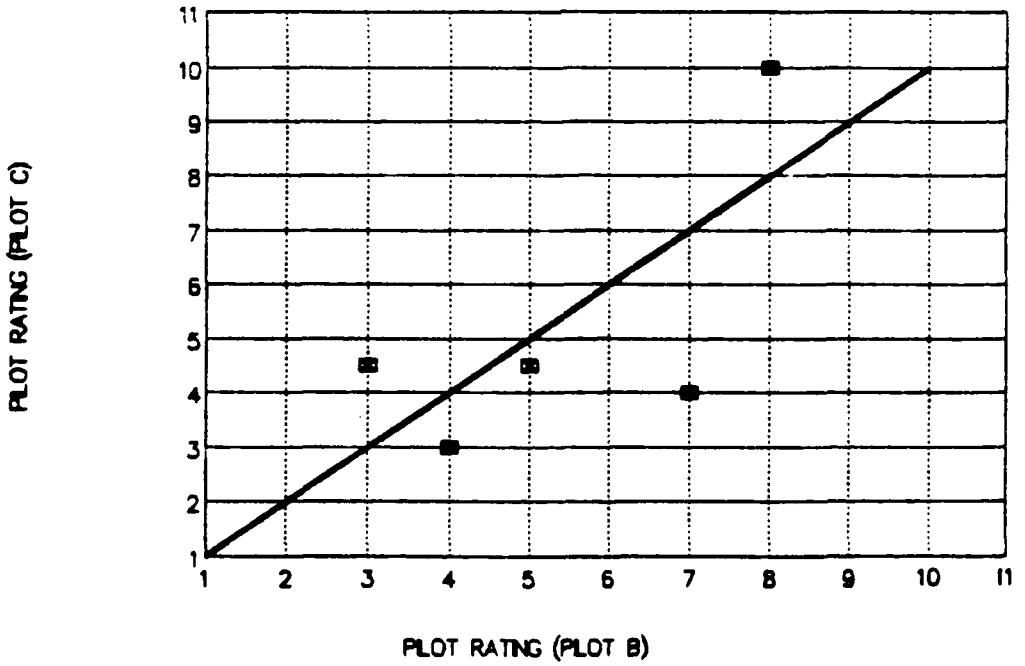

Figure 34. Pilot B and C PHQR Comparison

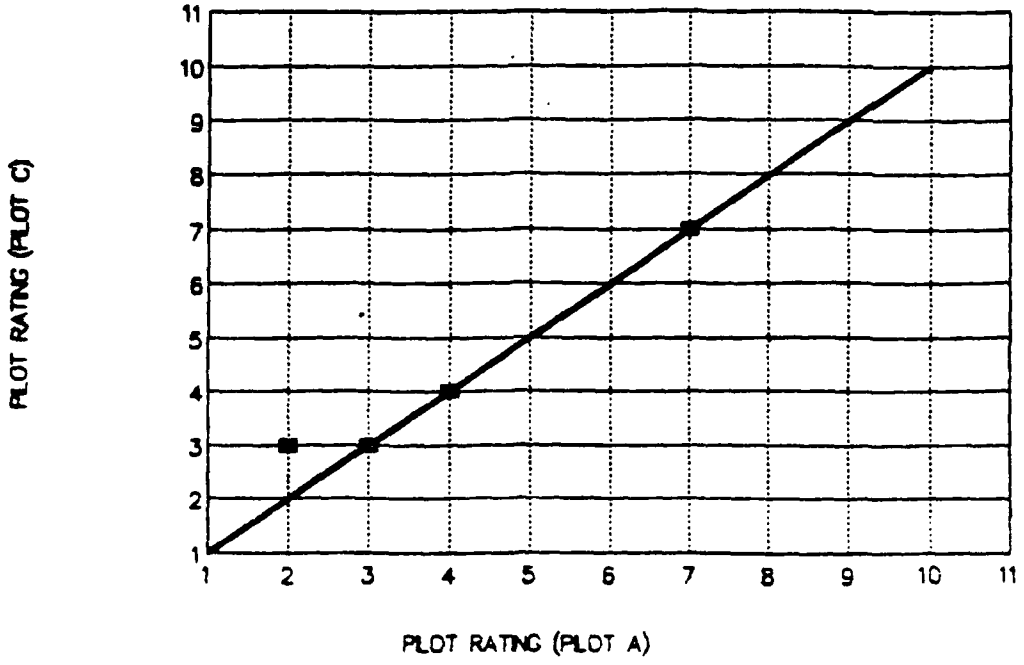

Figure 35. Pilot A and C PHQR Comparison

multi-engine background while pilot B had a fighter background. These two different flying backgrounds could influence pilot ratings. For example, when flying a large multi-engine aircraft, the pilot has a tendency to fly the approach and landing in an open loop manner using low gains. A pilot of a small fighter aircraft tends to be more closed loop in the approach and landing phase and uses higher gains. Flight test results showed that pilot B tended to rate configurations worse than pilot A or C. For example, pilot B gave configuration 3-8 a PHQR of 7, while pilot A rated the same configuration with identical dynamics a 3. The discrepancy in PHQRs was probably due to a handling

qualities "cliff". Comparison of HUD videotape showed that pilot B flew the aircraft more closed loop than pilot A, exposing a handling qualities deficiency that pilot A never saw.

Figures 33 through 35 also show a great deal of scatter between pilots when subjectively rating a configuration. This makes it impossible to predict pilot and PIO ratings perfectly. The prediction will never exactly fit the data. Despite the difficulty in accurately predicting pilot ratings, the flight control engineer needs a tool to predict the performance of a new design before it actually flies. The flight path error and crossover frequency prediction methods show a strong correlation to flight test data. The flight path error and crossover frequency rating prediction methods should be used as a tool in flight control system design.

VI. CONCLUSIONS AND RECOMMENDATIONS

The Optimal Control Model (OCM), using either the flight path error or the crossover frequency parameters, satisfactorily predicted both pilot handling qualities ratings (PHQR) and Pilot Induced Oscillation (PIO) ratings.

The flight path error prediction scheme predicted PHQRs within one rating 62 percent of the time and PIO ratings 96 percent of the time. This technique agreed with theory, predicting poorer ratings for larger values of flight path error.

The crossover frequency prediction scheme predicted PHQRs within one rating 80 percent of the time and PIO ratings 92 percent of the time. This technique showed that a higher crossover frequency yielded a better rating.

Both PIO prediction schemes were not as accurate at higher PIO ratings, due to PIO rating discrepancies in the original databases. As a result, new PIO prediction schemes for flight path error and crossover frequency were developed using a least squares regression of the flight test data. These new PIO prediction schemes should be flight tested to verify their accuracy.

Because of the subjective nature of PHQRs and PIO ratings, the flight test results varied from pilot to pilot. In general, fighter pilots gave configurations poorer PHQRs and PIO ratings than the multiengine pilots. Additionally,

the correlation between multiengine pilots was better than with fighter pilots.

The crossover frequency prediction scheme was the most accurate predictor of pilot ratings. This showed that pilots place more emphasis on workload than performance when using the handling qualities rating scale. The flight path error prediction scheme was slightly more accurate for PIO ratings. Both predictors agreed with classical control theory, showing correlation between flight path error, crossover frequency, and pilot/PIO ratings. The Optimal Control Model flight path error and crossover frequency ratings prediction methods are valid and should be used as a tool in flight control design.

APPENDIX A

NT-33A STABILITY DERIVATIVES
AND
FLIGHT CONTROL CONFIGURATIONS

Overall Aircraft Configuration

During the LAHOS, HAVE PIO, and HAVE CONTROL flight tests, the NT-33A was always flown in the power approach configuration (gear down, flaps 30 degrees, speed brake extended). The approach airspeed varied with aircraft fuel weight as shown below:

Fuel Remaining (Gals)	Approach Speed (KIAS)
150	125
250	130
350	135
450	140
550	140

A touchdown speed of 120 KIAS (U_0=205 feet/sec and W_0=25 feet/sec) was used for defining the LAHOS, HAVE PIO, and HAVE CONTROL dynamics and stability derivatives. Phugoid and lateral-directional characteristics were held constant. A listing of NT-33A parameters held constant throughout the evaluations are in Table 18.

For the LAHOS configurations, the gearing ratio between the elevator and the stick position was selected by the pilot for each evaluation. For HAVE PIO, the gearing ratio was selected for each configuration by the first pilot to fly it, from then on it was held constant. The HAVE CONTROL test team set the gain of the pitch rate to stick force transfer function at a constant value of $0.34M_{\delta_e}$.

Table 18

NT-33A PARAMETERS

PARAMETER	VALUE
ω_{nsp} (rad/sec)	variable
ζ_{sp}	variable
n/α (g/rad)	4.50
$1/T_{\theta 2}$ (1/sec)	0.70
ω_{np} (rad/sec)	0.17
ζ_p	0.15
$1/T_{\theta 1}$ (1/sec)	0.08
ω_{nd} (rad/sec)	1.30
ζ_d	0.20
φ/β	1.50
τ_r (sec)	0.30
F_{es}/in (lbs/in)	6.50
F_{as}/in (lbs/in)	3.00

Feel systems: $\dfrac{A}{s^2 + 2(.8)(26)s + 26^2}$ (in/lb)

Elevator: A = 84.50
Aileron: A = 169.00
Rudder: A = 11.47

Actuators: $\dfrac{75^2}{s^2 + 2(.7)(75)s + 75^2}$ (deg/in)

LAHOS Configurations

The stability derivatives and dynamics characteristics for the LAHOS baseline configurations are shown in Table 19.

Table 19: LAHOS Baseline Configurations

Parameter	1-1	2-1	3-1	4-1	5-1
ω_{sp}	1.03	2.30	2.19	2.00	3.90
ζ_{sp}	0.73	0.57	0.25	1.06	0.53
X_u	-0.041	-0.041	-0.041	-0.041	-0.041
X_w	0.11	0.11	0.11	0.11	0.11
X_q	0	0	0	0	0
X_{δ_e}	0.0032	0.0032	0.0032	0.0032	0.0032
Z_u	-0.25	-0.26	-0.26	-0.26	-0.26
Z_w	-0.75	-0.75	-0.75	-0.75	-0.75
Z_q	0.0	0.0	0.0	0.0	0.0
Z_{δ_e}	1.1	1.1	1.1	1.1	1.1
M_u	0.0	0.0	0.0	0.0	0.0
M_w	-0.00232	-0.01875	-0.02239	-0.00663	-0.05934
M_q	-0.76	-1.83	-0.29	-3.49	-3.25
M_{δ_e}	0.33685	0.33685	0.33685	0.33685	0.33685
θ_0	4.5	4.5	4.5	4.5	4.5

HAVE PIO Configurations

The stability derivatives and dynamics characteristics for the HAVE PIO baseline configurations are shown in Table 20.

Table 20: HAVE PIO Baseline Configurations

Parameter	2-1	3-1	4-1	5-1
ω_{sp}	2.41	4.22	3.04	1.70
ζ_{sp}	0.63	0.97	0.73	.68
X_u	-0.041	-0.041	-0.041	-0.041
X_w	0.11	0.11	0.11	0.11
X_q	0.0	0.0	0.0	0.0
X_{δ_e}	0.0032	0.0032	0.0032	0.0032
Z_u	-0.26	-0.26	-0.26	-0.26
Z_w	-0.80642	-0.92116	-0.84168	-0.76979
Z_q	0.0	0.0	0.0	0.0
Z_{δ_e}	1.1	1.1	1.1	1.1
M_u	0.0	0.0	0.0	0.0
M_w	-0.01960	-0.05474	-0.03040	-0.00838
M_q	-2.26560	-7.27889	-3.59834	-1.54220
M_{δ_e}	0.33685	0.33685	0.33685	0.33685
θ_0	4.5	4.5	4.5	4.5

Table 21 shows the prefilters used to modify the LAHOS HAVE PIO, and HAVE CONTROL baseline configurations.

Table 21: NT-33A Flight Control Prefilters

First Order Filters

	A	B	C	D	1	2	3	4	5
K	2.5	3.0	5.0	0.5	1.0	10.0	4.0	2.0	1.0
τ_1	4.0	3.33	2.0	20.0	---	----	---	---	---
τ_2	10.0	10.0	10.0	10.0	0.0	10.0	4.0	2.0	1.0

Second Order Filters

	6	7	8	9	10	12	13
K	256	144	81	36	16	4	9
ζ_1	0.7	0.7	0.7	0.7	0.7	0.7	0.7
ω_{n_1}	16	12	9	6	4	2	3

First Order Systems: $\dfrac{K(s+\tau_1)}{(s+\tau_2)}$

Second Order Systems: $\dfrac{K}{(s^2+2\zeta\omega_{n_1}+\omega_{n_1}{}^2)}$

Tables 22 and 23 show the LAHOS and HAVE PIO configurations flown and modeled using the optimal control model.

Table 22
LAHOS Flight Control System and Aircraft Dynamics Combinations

	Configuration				
Filter	1	2	3	4	5
-A	X	X			
-B	X				
-C	X	X	X	X	
-1	X	X	X	X	X
-2	X	X	X		
-3	X	X	X	X	X
-4	X	X		X	X
-5					X
-6	X	X	X	X	X
-7		X	X	X	X
-8	X				
-9		X			
-10		X		X	

Table 23

HAVE PIO Flight Control System and Aircraft Dynamics Combinations

	Configuration			
Filter	2	3	4	5
-B	X			
-D		X		
-1	X	X	X	X
-2			X	
-3		X		
-5	X			
-6		X		
-7	X			
-8	X	X		
-9				X
-10				X
-12		X		
-13		X		

HAVE CONTROL Configurations

To determine the approximate stability derivatives for the HAVE CONTROL baseline configurations, LAHOS 1-1 was used as a baseline, and the feedback characteristics of the NT-33A were used to estimate the new stability derivatives. This was done using the technique described in (7:113). The three stability derivatives modified were Z_w, M_w, and M_q as

$$\begin{aligned} Z_w' &= Z_w - Z_{\delta_e} K_\alpha / U_0 \\ M_w' &= M_w - M_{\delta_e} K_\alpha / U_0 \\ M_q' &= M_q - M_{\delta_e} K_q / U_0 \end{aligned} \qquad [58]$$

The gains K_α and K_q are the feedback gains used to derive the desired stability derivatives. Using the short period approximation, the stability derivatives can determine the short period damping ratio and natural frequency as

$$\omega_n^2 = Z_w' M_q' - M_w' U_0$$
$$2\zeta\omega_n = -M_q' - Z_w' \qquad [59]$$

LAHOS 1-1 values are substituted into [58] and then the results are substituted into [59] yielding

$$\omega_n^2 = 1.04587 + 0.25264K_q + 0.34093K_\alpha + 0.00181K_\alpha K_q$$
$$2\zeta\omega_n = 1.51 + 0.33685K_q + 1.1K_\alpha/205.0 \qquad [60]$$

K_q and K_α are determined for a given value of ζ and ω_n. K_q and K_α are then substituted back into [58] along with LAHOS 1-1 values to give

$$Z_w' = -0.075 - 1.1K_\alpha/205.0$$
$$M_w' = -0.0023213 - 0.33685K_\alpha/205.0 \qquad [61]$$
$$M_q' = -0.76 - 0.33685K_q$$

These equations provide the estimated stability derivatives used to determine the HAVE CONTROL configurations.

The stability derivatives and dynamics characteristics for the HAVE CONTROL baseline configurations are shown in Table 24.

Table 24: HAVE CONTROL Baseline Configurations

Parameter	1-1	2-1	3-1
ω_{sp}	1.00	2.00	3.20
ζ_{sp}	0.75	0.75	0.50
X_u	-0.041	-0.041	-0.041
X_w	0.11	0.11	0.11
X_q	0.0	0.0	0.0
X_{δ_e}	0.0032	0.0032	0.0032
Z_u	-0.25	-0.25	-0.25
Z_w	-0.74939	-0.77925	-0.87625
Z_q	0.0	0.0	0.0.
Z_{δ_e}	1.1	1.1	1.1
M_u	0.0	0.0	0.0
M_w	-0.002134	-0.01128	-0.04098
M_q	-0.75061	-2.22075	-2.32375
M_{δ_e}	0.33685	0.33685	0.33685
θ_0	4.5	4.5	4.5

Table 25 shows the HAVE CONTROL configurations modeled and flight tested using the optimal control model.

Table 25

HAVE CONTROL Flight Control System and Aircraft Dynamics Combinations

	Configuration		
Filter	1	2	3
-D		X	
-1	X	X	X
-2		X	
-3	X		X
-5		X	X
-6			X
-7		X	
-8			X

APPENDIX B

LAHOS 1-C SAMPLE INPUT AND OUTPUT FILES

LAHOS 1-C Input File

```
 $PIRDAT KTRG=2,NX=8,NX1=3,NU=1,NY=6,NW=1,
 A(1,1)=0,-.25,.5,A(1,2)=1,-.5,A(1,3)=0,0,-.5,
 A(4,4)=-.041,-.25,A(4,5)=.11,-.75,-.00232,
 A(4,6)=-25,205,-.76,1,A(4,7)=-32.075,-2.524,
 A(4,8)=.0032,1.1,.33685,0,-10,
 B(4,1)=.0064,2.2,.6737,0,-10,E(2,1)=.25,
 C(2,1)=.5,C(1,3)=1,-.5,C(2,4)=-.00122,0,.00122,
 C(1,5)=.00488,-.00366,-.00488,.00366,C(6,6)=1,
 C(1,7)=-1,-.0123,1,.0123,1,C(2,8)=.005366,0,-.005366,
 D(2,1)=.0107,0,-.0107,
 QY(1)=1,QR(1)=.000000732,WO=.0194955,T=.2,IDENTU=2,VU=-25,
 IDENTY=2,VY=6*-20,IDENTP=1,
 PYO(1)=.02,.02,.02,.02,.02,.02,
 TH(1)=.0009,.0035,.0009,.0035,.0009,.0035,
 ATTN(1)=6*.3333 $
 LAHOS 1-C YpYc DESCRIBING FUNCTION
 $PIRDAT ICODE=11 $
 $FRQDAT JX=5,MY1=1,MY2=2,MU=0,JS=0,
f(1)=1,1.5,1.6,1.7,1.8,1.9,2.0,2.5,3,3.5,3.6,3.7,3.8,3.9,
 4,4.5$
```

LAHOS 1-C Output File

```
 PROGRAM PIREP: LAHOS 1-C

        NO. OF STATES              8
        NOISE SHAPING STATES       3
        NO. OF CONTROLS            1
        NO. OF NOISE SOURCES       1
        NO. OF OUTPUTS             6
        KTRG                       2

         SYSTEM DYNAMICS ARE: XDOT=AX+BU+EW,      Y=CX+DU

    A  MATRIX:

 0.0000E+00    1.000       0.0000E+00  0.0000E+00  0.0000E+00
0.0000E+00
               0.0000E+00  0.0000E+00

-0.2500      -0.5000       0.0000E+00  0.0000E+00  0.0000E+00
0.0000E+00
```

```
                0.0000E+00   0.0000E+00

 0.5000        0.0000E+00 -0.5000        0.0000E+00   0.0000E+00
0.0000E+00
                0.0000E+00   0.0000E+00

 0.0000E+00   0.0000E+00   0.0000E+00 -4.1000E-02   0.1100
-25.00
                -32.08        3.2000E-03

 0.0000E+00   0.0000E+00   0.0000E+00 -0.2500       -0.7500
 205.0
                -2.524         1.100

 0.0000E+00   0.0000E+00   0.0000E+00   0.0000E+00 -2.3200E-03
-0.7600
                0.0000E+00   0.3368

 0.0000E+00   0.0000E+00   0.0000E+00   0.0000E+00   0.0000E+00
 1.000
                0.0000E+00   0.0000E+00

 0.0000E+00   0.0000E+00   0.0000E+00   0.0000E+00   0.0000E+00
0.0000E+00
                0.0000E+00   -10.00
```

```
          OPEN-LOOP EIGENVALUES:
                -0.2500       0.4330      J
                -0.2500      -0.4330      J
                -0.5000       0.0000E+00  J
                -0.7536       0.6955      J
                -0.7536      -0.6955      J
                -0.2192E-01   0.1303      J
                -0.2192E-01  -0.1303      J
                 -10.00       0.0000E+00  J
```

```
    B  MATRIX:

 0.0000E+00

 0.0000E+00

 0.0000E+00

 6.4000E-03

  2.200
```

0.6737

0.0000E+00

-10.00

C MATRIX:

0.0000E+00 0.0000E+00 1.000 0.0000E+00 4.8800E-03
0.0000E+00
-1.000 0.0000E+00

0.5000 0.0000E+00 -0.5000 -1.2200E-03 -3.6600E-03
0.0000E+00
-1.2300E-02 5.3660E-03

0.0000E+00 0.0000E+00 0.0000E+00 0.0000E+00 -4.8800E-03
0.0000E+00
1.000 0.0000E+00

0.0000E+00 0.0000E+00 0.0000E+00 1.2200E-03 3.6600E-03
0.0000E+00
1.2300E-02 -5.3660E-03

0.0000E+00 0.0000E+00 0.0000E+00 0.0000E+00 0.0000E+00
0.0000E+00
1.000 0.0000E+00

0.0000E+00 0.0000E+00 0.0000E+00 0.0000E+00 0.0000E+00
1.000
0.0000E+00 0.0000E+00

D MATRIX:

0.0000E+00

1.0700E-02

0.0000E+00

-1.0700E-02

0.0000E+00

0.0000E+00

E MATRIX:

0.0000E+00

```
 0.2500

 0.0000E+00

 0.0000E+00

 0.0000E+00

 0.0000E+00

 0.0000E+00

 0.0000E+00

          COST FUNCTIONAL WEIGHTINGS
     STATE

 0.0000E+00  0.0000E+00  0.0000E+00  0.0000E+00  0.0000E+00
0.0000E+00
              0.0000E+00  0.0000E+00
    OUTPUT

  1.000       0.0000E+00  0.0000E+00  0.0000E+00  0.0000E+00
0.0000E+00

    CONTRL

 0.0000E+00
    CT.RAT

 7.3200E-07
GRAMMIAN IS 6X 6 OF RANK  5
RICCATI SOLN IN  5 ITERATIONS

RICCATI SOLN IS PSD--RANK  5


 FEEDBACK CONTROL IS TN.UDOT+U=-LOPT.X, WHERE OPTIMAL
GAINS(LOPT):

 -31.96      -9.929      -84.53      7.2643E-02 -0.3544
 12.89
               117.0      0.2914


    TN MATRIX:

 0.1001
```

```
          EIGENVALUES:
                 0.1001        0.0000E+00 J

 FEEDBACK CONTROL IS ALSO UDOT=-LX(X)-LU(U) WHERE OOPTIMAL
GAINS,LX,LU:

 -319.1        -99.14        -844.0        0.7254        -3.539
 128.7
                 1168.         2.910         9.985

          CLOSED-LOOP EIGENVALUES:
                 -9.983        0.0000E+00 J
                 -2.237         4.014     J
                 -2.237        -4.014     J
                 -3.527         1.042     J
                 -3.527        -1.042     J
                -0.2678E-01    0.0000E+00 J
                -0.2497        0.4331     J
                -0.2497       -0.4331     J
                -0.5000        0.0000E+00 J

          CONTROLLER TIME DELAY:     0.200

          VARIANCE OF RANDOM TURBULENCE:

 1.9496E-02
          MOTOR NOISE:                                (RATIOS IN
DB)

 -25.00
          OBSERVATIONAL THRESHOLDS:

 9.0000E-04   3.5000E-03   9.0000E-04   3.5000E-03   9.0000E-04
3.5000E-03

          SENSOR NOISE:                               (RATIOS IN
DB)

 -20.00        -20.00        -20.00        -20.00        -20.00
-20.00

     ATTENTIONAL ALLOCATION:

 0.3333        0.3333        0.3333        0.3333        0.3333
0.3333

RICCATI SOLN IN  9 ITERATIONS
```

```
RICCATI SOLN IS PSD--RANK  4
RICCATI SOLN IN  8 ITERATIONS
RICCATI SOLN IN  5 ITERATIONS
RICCATI SOLN IN  3 ITERATIONS
RICCATI SOLN IN  2 ITERATIONS
RICCATI SOLN IN  2 ITERATIONS
RICCATI SOLN IN  2 ITERATIONS
RICCATI SOLN IN  2 ITERATIONS

     URMS AND MOTOR NOISE VARIANCE

 0.8063

 6.5017E-03

 6.4589E-03


    YRMS AND NOISE VARIANCE AT ITERATION  8)

 1.1690E-02  2.1885E-02  5.6014E-02  2.9999E-02  7.7936E-02
8.1268E-02


 1.4770E-05  5.8633E-05  3.0339E-04  1.0376E-04  5.8358E-04
6.7197E-04


 1.4853E-05  5.9449E-05  3.0342E-04  1.0306E-04  5.8173E-04
6.6901E-04



    COST GRADIENT WRTO F:

-1.2063E-04 -2.2282E-04 -4.8268E-07 -4.2473E-06 -2.0555E-06
-1.8620E-05


    TOTAL COST, J(U)= 0.1603E-03      SAMPLING COST=
0.1500E-03


    THE COST NORMALIZED PROJECTED GRADIENT VECTOR

-0.1136      -0.3099       0.1171       0.1099       0.1141
8.2308E-02

          OPTIMAL ESTIMATOR GAINS:

  4.305        2.110       0.3448       0.5889       0.3338
4.5621E-02
```

1.837	2.152	-5.8535E-03	0.2842	6.2493E-02	4.9144E-02
1.507	0.3962	0.2274	0.1470	0.1670	8.1684E-04
15.20	11.58	-20.58	-13.60	-20.14	-2.593
-88.85	-88.11	23.57	110.7	41.04	30.18
-0.4198	-0.8883	2.2248E-02	0.6470	0.1811	0.4443
-0.5585	-0.4663	0.3485	0.7325	0.3815	0.1573
-0.1650	2.172	4.1881E-02	-1.105	-0.4498	-2.634
0.5025	2.277	-5.0019E-02	-1.426	0.2349	2.192

*** RMS MODEL PREDICTIONS ***

INDEX	X	Y	VY	VYEFF	PY(DB) FC(%)
1	0.6981E-01	0.1169E-01	0.3607E-02	0.3843E-02	-15.2 16.7
2	0.3491E-01	0.2189E-01	0.6684E-02	0.7657E-02	-15.3 16.7
3	0.5700E-01	0.5601E-01	0.1719E-01	0.1742E-01	-15.2 16.7
4	18.28	0.3000E-01	0.9240E-02	0.1019E-01	-15.2 16.7
5	8.879	0.7794E-01	0.2393E-01	0.2416E-01	-15.2 16.7
6	0.8127E-01	0.8127E-01	0.2503E-01	0.2592E-01	-15.2 16.7
7	0.7794E-01	0.0000E+00	0.0000E+00	0.0000E+00	0.0 0.0
8	0.7009	0.0000E+00	0.0000E+00	0.0000E+00	0.0 0.0

```
          U             VU          PU(DB)        UDOT
   1     0.8063       0.8063E-01   -24.97        5.687

    TOTAL ATT'N= 2.00      TOTAL COST= 0.1603E-03      PERF.
COST= 0.1366E-03


    DISTURBANCE+STATE+CONTROL COVARIANCE MATRIX

 4.8739E-03  1.7462E-10  3.2493E-03 -0.2159       0.3150
7.4245E-04
              4.4453E-03 -2.2799E-03  1.9638E-03

 1.7462E-10  1.2185E-03 -8.1231E-04  0.1176       3.9503E-02
7.4009E-04
             -7.4244E-04 -3.1613E-03  3.3764E-03

 3.2493E-03 -8.1231E-04  3.2493E-03 -0.3826       0.1424
-3.1255E-04
              3.8202E-03  9.6565E-04 -1.1279E-03

-0.2159       0.1176      -0.3826       334.0       -90.45
0.1070
             -0.8206       0.1216      -3.2436E-02

 0.3150       3.9503E-02  0.1424       -90.45        78.83
0.1979
              0.4932       0.5899       -1.576

 7.4245E-04  7.4009E-04 -3.1255E-04  0.1070       0.1979
6.6045E-03
             -1.7171E-09 -4.3088E-02  2.9676E-02

 4.4453E-03 -7.4244E-04  3.8202E-03 -0.8206       0.4932
-1.7171E-09
              6.0740E-03  7.5924E-03 -1.1901E-02

-2.2799E-03 -3.1613E-03  9.6565E-04  0.1216       0.5899
-4.3088E-02
              7.5924E-03  0.4913      -0.4913

 1.9638E-03  3.3764E-03 -1.1279E-03 -3.2436E-02  -1.576
2.9676E-02
             -1.1901E-02 -0.4913       0.6501
              TIME  16:47:27      DATE  25-AUG-88


 PROGRAM PIREP: LAHOS 1-C YpYc DESCRIBING FUNCTION
```

FREQUENCY DOMAIN REPRESENTATION
CIRCULATORY DFCN USING OUTPUT 1 DERIVATIVE 2

FREQ	MAG	PHASE
1.000	8.026	-141.0
1.500	2.475	-146.5
1.600	1.763	-147.6
1.700	1.132	-148.7
1.800	0.5683	-149.9
1.900	0.6205E-01	-151.1
2.000	-0.3943	-152.4
2.500	-2.107	-160.0
3.000	-3.145	-168.6
3.500	-3.708	-178.1
3.600	-3.773	-180.1
3.700	-3.824	-182.1
3.800	-3.860	-184.2
3.900	-3.883	-186.3
4.000	-3.892	-188.4
4.500	-3.748	-199.8

ALL CASES PROCESSED

APPENDIX C

INFLIGHT PILOT RATING SCALES

INFLIGHT PILOT COMMENT CARD

Feel System Characteristics:

- **Forces/Displacements?**
- **Pitch Sensitivity?**

Pitch Attitude Control:

- Initial Response?
- Final Response?
- Predictability?
- Any special piloting techniques/compensation required?
- Tendency toward PIO?

Task Performance:

- Airspeed control?
- Touchdown point accuracy?
- Sink rate at touchdown?
- Runway alignment?
- Level of aggressiveness used to control touchdown point?
- Special control techniques required in flare?
- If approach was abandoned, was it due to poor handling qualities or PIO?

Additional Factors:

- Wind/Turbulence
- Lateral/directional characteristics

Summarize Evaluation:

- Major problems, good features

Review Ratings:

- PIO rating, Cooper-Harper Rating

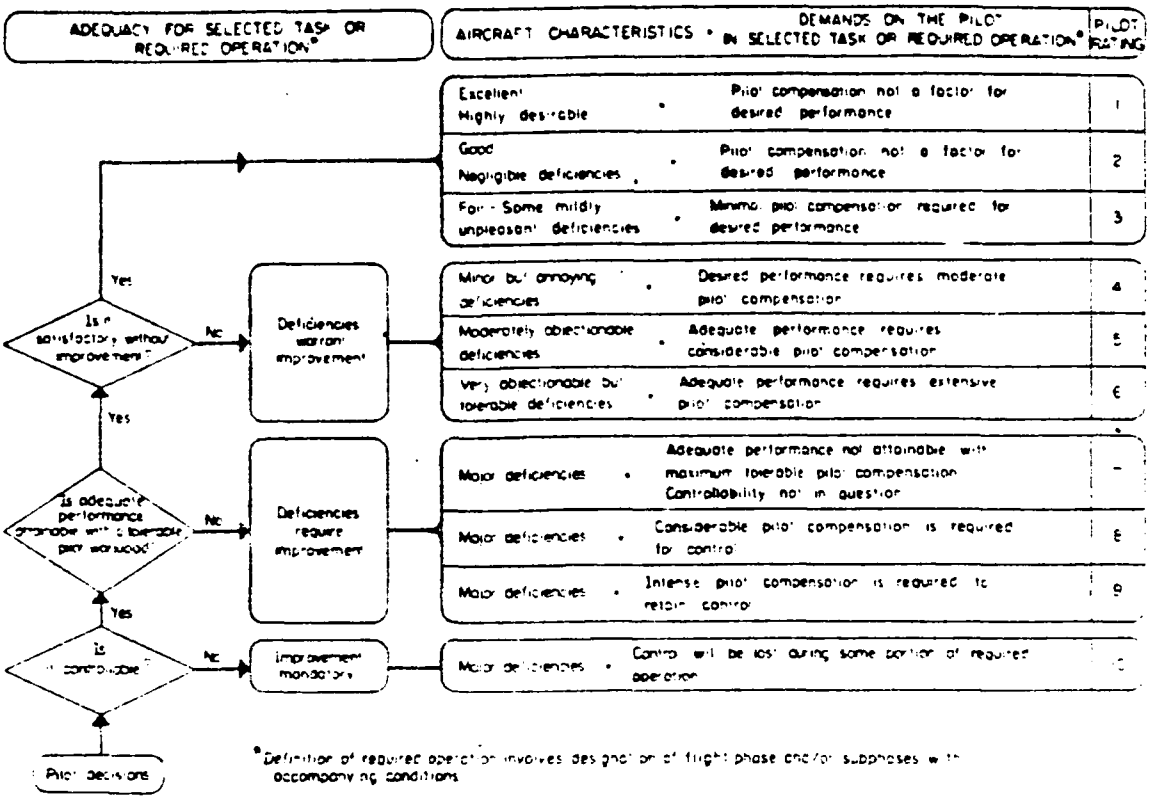

DEFINITIONS FROM TN-D-5153

COMPENSATION

The measure of additional pilot effort and attention required to maintain a given level of performance in the face of deficient vehicle characteristics

HANDLING QUALITIES

Those qualities or characteristics of an aircraft that govern the ease and precision with which a pilot is able to perform the tasks required in support of an aircraft role

MISSION

The composite of pilot-vehicle functions that must be performed to fulfill operational requirements. May be specified for a role, complete flight, flight phase, or flight subphase

PERFORMANCE

The precision of control with respect to aircraft movement that a pilot is able to achieve in performing a task. (Pilot-vehicle performance is a measure of handling performance. Pilot performance is a measure of the manner or efficiency with which a pilot moves the principal controls in performing a task.)

ROLE

The function or purpose that defines the primary use of an aircraft

TASK

The actual work assigned a pilot to be performed in completion of or as representative of a designated flight segment

WORKLOAD

The integrated physical and mental effort required to perform a specified piloting task

Figure 36. Pilot Handling Qualities Rating Scale

PILOT CONFIDENCE FACTORS

CLASS A

A pilot may usually assign a rating with a relatively high degree of confidence, although he may have mild reservations because of incomplete or inadequate simulation of motion cues, disturbances, visual information, or other factors affecting pilot workload.

Supplemetary tasks, if needed, can be adequately provided by the pilot.

CLASS B

A pilot can assign a rating with only a moderate level of confidence because of uncertainties introduced by a lack of representative environmental disturbances as well as incomplete or inadequate simulation of motion cues, disturbances, visual information, or other factors affecting pilot workload.

Supplementary tasks may be desired, but are not available.

CLASS C

A pilot can assign a rating with only minimum confidence because considerable pilot extrapolation is required due to an incomplete task, thereby requiring considerable reliance on self-imposed tasks and maneuvers for assessment.

This may also be aggravated by incomplete or very limited simulations of motion cues, disturbances, visual information, or other factors affecting pilot workload.

DESCRIPTION	NUMERICAL RATING
NO TENDENCY FOR PILOT TO INDUCE UNDESIRABLE MOTIONS	1
UNDESIRABLE MOTIONS TEND TO OCCUR WHEN PILOT INITIATES ABRUPT MANEUVERS OR ATTEMPTS TIGHT CONTROL. THESE MOTIONS CAN BE PREVENTED OR ELIMINATED BY PILOT TECHNIQUE.	2
UNDESIRABLE MOTIONS EASILY INDUCED WHEN PILOT INITIATES ABRUPT MANEUVERS OR ATTEMPTS TIGHT CONTROL. THESE MOTIONS CAN BE PREVENTED OR ELIMINATED BUT ONLY AT SACRIFICE TO TASK PERFORMANCE OR THROUGH CONSIDERABLE PILOT ATTENTION AND EFFORT.	3
OSCILLATIONS TEND TO DEVELOP WHEN PILOT INITIATES ABRUPT MANEUVERS OR ATTEMPTS TIGHT CONTROL. PILOT MUST REDUCE GAIN OR ABANDON TASK TO RECOVER.	4
DIVERGENT OSCILLATIONS TEND TO DEVELOP WHEN PILOT INITIATES ABRUPT MANEUVERS OR ATTEMPTS TIGHT CONTROL. PILOT MUST OPEN LOOP BY RELEASING OR FREEZING THE STICK.	5
DISTURBANCE OR NORMAL PILOT CONTROL MAY CAUSE DIVERGENT OSCILLATION. PILOT MUST OPEN CONTROL LOOP BY RELEASING OR FREEZING THE STICK	6

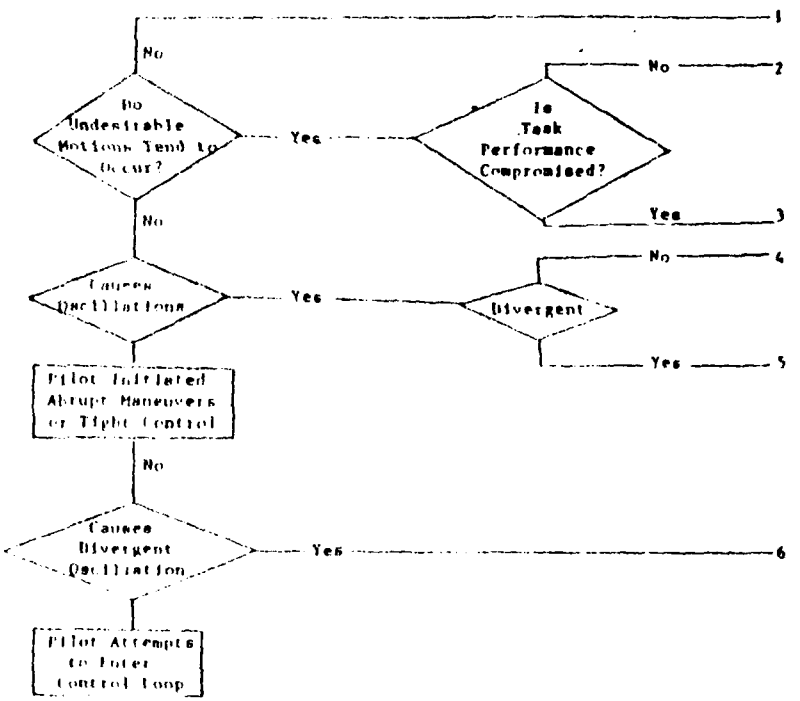

Figure 37. PIO Rating Scale

APPENDIX D

AIRCRAFT DESCRIPTION AND TEST INSTRUMENTATION

Aircraft Description

The NT-33A variable stability airplane, shown in Figure 38, is a T-33 jet trainer modified with a Variable Stability System. The VSS can be divided into two independent parts. The first part, the variable feel system, provides a variety of stick and rudder pedal forces, gradients, and displacements. The variable feel is provided by disconnecting the elevator, aileron, and rudder controls in the front cockpit from their respective control surfaces and connecting the controls to separate servomechanisms. The second part of the VSS is the response feedback flight control system. This part augments the normal T- 33 dynamics to represent those of the vehicle being simulated.

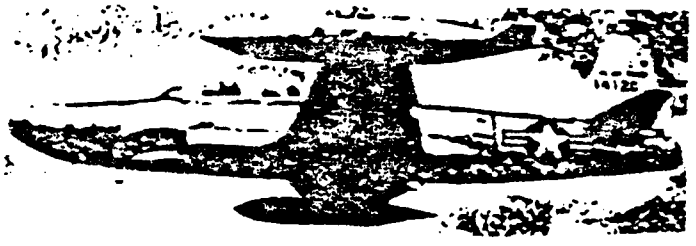

Figure 38. NT-33A Variable Stability Aircraft

The augmentation is accomplished by connecting the elevator, aileron, and rudder control surfaces to individual servos. These individual servos can be driven by a number of different inputs, such as the aircraft's artificial feel

system (pilot's commands, position or force), attitude and rate gyros, accelerometers, dynamic pressure pickups, angle of attack vane and sideslip probe. This arrangement, through a response-feedback system, allows the normal T-33 derivatives to be augmented to simulate the handling qualities of existing or hypothetical aircraft. A block diagram of the VSS is shown in Figure 39.

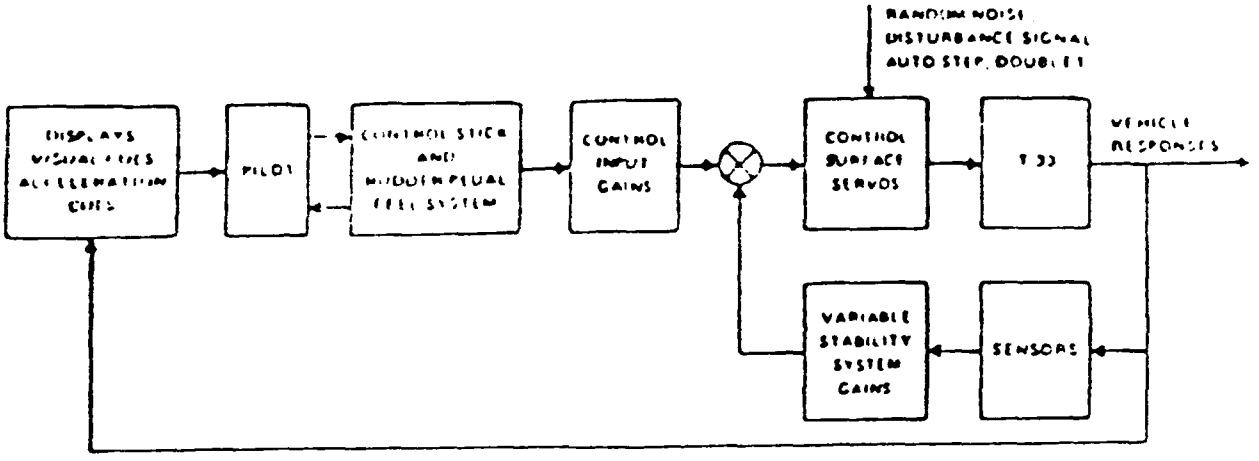

Figure 39. Variable Stability NT-33A Block Diagram

The original T-33 nose section has been replaced with the larger nose of an F-94 to provide the volume required for the electronic components of the response-feedback system and recording equipment. The physical layout of the control system is shown in Figure 40. Each control surface has an electro-hydraulic position servo which is actuated by inputs from the VSS. The servos operate in parallel with the normal T-33 control surface's actuating mechanisms.

Each of the surface position actuators has a hydraulic limiting circuit which limits the maximum hinge moment which can be generated by the flight control system. The rear cockpit controls have a direct mechanical connection to the aircraft control surfaces at all times.

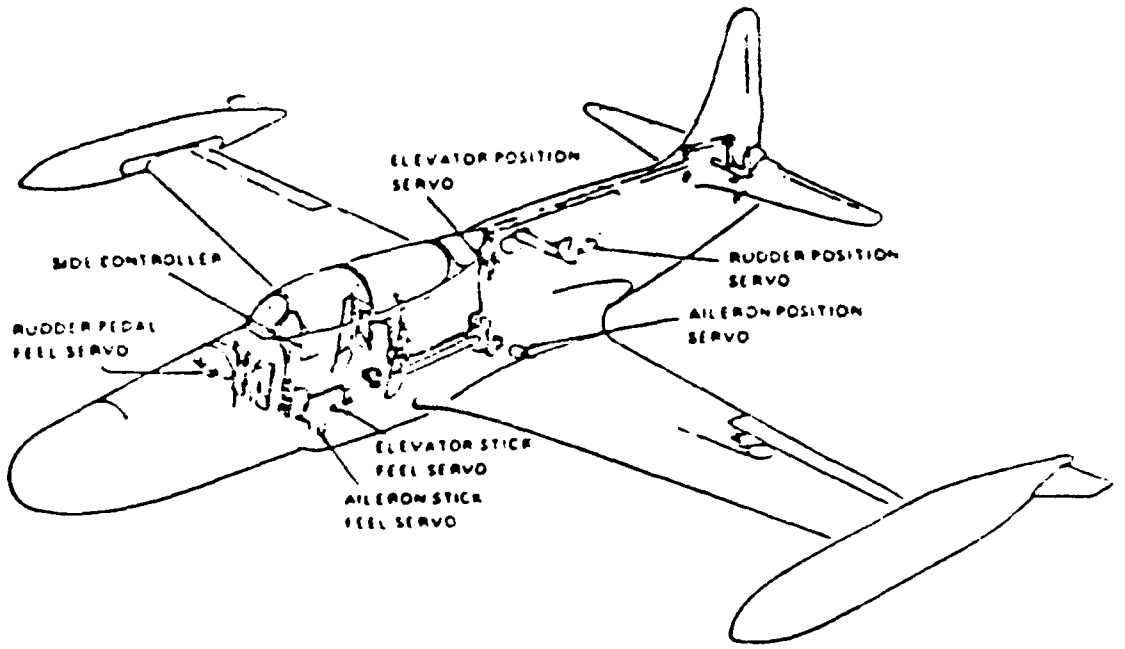

Figure 40. Control System Layout

NT-33A Safety Features

The primary safety feature in the airplane is the safety pilot; however, the NT-33A also has numerous safety provisions designed into the variable stability equipment.

Control Interlock System: The control buttons and switches for the various functions of the VSS are wired so that the proper sequence of operation of these controls must be observed to energize the various parts of the VSS. No action will result from a button or switch activated out of sequence. For example, interlocking circuits prevent servo engagement prior to auto balance engage.

Automatic Safety Trips: The automatic safety trip monitors the servovalve amplifier error signals and the normal and lateral accelerometer output signals. If these signals exceed preset values, the VSS is automatically shut off. Safety trip accelerometer limits have been set as follows:

a. n_z Pushover (- 0.3g on the g meter)

b. n_z Pullout (+ 4.8g on g meter)

c. n_y ($\pm$ 0.25g)

Audio-visual VSS Shut-off Warning System: When the VSS has been disengaged either automatically or manually, red lights will flash in both cockpits and a "beep, beep" will be heard in the interphone.

Special Aircraft Limitation: The variable stability NT-33A is limited to 375 KIAS with a never exceed speed of 400 KIAS.

Special Pilot Emergency Procedures: In addition to normal NT-33A emergency procedures, the following pertain specifically to the variable stability NT-33A:

-Manual VSS trip: The project pilot can manually disengage the VSS from the control surfaces and return control of the aircraft to the safety pilot. Disengage switches are located on both the centerstick and the sidestick.

-In the event of safety pilot incapacitation, the project pilot can fly the aircraft back to the base via his fly-by-wire controls with normal T-33 characteristics. This is accomplished by actuating the red guarded safety trip bypass switch located on the left side of the VSS engage panel and sequentially depressing the adjacent four buttons starting from the left. Subsequent buttons are pressed after the light below the previously pressed button is lit.

-If a feel system hardover should occur, the project pilot can activate the feel system hydraulic bypass switch and move the control stick out of the way to ensure non-interference during ejection.

Table 26: Test Instrumentation

NT-33A Digital Tape Parameters

DIGITAL CHANNEL NUMBER	RECORDED VARIABLE	ENGINEERING UNITS
1	Pressure Altitude	feet
2	Normal Acceleration	g's
3	Velocity (Indicated)	knots
4	Pitch Rate	degrees/second
5	Pitch Angle	degrees
6	Yaw Rate	degrees/second
7	Elevator Stick Deflection	inches
8	Angle of Sideslip	degrees
9	Event Mark	N/A
10	Radar Altitude	feet
11	Pitch Error	degrees
12	Roll Rate	degrees/second
13	Roll Angle	degrees
14	Longitudinal Acceleration	g's
15	Roll Error	degrees
16	Elevator Deflection	degrees
17	Lateral Acceleration	g's
18	Elevator Stick Force	pounds
19	Vertical Velocity	feet/sec
20	Rudder Deflection	degrees
21	Total Aileron Deflection	degrees
22	Change in Heading	degrees
23	Lateral Stick Deflection	inches
24	Angle of Attack	degrees
25	Aileron Stick Force	pounds
26	Rudder Pedal Deflection	inches
27	Rudder Pedal Force	pounds
28	Time Rate of AOA Change	degrees/second

APPENDIX E

INFLIGHT PILOT COMMENT CARDS

LEGEND

SP FREQ ----------	SHORT PERIOD NATURAL FREQUENCY (RAD/SEC)
DAMP RATIO ----------	DAMPING RATIO
PILOT A ----------	CAPT BAUM
PILOT B ----------	CAPT LINDSEY
PILOT C ----------	CAPT THOMAS
GEARING ----------	Overall gain of pitch rate to stick force transfer function (rad/sec/lb)
FCS ----------	Flight Control System with numerator(gain) and denominator(damping ratio and natural frequency)

INFLIGHT PILOT COMMENT CARD

FLT NO. 1	RUN NO. 1	SP FREQ = 1.0	DATE: 20 SEP 89
CONFIGURATION 1-3		DAMP RATIO = 0.75	PILOT: C
GEARING = $.34M\delta_e$		FCS = 4.0/(4)	IP: EASTER

C-H RATING = 7 PIO RATING = 4 CONFIDENCE RATING = A

FEEL SYSTEM CHARACTERISTICS:

FORCES:	MEDIUM
PITCH SENSITIVITY:	HIGH

PITCH ATTITUDE CONTROL:

INITIAL RESPONSE:	QUICK
FINAL RESPONSE:	QUICK
PREDICTABILITY:	LOW
PILOT COMPENSATION:	HIGH
PIO TENDENCY:	SLIGHT, BUT NOT DIVERGENT

TASK PERFORMANCE:

AIRSPEED CONTROL:	DESIRED
TOUCHDOWN POINT:	DESIRED
RUNWAY ALIGNMENT:	DESIRED
TOUCHDOWN SINK RATE:	LOW
AGGRESSIVENESS:	MEDIUM
SPECIAL CONTROL:	HIGH LEVELS TO AVOID PIO IN FLARE
REASON APP ABANDON:	N/A

ADDITIONAL FACTORS:

WIND:	CALM
TURBULENCE:	NONE
LAT-DIR PERFORMANCE:	GOOD

SUMMARIZE EVALUATION:

MAJOR PROBLEMS: BOUNCED TWICE ON TOUCHDOWN AND SLIGHT PIO UP AND AWAY

GOOD FEATURES:

INFLIGHT PILOT COMMENT CARD

FLT NO. 1	RUN NO. 2	SP FREQ = 1.0	DATE: 20 SEP 89
CONFIGURATION 1-1		DAMP RATIO = 0.75	PILOT: C
GEARING = $.34M\delta_e$		FCS = 1.0	IP: EASTER

C-H RATING = 3 PIO RATING = 2 CONFIDENCE RATING = B

FEEL SYSTEM CHARACTERISTICS:

FORCES:	MEDIUM
PITCH SENSITIVITY:	MEDIUM

PITCH ATTITUDE CONTROL:

INITIAL RESPONSE:	QUICK
FINAL RESPONSE:	AVERAGE
PREDICTABILITY:	FAIR
PILOT COMPENSATION:	MODERATE
PIO TENDENCY:	NONE

TASK PERFORMANCE:

AIRSPEED CONTROL:	DESIRED
TOUCHDOWN POINT:	DESIRED
RUNWAY ALIGNMENT:	DESIRED
TOUCHDOWN SINK RATE:	MEDIUM
AGGRESSIVENESS:	ABOVE AVERAGE
SPECIAL CONTROL:	PUSH OVER TO ATTAIN DESIRED
REASON APP ABANDON:	N/A

ADDITIONAL FACTORS:

WIND:	CALM
TURBULENCE:	NONE
LAT-DIR PERFORMANCE:	GOOD

SUMMARIZE EVALUATION:

MAJOR PROBLEMS: SLIGHT BALLOON WHICH REQUIRED PUSH OVER TO COMPENSATE

GOOD FEATURES:

INFLIGHT PILOT COMMENT CARD

FLT NO. 2	RUN NO. 1	SP FREQ = 2.0	DATE: 21 SEP 89
CONFIGURATION 2-1		DAMP RATIO = 0.75	PILOT: C
GEARING = .50Mδ_e		FCS = 1.0	IP: EASTER

C-H RATING = 3	PIO RATING = 1	CONFIDENCE RATING = A

FEEL SYSTEM CHARACTERISTICS:

FORCES:	MEDIUM
PITCH SENSITIVITY:	GOOD

PITCH ATTITUDE CONTROL:

INITIAL RESPONSE:	QUICK
FINAL RESPONSE:	QUICK
PREDICTABILITY:	GOOD
PILOT COMPENSATION:	LITTLE
PIO TENDENCY:	NONE

TASK PERFORMANCE:

AIRSPEED CONTROL:	DESIRED
TOUCHDOWN POINT:	DESIRED
RUNWAY ALIGNMENT:	DESIRED
TOUCHDOWN SINK RATE:	LOW
AGGRESSIVENESS:	MEDIUM
SPECIAL CONTROL:	NONE
REASON APP ABANDON:	N/A

ADDITIONAL FACTORS:

WIND:	CALM
TURBULENCE:	NONE
LAT-DIR PERFORMANCE:	GOOD

SUMMARIZE EVALUATION:

MAJOR PROBLEMS:

GOOD FEATURES: SUPER CONFIGURATION - I'D GIVE A 2.5 IF ALLOWED. BETTER THAN 1-1 CONFIGURATION THAT I GAVE A CH 3.

INFLIGHT PILOT COMMENT CARD

FLT NO. 2 RUN NO. 2	SP FREQ = 2.0	DATE: 21 SEP 89
CONFIGURATION 2-D	DAMP RATIO = 0.75	PILOT: C
GEARING = $.50M_{\delta_e}$	FCS = 0.5(20)/(10)	IP: EASTER

C-H RATING = 4.5 PIO RATING = 2 CONFIDENCE RATING = A

FEEL SYSTEM CHARACTERISTICS:

FORCES:	MEDIUM
PITCH SENSITIVITY:	GOOD

PITCH ATTITUDE CONTROL:

INITIAL RESPONSE:	QUICK
FINAL RESPONSE:	QUICK
PREDICTABILITY:	FAIR
PILOT COMPENSATION:	MODERATE
PIO TENDENCY:	MONE

TASK PERFORMANCE:

AIRSPEED CONTROL:	DESIRED
TOUCHDOWN POINT:	DESIRED
RUNWAY ALIGNMENT:	DESIRED
TOUCHDOWN SINK RATE:	LOW
AGGRESSIVENESS:	MEDIUM
SPECIAL CONTROL:	PITCH OVER IN FLARE AFTER BALLOON
REASON APP ABANDON:	N/A

ADDITIONAL FACTORS:

WIND:	CALM
TURBULENCE:	NONE
LAT-DIR PERFORMANCE:	GOOD

SUMMARIZE EVALUATION:

MAJOR PROBLEMS: 2ND OFFSET AHD MUCH HIGHER GAINS DUE TO LATE "CORRECT" CALL AND A DEFINITE BALLOONING TENDENCY WAS OBSERVED. THE COMPENSATION REQUIRED TO CORRECT WAS EASY.

GOOD FEATURES:

INFLIGHT PILOT COMMENT CARD

FLT NO. 3	RUN NO. 1	SP FREQ = 3.2	DATE: 22 SEP 89
CONFIGURATION 3-1		DAMP RATIO = 0.50	PILOT: A
GEARING = $1.1M_{\delta e}$		FCS = 1.0	IP: EASTER

C-H RATING = 2 PIO RATING = 1 CONFIDENCE RATING = B

FEEL SYSTEM CHARACTERISTICS:

FORCES:	GOOD
PITCH SENSITIVITY:	GOOD

PITCH ATTITUDE CONTROL:

INITIAL RESPONSE:	QUICK
FINAL RESPONSE:	QUICK
PREDICTABILITY:	GOOD
PILOT COMPENSATION:	NONE
PIO TENDENCY:	NONE

TASK PERFORMANCE:

AIRSPEED CONTROL:	DESIRED
TOUCHDOWN POINT:	DESIRED
RUNWAY ALIGNMENT:	DESIRED
TOUCHDOWN SINK RATE:	LOW
AGGRESSIVENESS:	MEDIUM
SPECIAL CONTROL:	NONE
REASON APP ABANDON:	N/A

ADDITIONAL FACTORS:

WIND:	CALM
TURBULENCE:	NONE
LAT-DIR PERFORMANCE:	GOOD

SUMMARIZE EVALUATION:

MAJOR PROBLEMS:	NONE
GOOD FEATURES:	QUICK, STABLE NICE FLYING

INFLIGHT PILOT COMMENT CARD

FLT NO. 3 RUN NO. 2	SP FREQ = 3.2	DATE: 22 SEP 89
CONFIGURATION 3-3	DAMP RATIO = 0.50	PILOT: A
GEARING = $1.1M_{\delta_e}$	FCS = 4.0/(4)	IP: EASTER

C-H RATING = 3 PIO RATING = 2 CONFIDENCE RATING = B

FEEL SYSTEM CHARACTERISTICS:

FORCES:	GOOD
PITCH SENSITIVITY:	GOOD

PITCH ATTITUDE CONTROL:

INITIAL RESPONSE:	QUICK
FINAL RESPONSE:	QUICK
PREDICTABILITY:	GOOD
PILOT COMPENSATION:	NONE
PIO TENDENCY:	SLIGHT

TASK PERFORMANCE:

AIRSPEED CONTROL:	DESIRED
TOUCHDOWN POINT:	DESIRED
RUNWAY ALIGNMENT:	DESIRED
TOUCHDOWN SINK RATE:	LOW
AGGRESSIVENESS:	MEDIUM
SPECIAL CONTROL:	SLIGHT FORE AND AFT STICK TRAVEL
REASON APP ABANDON:	N/A

ADDITIONAL FACTORS:

WIND:	CALM
TURBULENCE:	NONE
LAT-DIR PERFORMANCE:	GOOD

SUMMARIZE EVALUATION:

MAJOR PROBLEMS:

GOOD FEATURES:

INFLIGHT PILOT COMMENT CARD

FLT NO. 4	RUN NO. 1	SP FREQ = 2.0	DATE: 25 SEP 89
CONFIGURATION 2-2		DAMP RATIO = 0.75	PILOT: B
GEARING = .50M_{δ_e}		FCS = 10/(10)	IP: EASTER

C-H RATING = 4 PIO RATING = 1 CONFIDENCE RATING = B

FEEL SYSTEM CHARACTERISTICS:

FORCES:	LIGHT
PITCH SENSITIVITY:	LITTLE SENSITIVE

PITCH ATTITUDE CONTROL:

INITIAL RESPONSE:	QUICK
FINAL RESPONSE:	GOOD
PREDICTABILITY:	GOOD UNTIL TOUCHDOWN
PILOT COMPENSATION:	MODERATE
PIO TENDENCY:	NONE

TASK PERFORMANCE:

AIRSPEED CONTROL:	DESIRED
TOUCHDOWN POINT:	DESIRED
RUNWAY ALIGNMENT:	DESIRED
TOUCHDOWN SINK RATE:	MODERATE
AGGRESSIVENESS:	MODERATE
SPECIAL CONTROL:	FORCE A/C ONTO RUNWAY
REASON APP ABANDON:	N/A

ADDITIONAL FACTORS:

WIND:	CALM
TURBULENCE:	NONE
LAT-DIR PERFORMANCE:	GOOD

SUMMARIZE EVALUATION:

MAJOR PROBLEMS: HAD TO "GIVE UP" TO GET A/C ON RUNWAY - WANTED TO FLARE FOREVER

GOOD FEATURES:

INFLIGHT PILOT COMMENT CARD

FLT NO. 4	RUN NO. 2	SP FREQ = 2.0	DATE: 25 SEP 89
CONFIGURATION 2-5		DAMP RATIO = 0.75	PILOT: B
GEARING = $.50M_{\mathcal{f}_e}$		FCS = 1.0/(1)	IP: EASTER

C-H RATING = 8 PIO RATING = 5 CONFIDENCE RATING = A

FEEL SYSTEM CHARACTERISTICS:

FORCES:	HEAVY - 25-30 LBS
PITCH SENSITIVITY:	GOOD

PITCH ATTITUDE CONTROL:

INITIAL RESPONSE:	LOTS OF STICK REQUIRED, SLUGGISH
FINAL RESPONSE:	RATES UP, MUST LEAD INPUTS TO DAMP PIO
PREDICTABILITY:	UNPREDICTABLE
PILOT COMPENSATION:	LARGE LEADS REQUIRED
PIO TENDENCY:	LARGE

TASK PERFORMANCE:

AIRSPEED CONTROL:	UNSAT
TOUCHDOWN POINT:	ADEQUATE
RUNWAY ALIGNMENT:	DESIRED
TOUCHDOWN SINK RATE:	LARGE, AT BOTTOM OF PIO CYCLE
AGGRESSIVENESS:	HIGH
SPECIAL CONTROL:	LARGE CORRECTIONS DURING FLARE AND THEN OPEN LOOP FOR TOUCHDOWN
REASON APP ABANDON:	N/A

ADDITIONAL FACTORS:

WIND:	CALM
TURBULENCE:	NONE
LAT-DIR PERFORMANCE:	GOOD

SUMMARIZE EVALUATION:

MAJOR PROBLEMS: TENDENCY TO PIO DIVERGENT, ANY DISTRACTIONS WOULD HAVE MEANT LOSS OF CONTROL.

GOOD FEATURES:

INFLIGHT PILOT COMMENT CARD

FLT NO. 5	RUN NO. 1	SP FREQ = 3.2	DATE: 26 SEP 89
CONFIGURATION 3-5		DAMP RATIO = 0.50	PILOT: B
GEARING = $1.1M_{\delta_e}$		FCS = 1.0/(1)	IP: EASTER

C-H RATING = 6	PIO RATING = 4	CONFIDENCE RATING = A

FEEL SYSTEM CHARACTERISTICS:

FORCES:	GOOD
PITCH SENSITIVITY:	LAGGY, PITCH SENSITIVE

PITCH ATTITUDE CONTROL:

INITIAL RESPONSE:	VERY SLOW
FINAL RESPONSE:	PIO, SMALL OSCILLATIONS, LOW FREQ
PREDICTABILITY:	UNPREDICTABLE
PILOT COMPENSATION:	HIGH
PIO TENDENCY:	YES

TASK PERFORMANCE:

AIRSPEED CONTROL:	ADEQUATE
TOUCHDOWN POINT:	ADEQUATE
RUNWAY ALIGNMENT:	DESIRED
TOUCHDOWN SINK RATE:	MEDIUM
AGGRESSIVENESS:	HIGH
SPECIAL CONTROL:	AGGRESIVE CORRECTIONS THEN OPEN LOOP
REASON APP ABANDON:	N/A

ADDITIONAL FACTORS:

WIND:	CALM
TURBULENCE:	NONE
LAT-DIR PERFORMANCE:	GOOD

SUMMARIZE EVALUATION:

MAJOR PROBLEMS: HAD TO GO OPEN LOOP IN THE FLARE FLOATED, TENDED TO BALLOON, HAD TO FORCE THE A/C TO LAND

GOOD FEATURES:

INFLIGHT PILOT COMMENT CARD

FLT NO. 5 RUN NO. 2	SP FREQ = 3.2	DATE: 26 SEP 89
CONFIGURATION 3-6	DAMP RATIO = 0.50	PILOT: B
GEARING = $1.1M_{\delta_e}$	FCS = 256/[0.7,16]	IP: BALL

C-H RATING = 5 PIO RATING = 3 CONFIDENCE RATING = B

FEEL SYSTEM CHARACTERISTICS:

FORCES:	GOOD
PITCH SENSITIVITY:	SENSITIVE - BOBBLED

PITCH ATTITUDE CONTROL:

INITIAL RESPONSE:	SOME LAG
FINAL RESPONSE:	BOBBLE
PREDICTABILITY:	GOOD
PILOT COMPENSATION:	NONE
PIO TENDENCY:	YES, BOBBLE

TASK PERFORMANCE:

AIRSPEED CONTROL:	ADEQUATE
TOUCHDOWN POINT:	ADEQUATE
RUNWAY ALIGNMENT:	DESIRED
TOUCHDOWN SINK RATE:	LOW
AGGRESSIVENESS:	NORMAL
SPECIAL CONTROL:	FREEZE STICK IN FLARE
REASON APP ABANDON:	N/A

ADDITIONAL FACTORS:

WIND:	CALM
TURBULENCE:	NONE
LAT-DIR PERFORMANCE:	GOOD

SUMMARIZE EVALUATION:

MAJOR PROBLEMS: BOBBLE ALL THE WAY DOWN FINAL LIKE A HIGH FREQ/LOW AMPLITUDE LIMIT CYCLE, BUT WITH NO TENDENCY TO INCREASE IN AMPLITUDE. ALSO A/C FLOATED AND WAS DIFFICULT TO TOUCHDOWN.

GOOD FEATURES:

INFLIGHT PILOT COMMENT CARD

FLT NO. 6 RUN NO. 1	SP FREQ = 3.2	DATE: 3 OCT 89
CONFIGURATION 3-8	DAMP RATIO = 0.50	PILOT: A
GEARING = $1.1M_{\delta_e}$	FCS = 81.0/[0.7,9]	IP: BALL

C-H RATING = 3 PIO RATING = 1 CONFIDENCE RATING = B

FEEL SYSTEM CHARACTERISTICS:

FORCES:	MEDIUM
PITCH SENSITIVITY:	GOOD

PITCH ATTITUDE CONTROL:

INITIAL RESPONSE:	QUICK
FINAL RESPONSE:	QUICK
PREDICTABILITY:	GOOD
PILOT COMPENSATION:	SMALL
PIO TENDENCY:	VERY SLIGHT

TASK PERFORMANCE:

AIRSPEED CONTROL:	DESIRED
TOUCHDOWN POINT:	DESIRED
RUNWAY ALIGNMENT:	DESIRED
TOUCHDOWN SINK RATE:	LOW
AGGRESSIVENESS:	MEDIUM
SPECIAL CONTROL:	NONE
REASON APP ABANDON:	N/A

ADDITIONAL FACTORS:

WIND:	LIGHT
TURBULENCE:	NONE
LAT-DIR PERFORMANCE:	NO FACTOR

SUMMARIZE EVALUATION:

MAJOR PROBLEMS:	FLIGHT PATH MARKER TENDED TO OSCILLATE SLIGHTLY AFTER A PITCH INPUT, SMALL NOSE HUNT
GOOD FEATURES:	NO LAG OR DELAY NOTED

INFLIGHT PILOT COMMENT CARD

FLT NO. 6	RUN NO. 2	SP FREQ = 2.0	DATE: 3 OCT 89
CONFIGURATION 2-2		DAMP RATIO = 0.75	PILOT: A
GEARING = .50M_{δ_e}		FCS = 10/(10)	IP: BALL

C-H RATING = 2	PIO RATING = 1	CONFIDENCE RATING = B

FEEL SYSTEM CHARACTERISTICS:

FORCES:	MEDIUM
PITCH SENSITIVITY:	GOOD

PITCH ATTITUDE CONTROL:

INITIAL RESPONSE:	QUICK
FINAL RESPONSE:	QUICK
PREDICTABILITY:	GOOD
PILOT COMPENSATION:	NONE
PIO TENDENCY:	NONE

TASK PERFORMANCE:

AIRSPEED CONTROL:	DESIRED
TOUCHDOWN POINT:	DESIRED
RUNWAY ALIGNMENT:	DESIRED
TOUCHDOWN SINK RATE:	LOW
AGGRESSIVENESS:	MEDIUM
SPECIAL CONTROL:	NONE
REASON APP ABANDON:	N/A

ADDITIONAL FACTORS:

WIND:	LIGHT
TURBULENCE:	NONE
LAT-DIR PERFORMANCE:	GOOD

SUMMARIZE EVALUATION:

MAJOR PROBLEMS:	NONE
GOOD FEATURES:	GOOD, STABLE PITCH CONTROL

INFLIGHT PILOT COMMENT CARD

FLT NO. 7	RUN NO. 1	SP FREQ = 3.2	DATE: 3 OCT 89
CONFIGURATION 3-1		DAMP RATIO = 0.50	PILOT: C
GEARING = $1.1M_{\delta e}$		FCS = 1.0	IP: BALL

C-H RATING = 3	PIO RATING = 1	CONFIDENCE RATING = B

FEEL SYSTEM CHARACTERISTICS:

FORCES:	GOOD
PITCH SENSITIVITY:	GOOD

PITCH ATTITUDE CONTROL:

INITIAL RESPONSE:	GOOD
FINAL RESPONSE:	GOOD
PREDICTABILITY:	GOOD
PILOT COMPENSATION:	SLIGHT
PIO TENDENCY:	NONE

TASK PERFORMANCE:

AIRSPEED CONTROL:	DESIRED
TOUCHDOWN POINT:	DESIRED
RUNWAY ALIGNMENT:	DESIRED
TOUCHDOWN SINK RATE:	LOW
AGGRESSIVENESS:	AVERAGE
SPECIAL CONTROL:	NONE
REASON APP ABANDON:	N/A

ADDITIONAL FACTORS:

WIND:	SLIGHT X-WIND/TAILWIND
TURBULENCE:	NONE
LAT-DIR PERFORMANCE:	GOOD

SUMMARIZE EVALUATION:

MAJOR PROBLEMS:

GOOD FEATURES: GOOD FLYING A/C - WOULD HAVE GIVEN A CH OF 2 IF WINDS WERE CALM (FLOWN AT 1430) BUT MORE COMPENSATION WAS OBVIOUSLY REQUIRED DUE TO SLIGHT TAILWIND TO MEET DESIRED PERFORMANCE.

INFLIGHT PILOT COMMENT CARD

FLT NO. 7	RUN NO. 2	SP FREQ = 2.0	DATE: 3 OCT 89
CONFIGURATION 2-7		DAMP RATIO = 0.75	PILOT: C
GEARING = .50Mζ_e		FCS = 144/[0.7,12]	IP: BALL

C-H RATING = 4.5 PIO RATING = 1 CONFIDENCE RATING = B

FEEL SYSTEM CHARACTERISTICS:

FORCES:	GOOD
PITCH SENSITIVITY:	AVERAGE

PITCH ATTITUDE CONTROL:

INITIAL RESPONSE:	GOOD
FINAL RESPONSE:	GOOD
PREDICTABILITY:	BELOW AVERAGE
PILOT COMPENSATION:	MODERATE
PIO TENDENCY:	NONE

TASK PERFORMANCE:

AIRSPEED CONTROL:	DESIRED
TOUCHDOWN POINT:	DESIRED/ADEQUATE
RUNWAY ALIGNMENT:	DESIRED
TOUCHDOWN SINK RATE:	LOW
AGGRESSIVENESS:	HIGH
SPECIAL CONTROL:	PUSH OVER TO COUNTER BALLOON
REASON APP ABANDON:	N/A

ADDITIONAL FACTORS:

WIND:	SLIGHT X-WIND/TAILWIND
TURBULENCE:	NONE
LAT-DIR PERFORMANCE:	GOOD

SUMMARIZE EVALUATION:

MAJOR PROBLEMS: SLIGHT BALLOON DUE POSSIBLY TO WINDS RESULTED IN LESS THAN DESIRED PREDICTABILITY AND LONG TOUCHDOWNS

GOOD FEATURES:

INFLIGHT PILOT COMMENT CARD

FLT NO. 8	RUN NO. 1	SP FREQ = 1.0	DATE: 4 OCT 89
CONFIGURATION 1-1		DAMP RATIO = 0.75	PILOT: B
GEARING = $.34M_{\delta_e}$		FCS = 1.0	IP: BALL

C-H RATING = 4	PIO RATING = 2	CONFIDENCE RATING = A

FEEL SYSTEM CHARACTERISTICS:

FORCES:	GOOD
PITCH SENSITIVITY:	GOOD

PITCH ATTITUDE CONTROL:

INITIAL RESPONSE:	QUICK
FINAL RESPONSE:	QUICK
PREDICTABILITY:	GOOD
PILOT COMPENSATION:	SLIGHT
PIO TENDENCY:	NONE

TASK PERFORMANCE:

AIRSPEED CONTROL:	DESIRED
TOUCHDOWN POINT:	DESIRED
RUNWAY ALIGNMENT:	DESIRED
TOUCHDOWN SINK RATE:	LOW
AGGRESSIVENESS:	HIGH
SPECIAL CONTROL:	FORCE NOSE ONTO RUNWAY IN FLARE
REASON APP ABANDON:	N/A

ADDITIONAL FACTORS:

WIND:	CALM
TURBULENCE:	NONE
LAT-DIR PERFORMANCE:	GOOD

SUMMARIZE EVALUATION:

MAJOR PROBLEMS: TENDED TO FLOAT IN FLARE

GOOD FEATURES:

INFLIGHT PILOT COMMENT CARD

FLT NO. 8 RUN NO. 2	SP FREQ = 2.0	DATE: 4 OCT 89
CONFIGURATION 2-7	DAMP RATIO = 0.75	PILOT: B
GEARING = $.50M_{fe}$	FCS = 144/[0.7,12]	IP: BALL

C-H RATING = 5 PIO RATING = 3 CONFIDENCE RATING = A

FEEL SYSTEM CHARACTERISTICS:

FORCES:	SLIGHTLY HEAVY
PITCH SENSITIVITY:	SLUGGISH

PITCH ATTITUDE CONTROL:

INITIAL RESPONSE:	SLUGGISH
FINAL RESPONSE:	RATES INCREASE
PREDICTABILITY:	GOOD, SOME LEAD REQUIRED
PILOT COMPENSATION:	SLIGHT
PIO TENDENCY:	NO, SLIGHT UNDESIRABLE MOTION

TASK PERFORMANCE:

AIRSPEED CONTROL:	DESIRED
TOUCHDOWN POINT:	DESIRED
RUNWAY ALIGNMENT:	DESIRED
TOUCHDOWN SINK RATE:	DROPPED IN
AGGRESSIVENESS:	MODERATE
SPECIAL CONTROL:	OPEN LOOP IN FLARE
REASON APP ABANDON:	N/A

ADDITIONAL FACTORS:

WIND:	CALM
TURBULENCE:	NONE
LAT-DIR PERFORMANCE:	GOOD

SUMMARIZE EVALUATION:

MAJOR PROBLEMS:

GOOD FEATURES:

INFLIGHT PILOT COMMENT CARD

FLT NO. 9 RUN NO. 1	SP FREQ = 2.0	DATE: 4 OCT 89
CONFIGURATION 2-D	DAMP RATIO = 0.75	PILOT: B
GEARING = $.50M_{\delta_e}$	FCS = 0.5(20)/(10)	IP: BALL

C-H RATING = 3 PIO RATING = 1 CONFIDENCE RATING = A

FEEL SYSTEM CHARACTERISTICS:

FORCES:	GOOD
PITCH SENSITIVITY:	GOOD

PITCH ATTITUDE CONTROL:

INITIAL RESPONSE:	GOOD
FINAL RESPONSE:	GOOD
PREDICTABILITY:	GOOD
PILOT COMPENSATION:	MODERATE
PIO TENDENCY:	NONE

TASK PERFORMANCE:

AIRSPEED CONTROL:	DESIRED
TOUCHDOWN POINT:	DESIRED
RUNWAY ALIGNMENT:	DESIRED
TOUCHDOWN SINK RATE:	MODERATE
AGGRESSIVENESS:	MODERATE
SPECIAL CONTROL:	GAVE UP TO MAKE A/C LAND
REASON APP ABANDON:	N/A

ADDITIONAL FACTORS:

WIND:	CALM
TURBULENCE:	NONE
LAT-DIR PERFORMANCE:	GOOD

SUMMARIZE EVALUATION:

MAJOR PROBLEMS: GOOD CONFIGURATION EXCEPT HAD TO "GIVE UP" TO MAKE A/C LAND

GOOD FEATURES:

INFLIGHT PILOT COMMENT CARD

FLT NO. 9	RUN NO. 2	SP FREQ = 3.2	DATE: 4 OCT 89
CONFIGURATION 3-8		DAMP RATIO = 0.50	PILOT: B
GEARING = $1.1M_{\delta_e}$		FCS = 81,0/[0.7,9]	IP: BALL

C-H RATING = 7 PIO RATING = 4 CONFIDENCE RATING = B

FEEL SYSTEM CHARACTERISTICS:

FORCES:	STIRRING THE STICK TO CONTROL A/C
PITCH SENSITIVITY:	SLUGGISH

PITCH ATTITUDE CONTROL:

INITIAL RESPONSE:	SLUGGISH
FINAL RESPONSE:	SLUGGISH, THEN RATED UP
PREDICTABILITY:	UNPREDICTABLE
PILOT COMPENSATION:	OPEN LOOP IN FLARE
PIO TENDENCY:	LARGE

TASK PERFORMANCE:

AIRSPEED CONTROL:	DIFFICULT
TOUCHDOWN POINT:	ADEQUATE
RUNWAY ALIGNMENT:	DESIRED
TOUCHDOWN SINK RATE:	DROPPED IN
AGGRESSIVENESS:	OPEN LOOP TO LAND
SPECIAL CONTROL:	OPEN LOOP TO PREVENT PIO
REASON APP ABANDON:	N/A

ADDITIONAL FACTORS:

WIND:	LIGHT
TURBULENCE:	NONE
LAT-DIR PERFORMANCE:	GOOD

SUMMARIZE EVALUATION:

MAJOR PROBLEMS:	PIO PRONE
GOOD FEATURES/COMMENTS:	DIFFICULT TO RATE CH - HAD TO DECIDE BETWEEN A 6 AND 7.

INFLIGHT PILOT COMMENT CARD

FLT NO. 10	RUN NO. 1	SP FREQ = 3.2	DATE: 5 OCT 89
CONFIGURATION 3-5		DAMP RATIO = 0.50	PILOT: A
GEARING = $1.1M_{\sqrt{\theta}}$		FCS = 1.0/(1)	IP: BALL

C-H RATING = 5 PIO RATING = 3 CONFIDENCE RATING = B

FEEL SYSTEM CHARACTERISTICS:

FORCES:	MEDIUM
PITCH SENSITIVITY:	GOOD

PITCH ATTITUDE CONTROL:

INITIAL RESPONSE:	SLOW/DELAYED
FINAL RESPONSE:	GOOD
PREDICTABILITY:	GOOD
PILOT COMPENSATION:	LOWER GAIN AND LEAD INPUTS
PIO TENDENCY:	SLIGHT

TASK PERFORMANCE:

AIRSPEED CONTROL:	DESIRED
TOUCHDOWN POINT:	ADEQUATE
RUNWAY ALIGNMENT:	DESIRED
TOUCHDOWN SINK RATE:	LOW
AGGRESSIVENESS:	LOW
SPECIAL CONTROL:	LOWERED GAIN IN FLARE
REASON APP ABANDON:	N/A

ADDITIONAL FACTORS:

WIND:	CALM
TURBULENCE:	NONE
LAT-DIR PERFORMANCE:	GOOD

SUMMARIZE EVALUATION:

MAJOR PROBLEMS: WITH MEDIUM GAIN UNDESIRABLE MOTIONS OCCURED THAT AFFECTED TASK PERFORMANCE, AND WHEN PILOT LOWERED GAIN UNDESIRABLE MOTIONS DISAPPEARED.

GOOD FEATURES:

INFLIGHT PILOT COMMENT CARD

FLT NO. 10	RUN NO. 2	SP FREQ = 2.0	DATE: 5 OCT 89
CONFIGURATION 2-1		DAMP RATIO = 0.75	PILOT: A
GEARING = $.50M_{\delta_e}$		FCS = 1.0	IP: BALL

C-H RATING = 2 PIO RATING = 1 CONFIDENCE RATING = B

FEEL SYSTEM CHARACTERISTICS:

FORCES:	MEDIUM
PITCH SENSITIVITY:	GOOD

PITCH ATTITUDE CONTROL:

INITIAL RESPONSE:	QUICK
FINAL RESPONSE:	QUICK
PREDICTABILITY:	GOOD
PILOT COMPENSATION:	NONE
PIO TENDENCY:	NONE

TASK PERFORMANCE:

AIRSPEED CONTROL:	DESIRED
TOUCHDOWN POINT:	DESIRED
RUNWAY ALIGNMENT:	DESIRED
TOUCHDOWN SINK RATE:	LOW
AGGRESSIVENESS:	MEDIUM
SPECIAL CONTROL:	NONE
REASON APP ABANDON:	N/A

ADDITIONAL FACTORS:

WIND:	CALM
TURBULENCE:	NONE
LAT-DIR PERFORMANCE:	GOOD

SUMMARIZE EVALUATION:

MAJOR PROBLEMS:

GOOD FEATURES:

INFLIGHT PILOT COMMENT CARD

FLT NO. 11	RUN NO. 1	SP FREQ = 3.2	DATE: 10 OCT 89
CONFIGURATION 3-8		DAMP RATIO = 0.50	PILOT: A
GEARING = $1.1M_{\delta_e}$		FCS = 81.0/[0.7,9]	IP: BALL

C-H RATING = 4 PIO RATING = 2 CONFIDENCE RATING = B

FEEL SYSTEM CHARACTERISTICS:

FORCES:	GOOD
PITCH SENSITIVITY:	A LITTLE SENSITIVE

PITCH ATTITUDE CONTROL:

INITIAL RESPONSE:	QUICK
FINAL RESPONSE:	QUICK
PREDICTABILITY:	FAIR
PILOT COMPENSATION:	HAD TO REDUCE GAIN
PIO TENDENCY:	LOW

TASK PERFORMANCE:

AIRSPEED CONTROL:	DESIRED
TOUCHDOWN POINT:	DESIRED
RUNWAY ALIGNMENT:	DESIRED
TOUCHDOWN SINK RATE:	GOOD
AGGRESSIVENESS:	MEDIUM
SPECIAL CONTROL:	HAD TO LOWER GAIN IN THE FLARE
REASON APP ABANDON:	N/A

ADDITIONAL FACTORS:

WIND:	CALM
TURBULENCE:	NONE
LAT-DIR PERFORMANCE:	GOOD

SUMMARIZE EVALUATION:

MAJOR PROBLEMS: JUMPY, UNDESIRABLE MOTIONS, MODERATE COMPENSATION

GOOD FEATURES:

INFLIGHT PILOT COMMENT CARD

FLT NO. 11 RUN NO. 2	SP FREQ = 3.2	DATE: 10 OCT 89
CONFIGURATION 3-6	DAMP RATIO = 0.50	PILOT: A
GEARING = $1.1M_{\delta_e}$	FCS = 256/[0.7,16]	IP: BALL

C-H RATING = 6 PIO RATING = 3 CONFIDENCE RATING = B

FEEL SYSTEM CHARACTERISTICS:

FORCES:	OK
PITCH SENSITIVITY:	SLIGHT

PITCH ATTITUDE CONTROL:

INITIAL RESPONSE:	QUICK - JUMPY
FINAL RESPONSE:	QUICK
PREDICTABILITY:	GOOD
PILOT COMPENSATION:	EXTENSIVE-LOWER GAIN IN THE FLARE
PIO TENDENCY:	MEDIUM - NOT OSCILLATORY

TASK PERFORMANCE:

AIRSPEED CONTROL:	DESIRED
TOUCHDOWN POINT:	ADEQUATE
RUNWAY ALIGNMENT:	DESIRED
TOUCHDOWN SINK RATE:	LOW
AGGRESSIVENESS:	MEDIUM
SPECIAL CONTROL:	LOWERED GAIN IN FLARE
REASON APP ABANDON:	N/A

ADDITIONAL FACTORS:

WIND:	CALM
TURBULENCE:	NONE
LAT-DIR PERFORMANCE:	GOOD

SUMMARIZE EVALUATION:

MAJOR PROBLEMS: JUMPY/UNDESIRABLE MOTIONS REQUIRING EXTENSIVE PILOT COMPENSATION

GOOD FEATURES:

INFLIGHT PILOT COMMENT CARD

FLT NO. 11 RUN NO. 3	SP FREQ = 1.0	DATE: 10 OCT 89
CONFIGURATION 1-3	DAMP RATIO = 0.75	PILOT: A
GEARING = $.34M_{\delta e}$	FCS = 4.0/(4)	IP: BALL

C-H RATING = 7 PIO RATING = 4 CONFIDENCE RATING = A

FEEL SYSTEM CHARACTERISTICS:

FORCES:	GOOD
PITCH SENSITIVITY:	SLUGGISH

PITCH ATTITUDE CONTROL:

INITIAL RESPONSE:	SLOW-POOR
FINAL RESPONSE:	GOOD
PREDICTABILITY:	POOR
PILOT COMPENSATION:	EXCESSIVE
PIO TENDENCY:	HIGH

TASK PERFORMANCE:

AIRSPEED CONTROL:	DESIRED
TOUCHDOWN POINT:	ADEQUATE
RUNWAY ALIGNMENT:	DESIRED
TOUCHDOWN SINK RATE:	LOW
AGGRESSIVENESS:	MEDIUM
SPECIAL CONTROL:	LOWERED GAINS IN FLARE
REASON APP ABANDON:	N/A

ADDITIONAL FACTORS:

WIND:	CALM
TURBULENCE:	NONE
LAT-DIR PERFORMANCE:	GOOD

SUMMARIZE EVALUATION:

MAJOR PROBLEMS: SLOW-LAGGY-PIO, UNPREDICTABLE, COULD BE A "CLIFF" IF PILOT DOES NOT LOWER GAINS IN FLARE

GOOD FEATURES:

INFLIGHT PILOT COMMENT CARD

FLT NO. 12	RUN NO. 1	SP FREQ = 3.2	DATE: 10 OCT 89
CONFIGURATION 3-3		DAMP RATIO = 0.50	PILOT: C
GEARING = $1.1M_{\delta_e}$		FCS = 4.0/(4)	IP: BALL

C-H RATING = 3	PIO RATING = 1	CONFIDENCE RATING = B

FEEL SYSTEM CHARACTERISTICS:

FORCES:	MEDIUM
PITCH SENSITIVITY:	GOOD

PITCH ATTITUDE CONTROL:

INITIAL RESPONSE:	GOOD
FINAL RESPONSE:	GOOD
PREDICTABILITY:	GOOD
PILOT COMPENSATION:	NONE
PIO TENDENCY:	NONE

TASK PERFORMANCE:

AIRSPEED CONTROL:	DESIRED
TOUCHDOWN POINT:	DESIRED
RUNWAY ALIGNMENT:	DESIRED
TOUCHDOWN SINK RATE:	HIGHER THAN NORMAL
AGGRESSIVENESS:	MODERATE
SPECIAL CONTROL:	NONE
REASON APP ABANDON:	N/A

ADDITIONAL FACTORS:

WIND:	CALM
TURBULENCE:	NONE
LAT-DIR PERFORMANCE:	GOOD

SUMMARIZE EVALUATION:

MAJOR PROBLEMS: TENDS TO QUIT FLYING IN THE FLARE AND RESULTS IN DROPPED IN LANDINGS

GOOD FEATURES:

INFLIGHT PILOT COMMENT CARD

FLT NO. 12 RUN NO. 2	SP FREQ = 2.0	DATE: 10 OCT 89
CONFIGURATION 2-5	DAMP RATIO = 0.75	PILOT: C
GEARING= .50M$\int_e$	FCS = 1.0/(1)	IP: BALL

C-H RATING = 10 PIO RATING = 6 CONFIDENCE RATING = A

FEEL SYSTEM CHARACTERISTICS:

FORCES:	UNSAT - TOO HEAVY
PITCH SENSITIVITY:	UNSAT - TOO SLOW

PITCH ATTITUDE CONTROL:

INITIAL RESPONSE:	UNSAT
FINAL RESPONSE:	UNSAT
PREDICTABILITY:	UNPREDICTABLE
PILOT COMPENSATION:	IMPOSSIBLE
PIO TENDENCY:	EXCESSIVE

TASK PERFORMANCE:

AIRSPEED CONTROL:	DESIRED
TOUCHDOWN POINT:	UNSAT
RUNWAY ALIGNMENT:	DESIRED
TOUCHDOWN SINK RATE:	DID NOT GET THAT FAR
AGGRESSIVENESS:	EXCESSIVELY HIGH
SPECIAL CONTROL:	N/A
REASON APP ABANDON:	POOR HANDLING QUALITIES AND PIO

ADDITIONAL FACTORS:

WIND:	CALM
TURBULENCE:	NONE
LAT-DIR PERFORMANCE:	GOOD

SUMMARIZE EVALUATION:

MAJOR PROBLEMS: EXCESSIVE BALLOON STARTING FLARE AND LOW FREQ PIO WHICH SEEMED TO BE CAUSED BY ALOT OF LAG IN THE SYSTEM. TO OBTAIN DESIRED/ADEQUATE PERFORMANCE WOULD HAVE MEANT A PUSH OVER THAT WOULD HAVE EXCEEDED A/C LIMITS ON LANDING.

GOOD FEATURES: IT HAD NONE!!

INFLIGHT PILOT COMMENT CARD

FLT NO. 12	RUN NO. 3	SP FREQ = 3.2	DATE: 10 OCT 89
CONFIGURATION 3-8		DAMP RATIO = 0.50	PILOT: C
GEARING = $1.1M_{\mathcal{J}_e}$		FCS = 81.0/[0.7,9]	IP: BALL

C-H RATING = 4 PIO RATING = 2 CONFIDENCE RATING = A

FEEL SYSTEM CHARACTERISTICS:

FORCES:	GOOD
PITCH SENSITIVITY:	EXCESSIVE, BOBBLES

PITCH ATTITUDE CONTROL:

INITIAL RESPONSE:	GOOD
FINAL RESPONSE:	GOOD
PREDICTABILITY:	GOOD
PILOT COMPENSATION:	NONE
PIO TENDENCY:	NONE

TASK PERFORMANCE:

AIRSPEED CONTROL:	GOOD
TOUCHDOWN POINT:	DESIRED
RUNWAY ALIGNMENT:	DESIRED
TOUCHDOWN SINK RATE:	GOOD
AGGRESSIVENESS:	AVERAGE
SPECIAL CONTROL:	ALOT OF STICK MOVEMENTS TO COUNTER PITCH BOBBLES
REASON APP ABANDON:	N/A

ADDITIONAL FACTORS:

WIND:	NONE
TURBULENCE:	NONE
LAT-DIR PERFORMANCE:	GOOD

SUMMARIZE EVALUATION:

MAJOR PROBLEMS:	PITCH BOBBLES
GOOD FEATURES:	OVERALL GOOD FLYING A/C EXCEPT FOR PITCH BOBBLES

APPENDIX F

NT-33A CONFIGURATION IDENTIFICATIONS

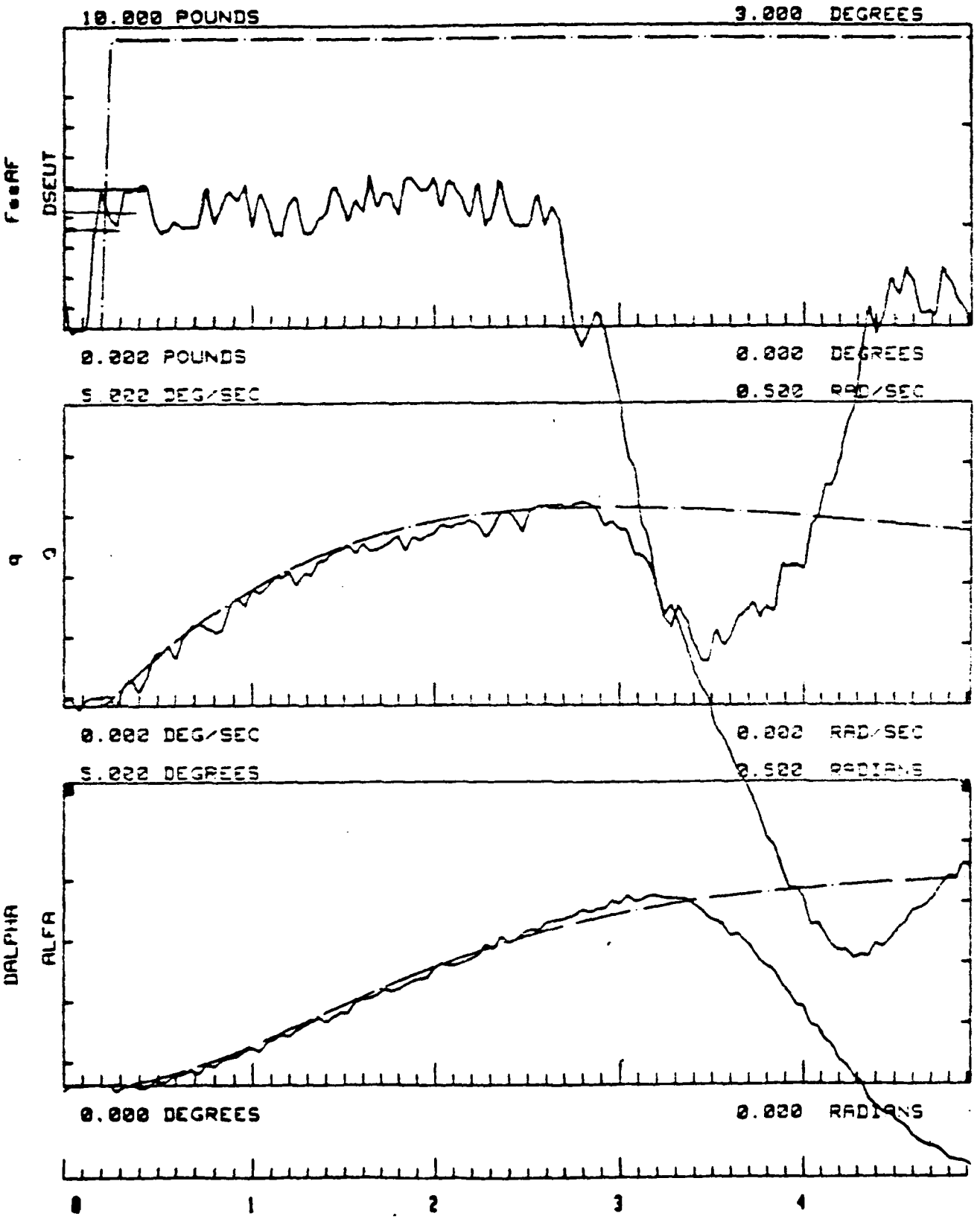

Figure 41. System Verification by CALSPAN - Configuration 1-1

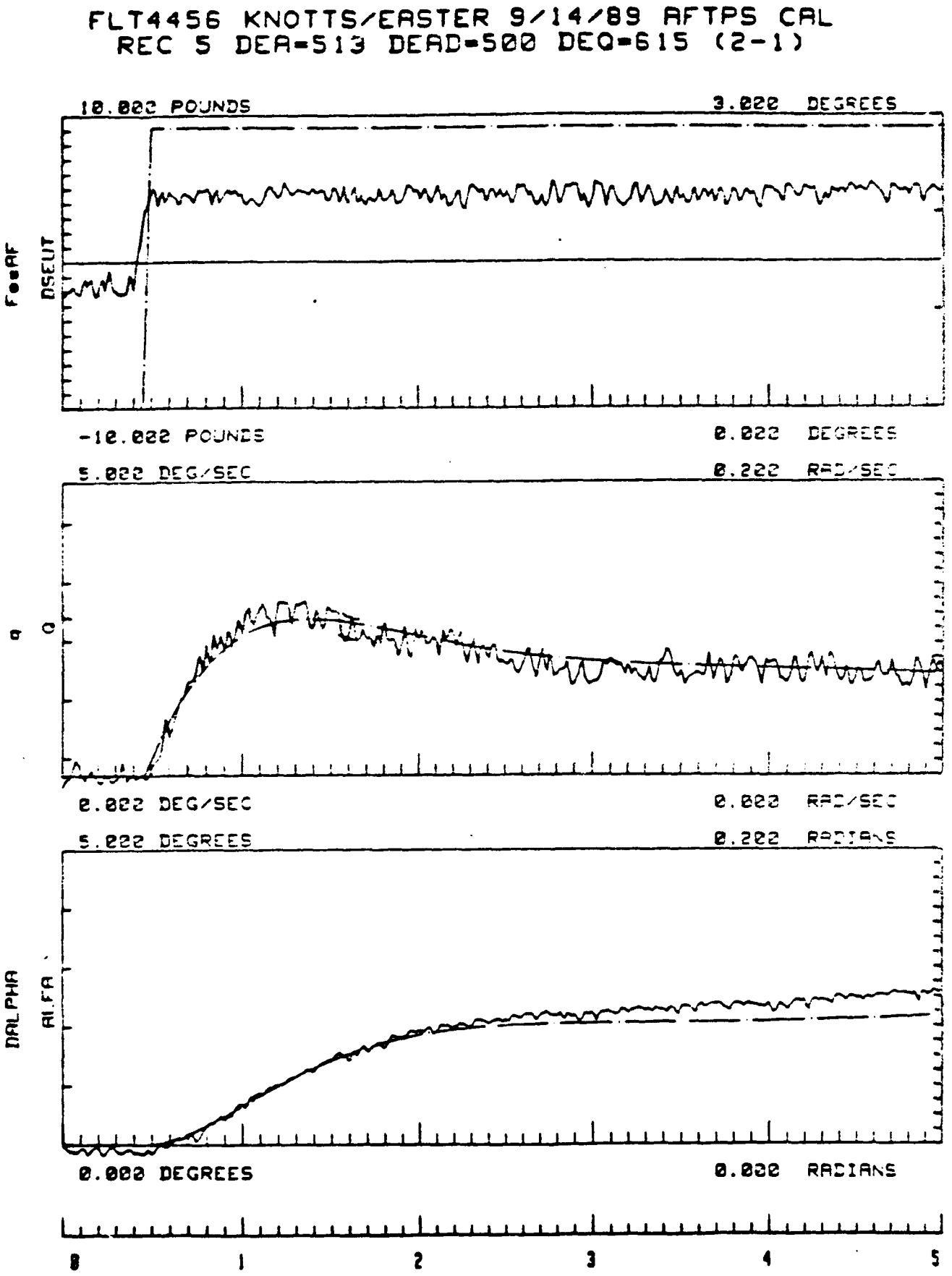

Figure 42. System Verification by CALSPAN - Configuration 2-1

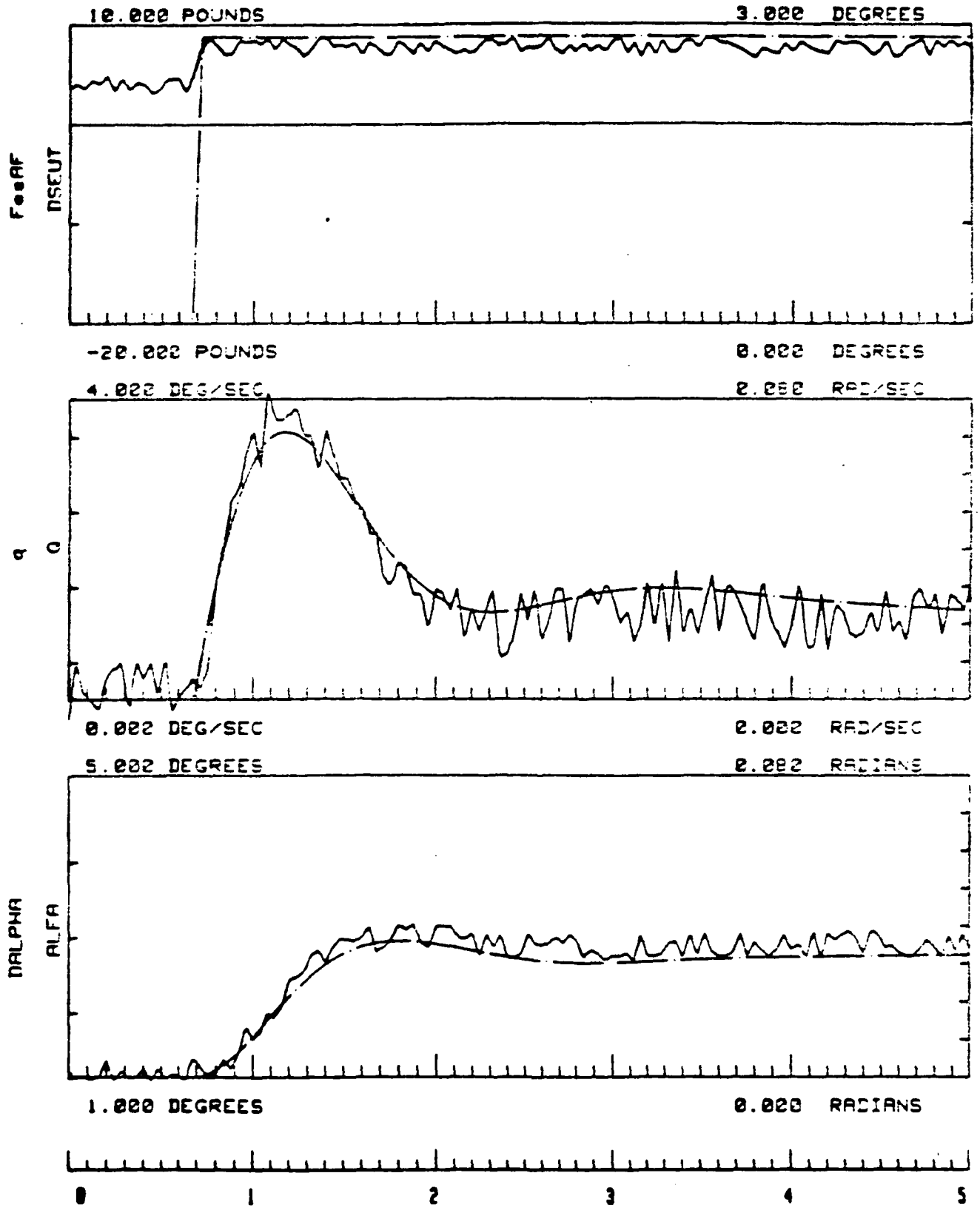

Figure 43. System Verification by CALSPAN - Configuration 3-1

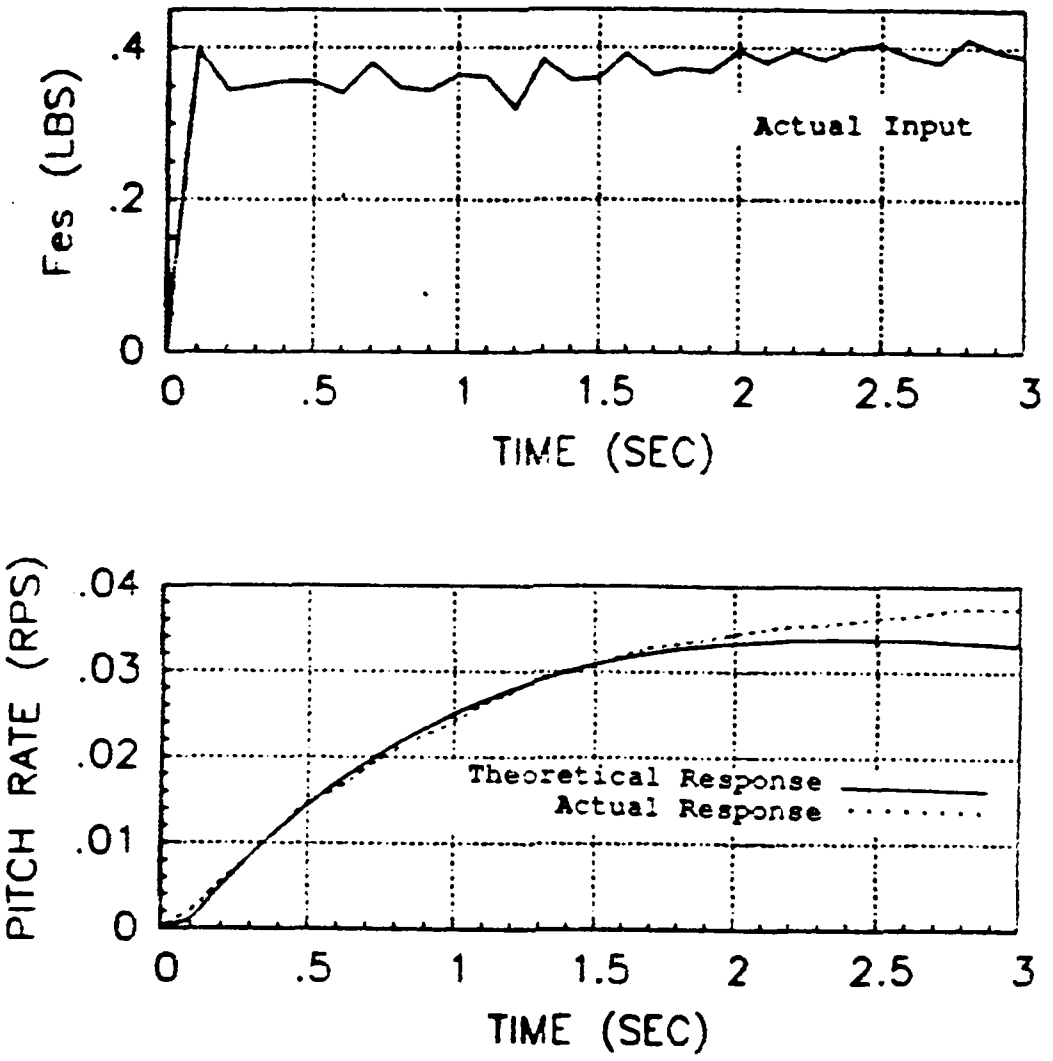

Figure 44. System Verification - Configuration 1-1

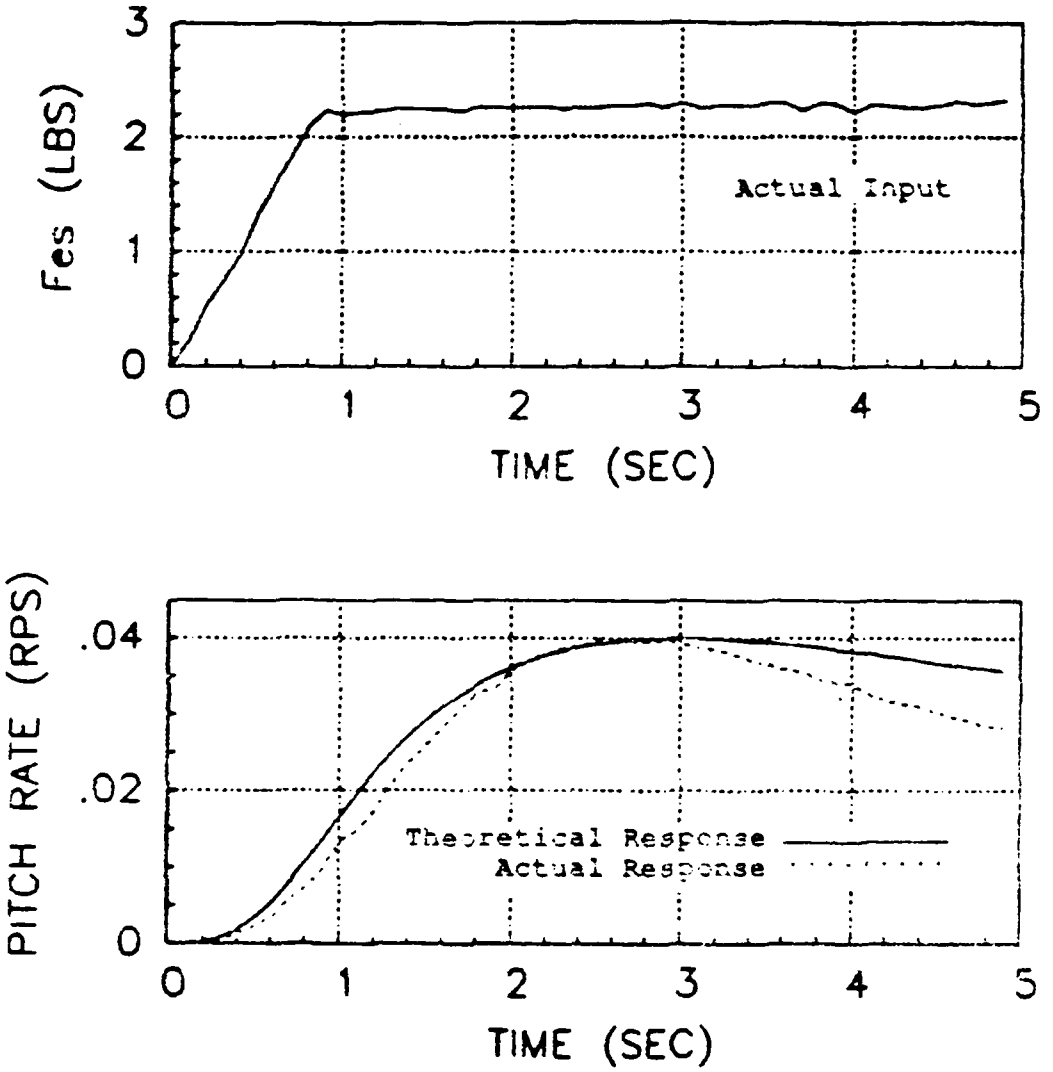

Figure 45. System Verification - Configuration 1-3

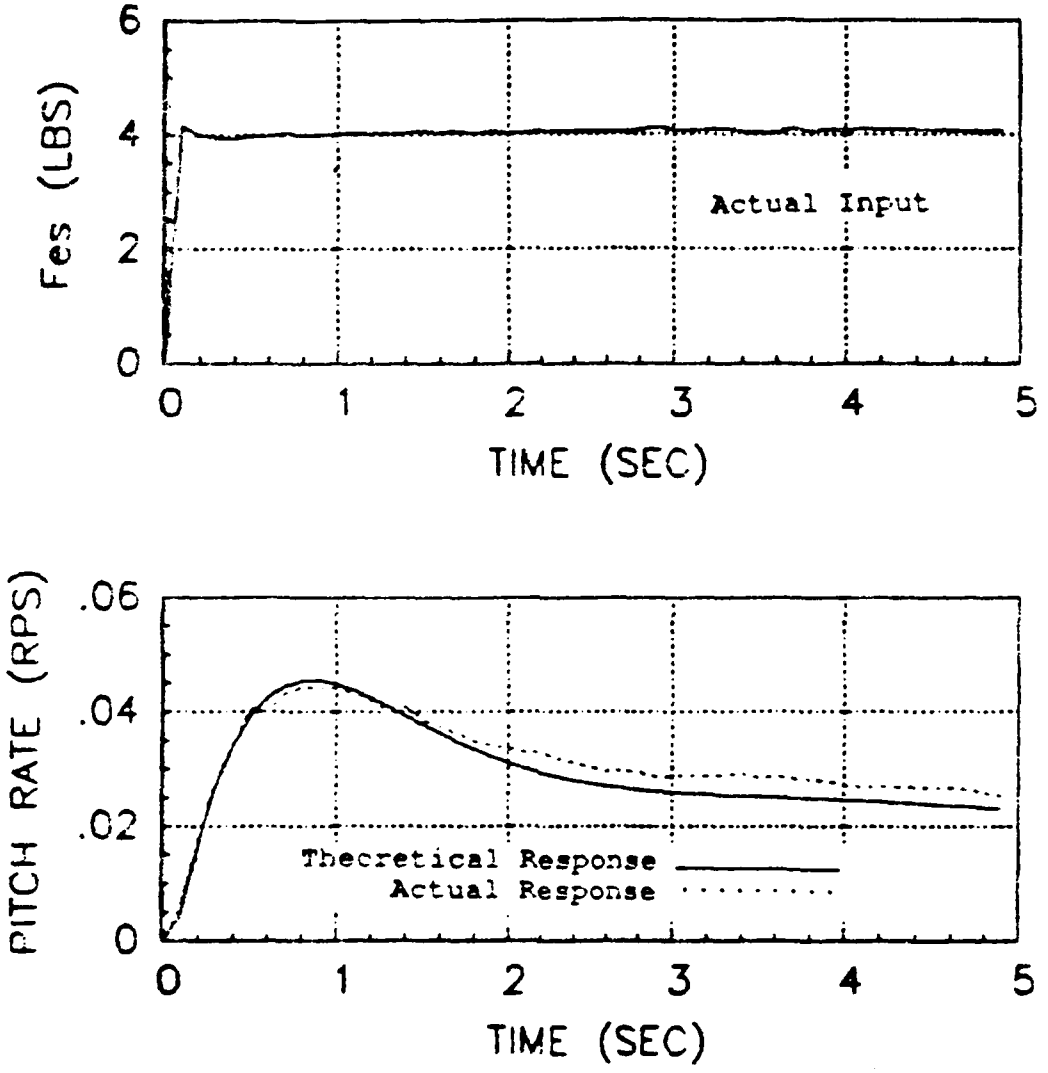

Figure 46. System Verification - Configuration 2-1

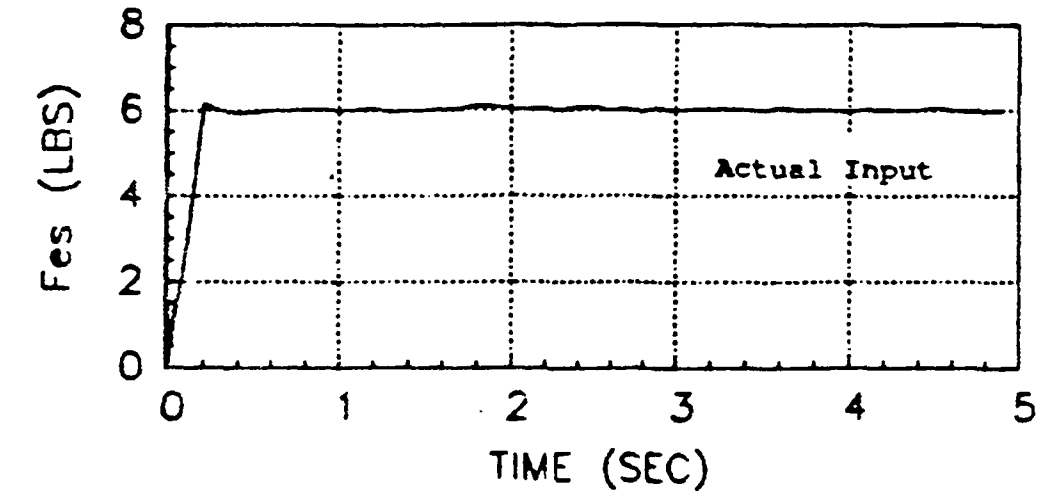

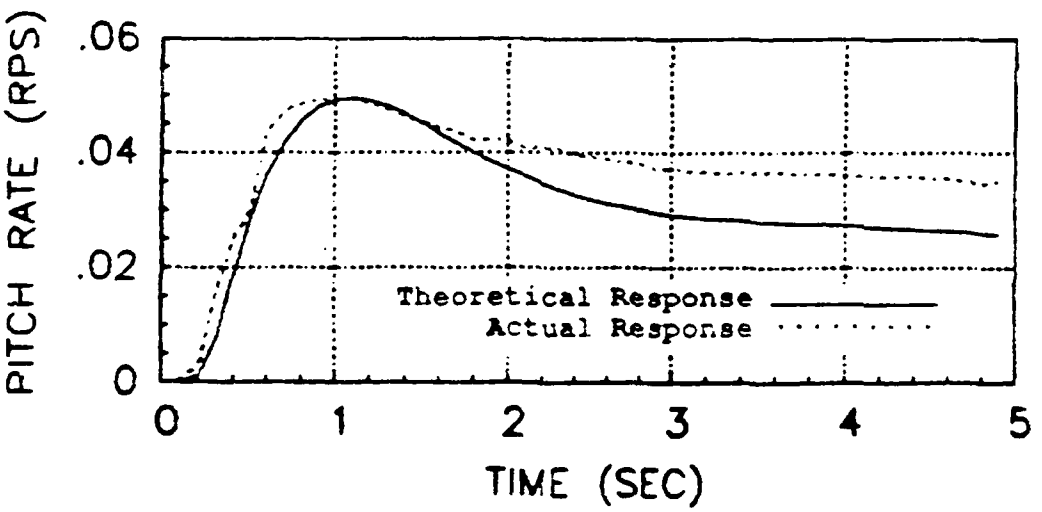

Figure 47. System Verification - Configuration 2-D

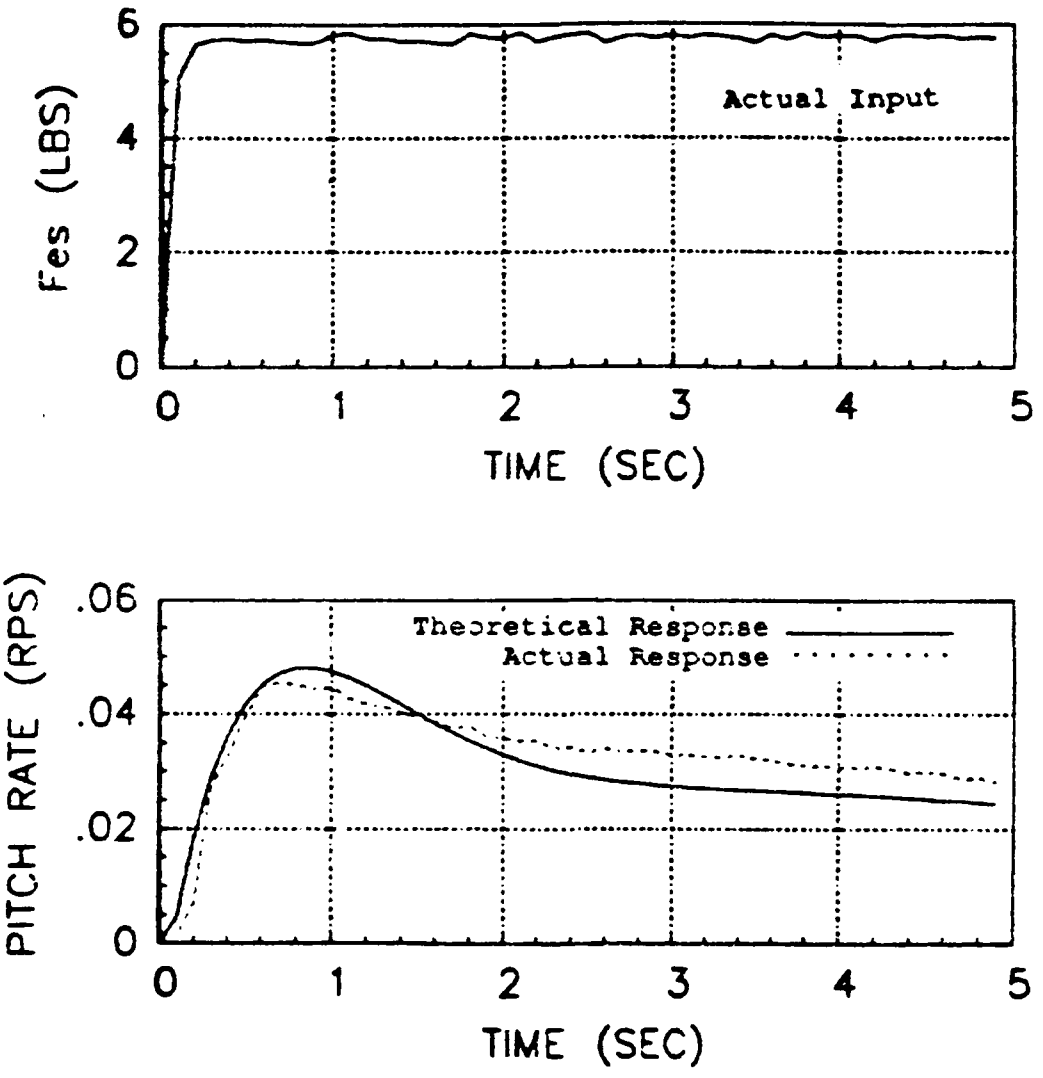

Figure 48. System Verification - Configuration 2-2

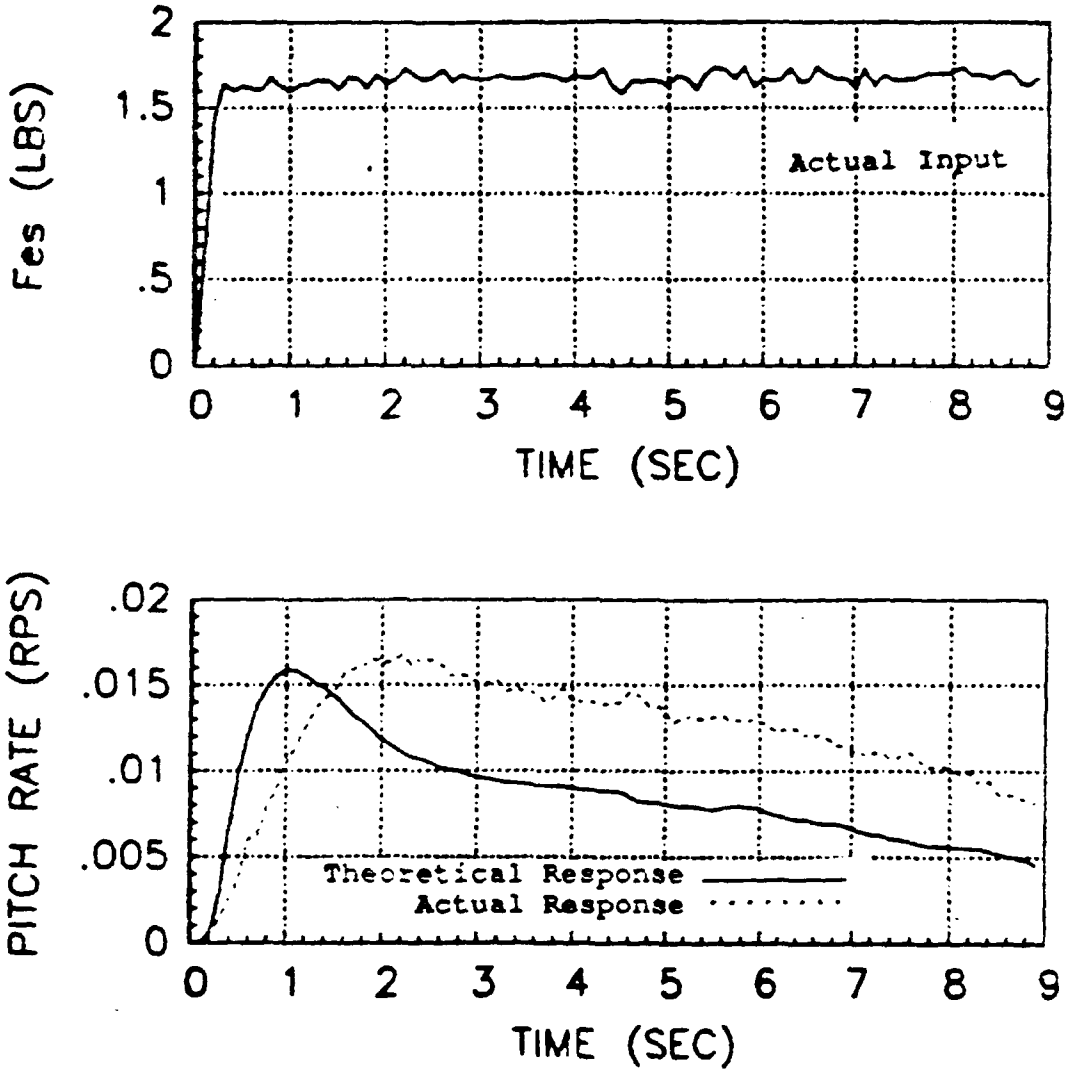

Figure 49. System Verification - Configuration 2-5

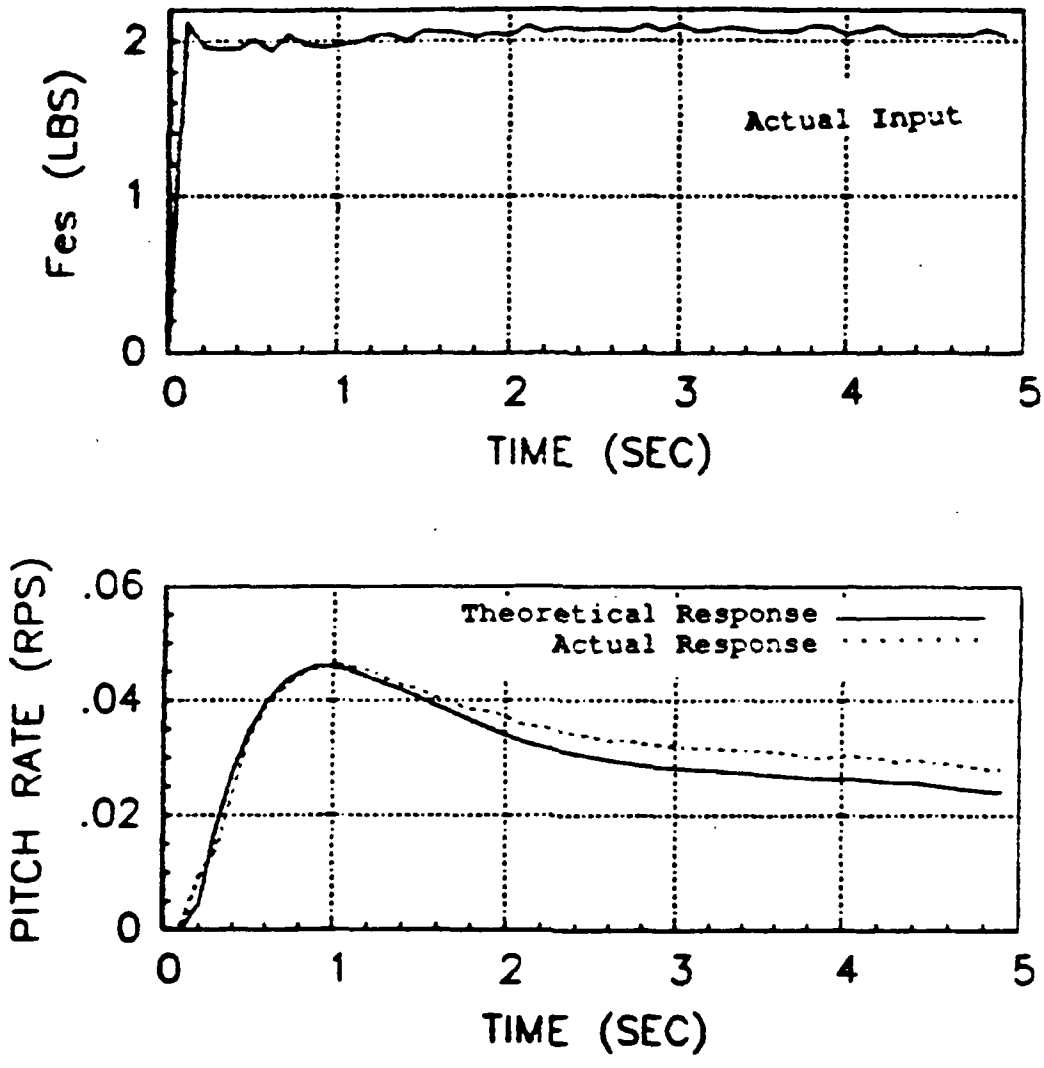

Figure 50. System Verification - Configuration 2-7

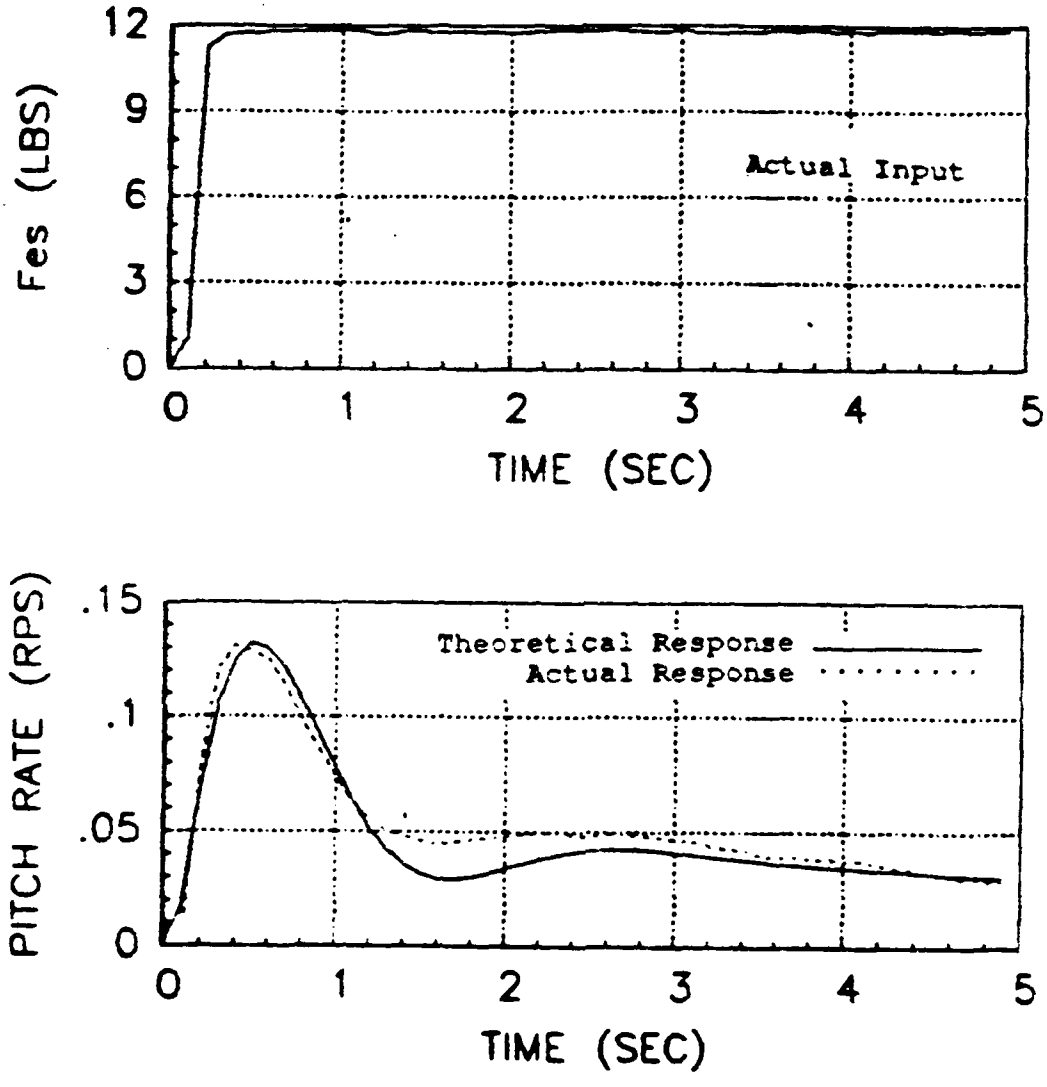

Figure 51. System Verification - Configuration 3-1

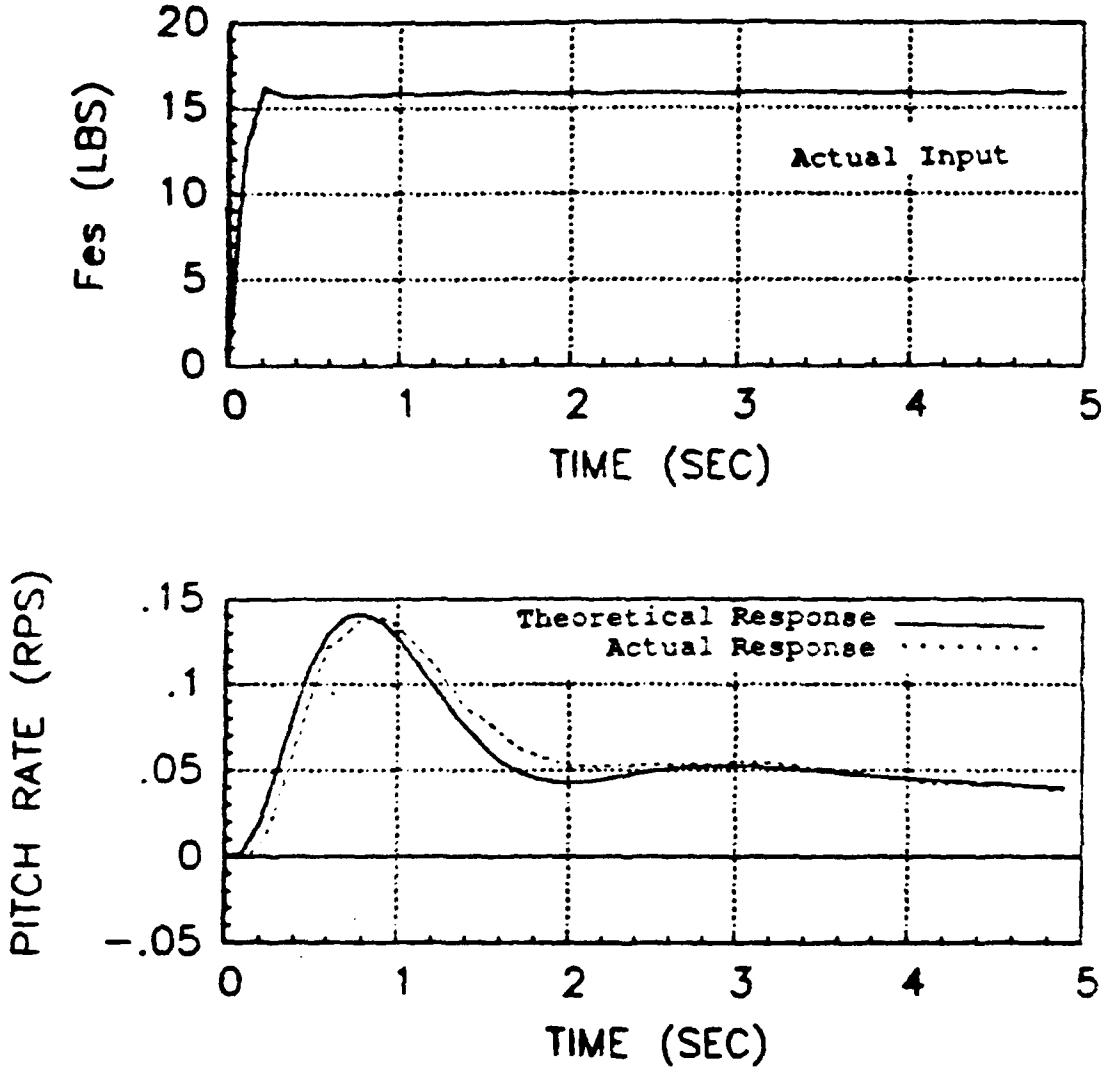

Figure 52. System Verification - Configuration 3-3

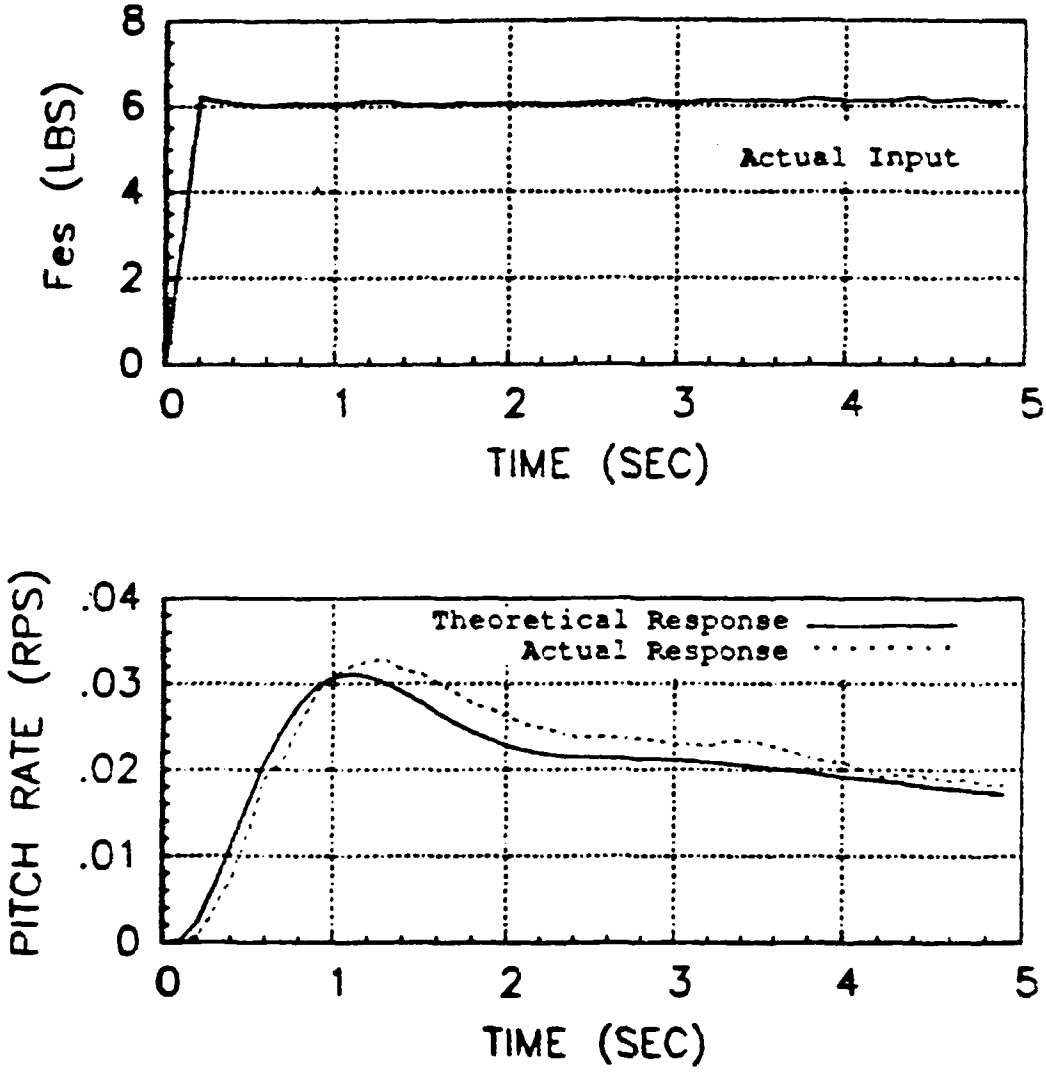

Figure 53. System Verification - Configuration 3-5

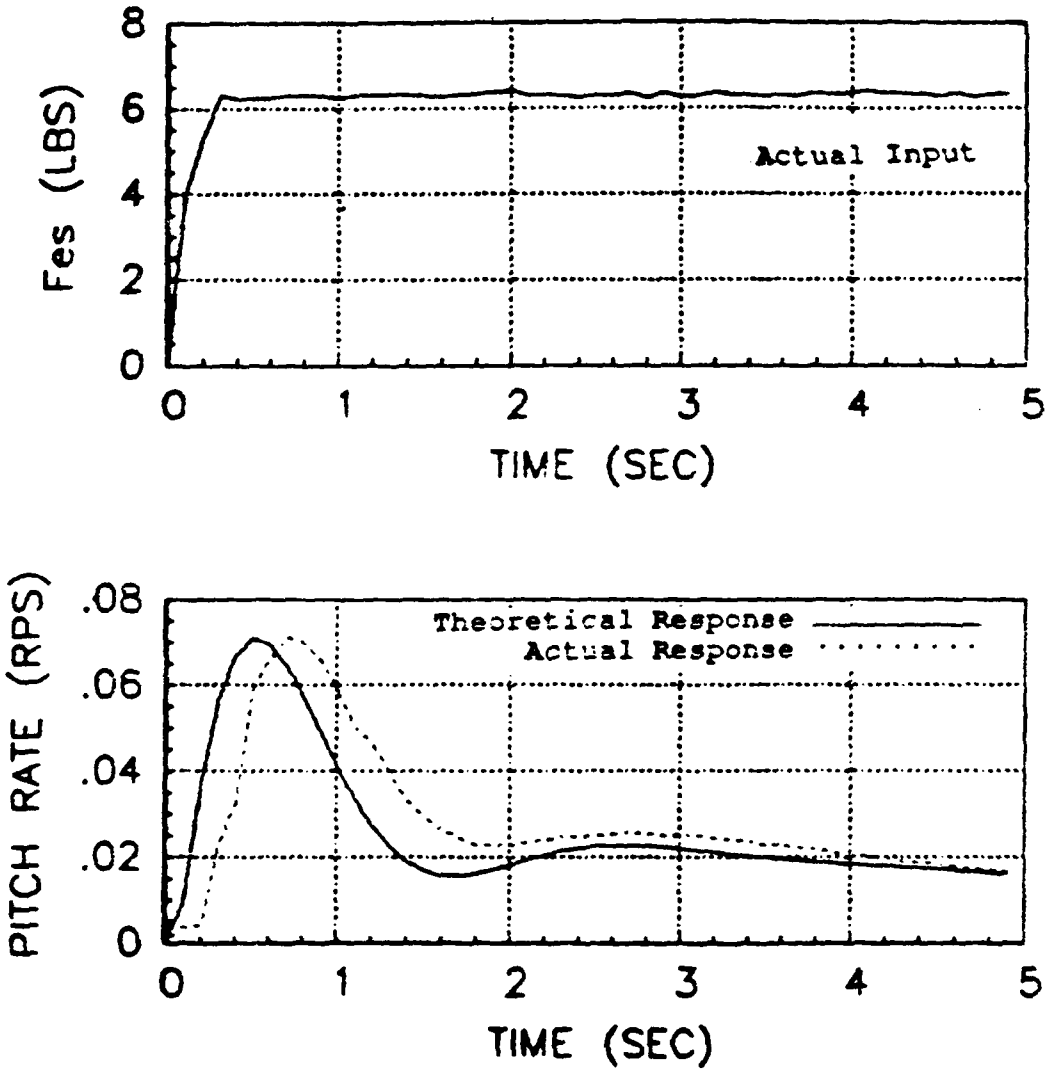

Figure 54. System Verification - Configuration 3-6

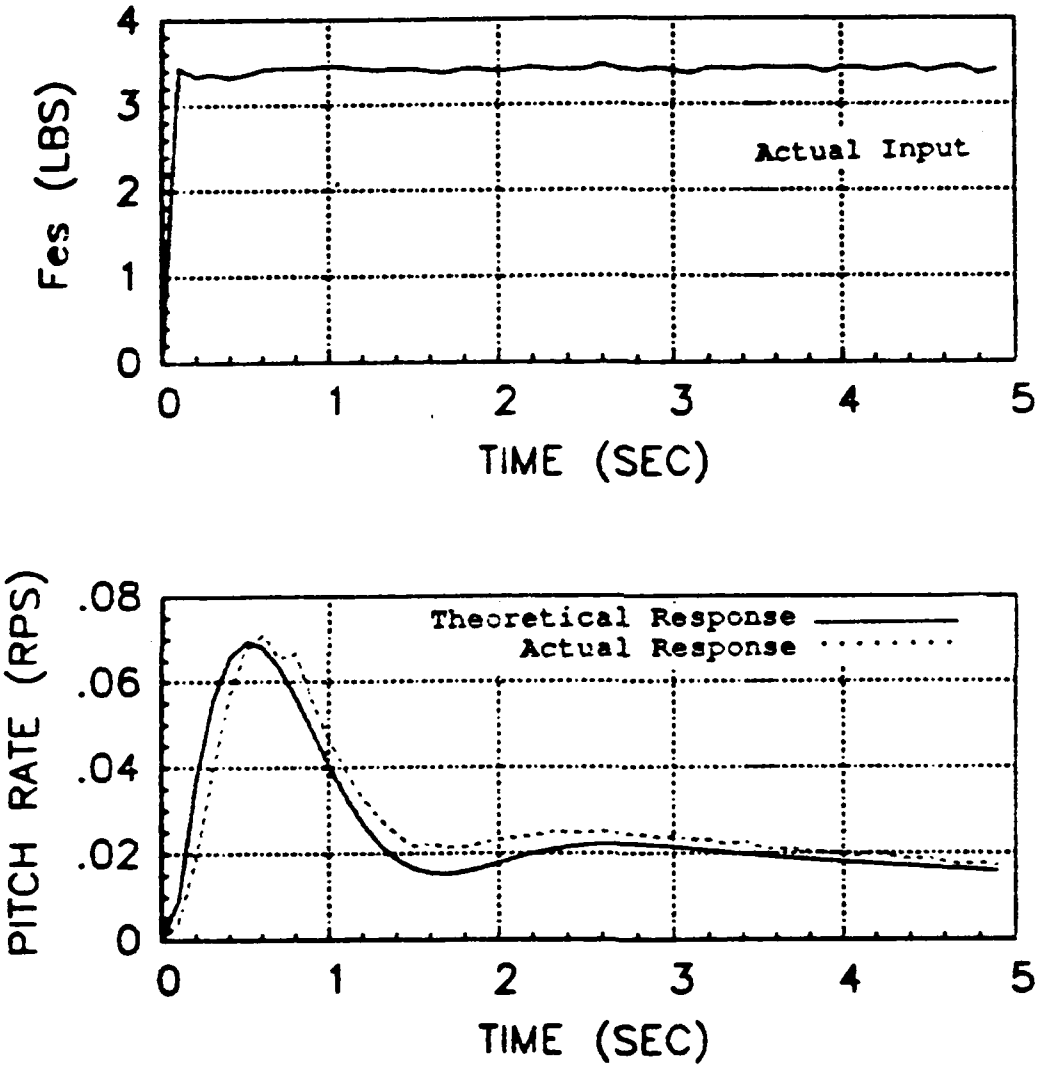

Figure 55. System Verification - Configuration 3-8

Bibliography

1. Smith, R. H., A Theory for Longitudinal Short-Period Pilot Induced Oscillations, AFFDL-TR-77-57, Air Force Flight Dynamics Laboratory, Wright-Patterson AFB, OH, June 1977.

2. Ashkenas, I., H. Jex, and D. McRuer, Pilot-Induced Oscillations: Their Cause and Analysis, NORAIR Report No. NOR-64-143, Northrup Corporation, June 1964.

3. Military Standard, Flying Qualities of Piloted Airplanes, MIL- STD-1797, April 1987.

4. Kleinman, D. L., S. Baron, and W. H. Levison, "An Optimal Control Model of Human Response, Pt I & II," Automatica, Vol 6, May 1970, pp. 357-383.

5. Curry, R. E., W. C. Hoffman, and L. R. Young, Pilot Modeling for Manned Simulation, Vols. I and II, AFFDL-TR-76-124, Air Force Flight Dynamics Laboratory, Wright-Patterson AFB, OH, 1976.

6. Smith, R. E., Effects of Control System Dynamics on Fighter Approach and Landing Handling Qualities, Vol.I, AFFDL-TR-78-122, Air Force Flight Dynamics Laboratory, Wright-Patterson AFB, OH, March 1978.

7. Bjorkman, E. A., Flight Test Evaluation of Techniques to Predict Longitudinal Pilot Induced Oscillations, M. S. Thesis, Air Force Institute of Technology, WPAFB, OH, December 1986.

8. McRuer, D. T., I. Ashkenas, and D. Graham, Aircraft Dynamics and Automatic Control, Princeton, N. J., 1973.

9. Levison, W. H., D. L. Kleinman, and S. Baron, "A Model For Human Controller Remnant," IEEE Transactions on Man-Machine Systems 10, December 1969.

10. Rynaskii, E. G. and R. F. Whitbeck, The Theory and Application of Linear Optimal Control, AFFDL-TR-65-28, Air Force Flight Dynamics Laboratory, Wright-Patterson AFB, OH, January 1966.

11. Baron, S.; et al., Application of Optimal Control Theory to the Prediction of Human Performance in a Complex Task, AFFDL-TR-69-81, Air Force Flight Dynamics Laboratory, Wright-Patterson AFB, OH, March 1970.

12. Kleinman, D. L., "Optimal Control of Linear Systems with Time-Delay and Observation Noise," IEEE Transactions on Automatic Control, Vol. AC-14, Oct. 1969, pp. 524-527

13. Levison, W. H., J. I. Elkind, and J. L. Ward, Studies of Multivariable Manual Control Systems: A Model for Task Interference, NASA-CR-1746, May 1971.

14. Bryson, A. E. and Y. C. Ho, Applied Optimal Control, New York, Wiley, 1975

15. Anderson, M. R. and D. K. Schmidt, "Closed-Loop Pilot Vehicle Analysis of the Approach and Landing Task," Journal of Guidance, Dynamics, and Control, Vol 10, No. 2, Mar-Apr 1987, pp187-194.

16. Neal, T. P. and R. E. Smith, An In-Flight Investigation to Develop System Design Criteria for Fighter Airplanes, Vol. 1, AFFDL-TR-70-74, Air Force Flight Dynamics Laboratory, Wright-Patterson AFB, OH, Dec. 1970.

17. Boettcher, K., D. K. Schmidt, and L. Case, Display Systems Dynamics Requirements For Flying Qualities, AFWAL-TR-88-3017, Air Force Weapons Laboratory, Wright-Patterson AFB, OH, May 1988.

18. USAF Series T-33 Aircraft, T.O. 1T-33A-1, 31 January 1973, Change 7, 30 August 1976.

19. Partial Flight Manual, NT-33A S/N 51-4120.

20. G.W. Hall, R.W. Huber, AFFDL-TR-70-71, System Description and Performance Data for the USAF/CAL Variable Stability T-33 Airplane, Cornell Aeronautical Laboratory, Inc, August 1970.

21. Aircrew Operations, Air Force Flight Test Center (AFFTC) Regulation 55-2, Volume I, Air Force Flight Test Center, Edwards AFB, CA, 29 November 1988.

VITA

Capt Steven W. Lindsey [redacted]. He graduated from high school in Temple City, California, in 1978. He then attended the United States Air Force Academy, receiving the Bachelor of Science in Engineering Sciences in June 1982. After receiving a commission in the USAF in June, 1982, he entered undergraduate pilot training at Reese Air Force Base, Texas. Capt Lindsey graduated from pilot training in June, 1983, and then was an operational fighter pilot in RF-4C Phantoms at Bergstrom Air Force Base, Texas. He then became an RF-4C academic instructor and instructor pilot at Bergstrom Air Force Base until entering the joint AFIT/TPS program in August 1987.

[redacted]

UNCLASSIFIED
SECURITY CLASSIFICATION OF THIS PAGE

REPORT DOCUMENTATION PAGE

Form Approved OMB No. 0704-0188

1a. REPORT SECURITY CLASSIFICATION: UNCLASSIFIED	1b. RESTRICTIVE MARKINGS: NONE
2a. SECURITY CLASSIFICATION AUTHORITY	3. DISTRIBUTION/AVAILABILITY OF REPORT
2b. DECLASSIFICATION/DOWNGRADING SCHEDULE	UNLIMITED
4. PERFORMING ORGANIZATION REPORT NUMBER(S)	5. MONITORING ORGANIZATION REPORT NUMBER(S)
6a. NAME OF PERFORMING ORGANIZATION: SCHOOL OF ENGINEERING, AIR FORCE INSTITUTE OF TECH / 6b. OFFICE SYMBOL (If applicable): AFIT/ENY	7a. NAME OF MONITORING ORGANIZATION
6c. ADDRESS (City, State, and ZIP Code): WRIGHT-PATTERSON AFB, OHIO 45433	7b. ADDRESS (City, State, and ZIP Code)
8a. NAME OF FUNDING/SPONSORING ORGANIZATION / 8b. OFFICE SYMBOL (If applicable)	9. PROCUREMENT INSTRUMENT IDENTIFICATION NUMBER
8c. ADDRESS (City, State, and ZIP Code)	10. SOURCE OF FUNDING NUMBERS: PROGRAM ELEMENT NO. / PROJECT NO. / TASK NO / WORK UNIT ACCESSION NO

11. TITLE (Include Security Classification)
See Box 19

12. PERSONAL AUTHOR(S)
Steven W. Lindsey, Captain, USAF

13a. TYPE OF REPORT	13b. TIME COVERED	14. DATE OF REPORT (Year, Month, Day)	15. PAGE COUNT
MS Thesis	FROM _____ TO _____	1989 December	191

16. SUPPLEMENTARY NOTATION

17. COSATI CODES			18. SUBJECT TERMS (Continue on reverse if necessary and identify by block number)
FIELD	GROUP	SUB-GROUP	Pilot Induced Oscillation, Flight Control System, Variable Stability Aircraft, Flying Qualities, Handling Qualities, Cooper-Harper, NT-33, Optimal Control Model, Approach
01	04		
01	03	12	

19. ABSTRACT (Continue on reverse if necessary and identify by block number)

Title: PREDICTION OF LONGITUDINAL PILOT INDUCED OSCILLATIONS USING THE OPTIMAL CONTROL MODEL

Thesis Chairman: Dr. Robert A. Calico
Professor of Aerospace Engineering

20. DISTRIBUTION/AVAILABILITY OF ABSTRACT: ☒ UNCLASSIFIED/UNLIMITED ☐ SAME AS RPT. ☐ DTIC USERS	21. ABSTRACT SECURITY CLASSIFICATION: UNCLASSIFIED
22a. NAME OF RESPONSIBLE INDIVIDUAL: Dr. Robert A. Calico, Professor	22b. TELEPHONE (Include Area Code): 513-225-2362 / 22c. OFFICE SYMBOL: AFIT/ENY

DD Form 1473, JUN 86 — Previous editions are obsolete. — SECURITY CLASSIFICATION OF THIS PAGE: UNCLASSIFIED

The purpose of this study was to evaluate the Optimal Control Model (OCM) in predicting handling qualities and PIO pilot ratings during the approach and landing task. Using two existing PIO databases, analytical prediction schemes were developed using the OCM. The two prediction schemes used were flight path error and crossover frequency. The prediction schemes were then applied to twelve different aircraft/flight control system landing configurations. The twelve configurations were flight tested using a USAF/Calspan variable stability NT-33A.

The OCM was able to predict pilot handling qualities ratings (PHQR) accurately (within one pilot rating) 80 percent of the time. PIO ratings were accurately predicted 96 percent of the time. Due to a PIO rating problem in the original databases, the PIO prediction schemes were modified using flight test data. Additional flight test configurations should be flown to verify the revised flight path error and crossover frequency prediction schemes.

Because of the subjective nature of PHQRs and PIO ratings, the flight test results varied between pilots. Flight test results showed that the fighter pilot gave configurations poorer PHQRs and PIO ratings than the multiengine pilots. Additionally, the correlation between multiengine pilots was better than with the fighter pilot.

The crossover frequency prediction scheme was the most accurate predictor of pilot ratings, while the flight path error prediction scheme was slightly more accurate for PIO ratings. Both predictors agreed with classical control theory, showing correlation between flight path error, crossover frequency, and pilot/PIO ratings. The flight path error and crossover frequency rating prediction methods should be used as a tool in flight control system design.